A study of neutrino interactions constituting the background to electron neutrino appearance in T2K experiment

Paweł Przewłocki

Ph. D. thesis
written under supervision of
prof. dr hab. Danuta Kiełczewska

Andrzej Sołtan Institute for Nuclear Studies

2010

Abstract

Several studies for Tokai2Kamioka (T2K) experiment are presented. The primary aim of the thesis was to study background to electron neutrino appearance. The uncertainty of NC neutral pion production has been estimated to 6-10% in the relevant neutrino energy region (1-4 GeV) basing on reanalyzed data of historical bubble chamber experiments. Neutral pion identification capabilities of liquid argon TPC detection technique have been verified with a result of less than 1% inefficiency. Various method of neutrino energy and four-momentum transfer squared (Q^2) reconstruction have also been carefully evaluated and their weak points revealed. Finally, in the SMRD detector optimization study, an optimal layout of scintillation modules for this detector has been determined.

Thank you!

I want to say a big THANK YOU to prof. Danuta Kiełczewska, my supervisor, for help, guidance, patience and lots, lots of other things.

A warm thank you also goes to prof. Ewa Rondio, who has been my supervisor earlier, at the beginning of my Ph. D. studies.

Without the support of Danka and Ewa this thesis would have never come into existence. Thank you!

Cheers to Piotrek Mijakowski, Magda Posiadała, Robert Sulej, Tomek Palczewski, Justyna Łagoda, Krzysiek Graczyk, Jarek Nowak, Dorota Stefan, Łukasz Mączewski, Beata Brzozowska, Piotrek Traczyk and others for having fun together during my Ph.D. studies.

I would like to thank Warsaw Neutrino Group, along with groups from Wrocław, Katowice and Kraków for a nice and fruitful cooperation.

The author wishes also to thank T2K SMRD Group, and prof. Thomas Kutter in particular, and also many other people (among them prof. Jan Sobczyk and prof. Takuya Hasegawa) for help and support.

This Ph. D. Thesis was supported by grant N N202 029933.

Contents

List of tables

List of figures

Chapter 1
Introduction

1.1 Motivation

A combination of experiments worldwide have now demonstrated that neutrinos have mass and oscillate, which is the first confirmed evidence for physics beyond the Standard Model. Neutrino oscillation analysis is extremely important for understanding of nature of mixing in neutrino sector; it has also cosmological implications. There are many questions still to be answered, the most important of which are: Is third mixing angle θ_{13} non zero? Is there a CP violation in neutrino sector? More precise estimation of other neutrino oscillation parameters is also necessary.

The Tokai2Kamioka (T2K) experiment (currently starting its operation in Japan) is a long baseline neutrino experiment designed to provide answers to these questions. A strong, artificial neutrino beam, produced in J-PARC accelerator complex in Tokai will be directed at Kamioka mine, a far station of the experiment, 295 km away from the beam source. Neutrinos undergo the oscillation process and reach Super-Kamiokande, a large water Cherenkov detector situated in the mine. Phase I of the experiment will extend our sensitivity to θ_{13} by a factor of about ten. A proposed second phase of the experiment could extend this sensitivity even further, and also begin to have sensitivity to CP violation if θ_{13} is large enough, by comparing running with neutrinos and anti-neutrinos.

The author of this thesis is a member of T2K collaboration. Analyses presented in the thesis were done during preparation phase of T2K and deal with issues that are essential for the experiment.

1.2 Layout of the thesis

Chapter 2 is introductory and present the current status of neutrino oscillation searches. The formalism of oscillations as well as the most historically important experimental achievements in the field are also discussed. Chapter 3 describes experimental data and theoretical description of neutrino interactions in matter, in particular for the neutrino energies

specific to T2K experiment. Simulation algorithms and software used in further chapters are also presented and evaluated. Chapter 4 provides a detailed description of the T2K experimental setup. An SMRD detector optimization study is featured in this chapter. Chapter 5 is dedicated to evaluation of different methods of reconstructing neutrino energy and four-momentum transfer squared for neutrino interactions in T2K experiment. Chapter 6 presents the main study of the thesis – estimation of pion production uncertainties in context of the T2K experiment. Finally, Chapter 7 sheds some light on a relatively new and interesting detection technique – liquid argon TPC – and presents an analysis of identification of neutral pion background using such a detector. Chapter 8 summarizes the results.

The following analyses in this thesis were carried out by the author:

- Pion production uncertainty estimation for T2K experiment presented in Chapter 6,
- Multi-pion contribution estimation, presented in the same Chapter,
- Pion identification study in liquid argon TPC detector, a part of possible 2 km station of T2K (Chapter 7),
- Neutrino energy reconstruction and four-momentum transfer squared reconstruction studies presented in Chapter 5,
- SMRD detector optimization study, presented in Chapter 4, Section 3.
- Verification of FSI implementation in Nuance neutrino generator (Chapter 3, Section 2.3).

The pion production uncertainty estimation was a part of a broader study, and results of this study were published in Phys. Rev. D 80, 093001 (2009) (Ref. [G09] of this thesis). Partial results of this analysis were repeatedly presented on T2K collaboration meetings. Some of the Nuance FSI implementation discussion was published in Acta Phys. Pol. B 40, 2593 (2009). For a full list of publications, see below.

The author was also actively involved in technical work for T2K and ICARUS experiments. The list of performed tasks includes:

- taking part in Super-Kamiokande detector restoration in Mozumi, Japan (January – February, 2006). The author was a member of American group taking care of the outer detector,
- testing electronics (TFB boards, MPPC sensors, cables, etc) for T2K SMRD detector in J-PARC complex, Tokai, Japan (October – November, 2008),

- testing electronics for ICARUS experiment in LNGS laboratories, Assergi, Italy (February, 2007).

1.3 List of publications

- K. M. Graczyk, D. Kielczewska, P. Przewlocki, and J. T. Sobczyk, *C5A axial form factor from bubble chamber experiments,* Phys. Rev. D 80, 093001 (2009) (Ref. [G09]).
- A. Ankowski et al. [ICARUS Collaboration], *Energy Reconstruction of Electromagnetic Showers from π^0 Decays with the ICARUS T600 Liquid Argon TPC,* Acta Phys. Pol. B 41, 103 (2010).
- P. Przewlocki, *Running Nuance,* Acta Phys. Pol. B 40, 2513 (2009) (*proceedings of 45th Karpacz Winter School in Theoretical Physics, Lądek Zdrój, 2009*).
- P. Przewlocki, *Single Pion Production. Theoretical Dependencies and Experimental Limitations,* Acta Phys. Pol. B 40, 2593 (2009) (*proceedings of 45th Karpacz Winter Workshop in Theoretical Physics, Lądek Zdrój, 2009*).
- M. Antonello, V. Caracciolo, G. Christodoulou, J. Dobson, E. Frank, T. Golan, V. Lee, S. Mania, P. Przewlocki, B. Rossi, D. Stefan, R. Sulej, T. Szeglowski, R. Tacik, T. Wachala *Study of Pion Production in ν_μ CC Interactions on ^{16}O Using Different MC Generators,* Acta Phys. Pol. B 40, 2519 (2009).
- J. Lagoda, D. Kielczewska, M. Posiadala, R. Sulej, K. Zaremba, T. Kozlowski, K. Kurek, P. Mijakowski, P. Przewlocki, E. Rondio, J. Stepaniak, M. Szeptycka, *Polarization Effects in tau Production by Neutrino,* Acta Phys. Pol. B Vol. B (2007) 6, 2007.
- P. Przewlocki, *ICARUS - The Liquid Argon Detector for Neutrino Physics,* Acta Phys. Pol. B Vol. 37 No 4 1245-125 , 2006 (*proceedings of International Workshop on High Energy Photon Linear Colliders, Kazimierz nad Wisłą, 2005*).
- P. Przewlocki , *π^0 Identification Analysis for the LAr Detector in 2km Station of T2K Experiment* , Acta Phys. Pol. B Vol 37 No 8 2395-2402, 2006 (*proceedings of XX Max Born Symposium, Wrocław, 2005*).
- A. Ankowski et al. [ICARUS Collaboration], *Characterization of ETL 9357FLA photomultiplier tubes for cryogenic temperature applications* Nucl. Instr. Meth. A Vol. 556 No 1 146-157, 2006.

- A. Ankowski et al. [ICARUS Collaboration], *Measurement of Through-Going Particle Momentum by Means of Multiple Scattering with the ICARUS T600 TPC*, European Physical Journal C 48, 667-676, 2006.
- J. Jakubas-Przewłocka, P. Przewłocki, A. Sawicki, *Assesment of changes due to the long-term effect of estrogen and calcium defficiency in the trabecular bone structure in rats*, Clinical and Experimental Rheumatology 2005, Vol. 23., 385-388., 2005.
- J. Jakubas-Przewlocka, A. Sawicki, P. Przewlocki, *Assessment of trabecular bone structure in postmenopausal and senile osteoporosis in women by image analysis*, Scand J Rheumatol. 2003;32(5):295-9.

1.4 Talks and posters presented at international conferences and workshops

- P. Przewłocki, K.M. Graczyk, D. Kiełczewska**,** J.T. Sobczyk, *Pion production uncertainty in context of Tokai2Kamioka (T2K) experiment,* a poster presented at European Strategy for Future Neutrino Physics Workshop, CERN, Geneva, Switzerland, 2009.
- P. Przewlocki, *Running Nuance,* 45th Karpacz Winter School in Theoretical Physics, Lądek Zdrój, Poland, 2009.
- P. Przewlocki, *Single Pion Production. Theoretical Dependencies and Experimental Limitations,* 45th Karpacz Winter Workshop in Theoretical Physics, Lądek Zdrój, Poland, 2009.
- P. Przewlocki , π^0 *Identification Analysis for the LAr Detector in 2km Station of T2K Experiment* , XX Max Born Symposium, Wrocław, Poland, 2005.
- P. Przewlocki [for ICARUS Collaboration], *ICARUS - The Liquid Argon Detector for Neutrino Physics,* International Workshop on High Energy Photon Linear Colliders, Kazimierz nad Wisłą, Poland, 2005.

Chapter 2
Neutrino oscillations

Neutrinos are neutral and almost massless elementary particles. Their existence has been first postulated by Wolfgang Pauli in 1930, under the name of neutrons, to explain continuous energy spectrum of electrons produced in beta decay [G07]. Such spectrum suggested 3 particles in the final state instead of two (recoil nucleus and electron). The current name was coined by Enrico Fermi two years later.

Neutrinos interact with matter only weakly – this allows them to travel very long distance without any disturbances. A mean free path of neutrino in water is larger than a light year.

In the Standard Model neutrinos are massless (as until recently there was no convincing data suggesting existence of non-zero mass) and bound to two lepton number conservation rules:

- lepton number conservation, $\Delta L = 0$ – total number of leptons in any reaction has to be conserved,
- flavor lepton number conservation, $\Delta L_{e,\mu,\tau} = 0$ – number of leptons of a given flavor has to stay the same.

As a consequence of the latter, neutrinos are not allowed to change flavor. However, there exist now strong experimental evidence that prove otherwise, due to observation of what is interpreted as neutrino oscillations.

2.1 Description of the phenomenon

Neutrino oscillations are a quantum mechanical phenomenon, first proposed by Bruno Pontecorvo in the 1950s in analogy with kaon oscillations [P57]. Pontecorvo's original idea included sterile neutrinos, since by that time only electron neutrinos were known. In 1962 Maki, Nakagawa and Sakata considered for the first time a model with oscillation of different neutrino flavors (muon neutrino was discovered the same year) [M62]. The modern neutrino oscillation theory was developed in 1970s by many physicists, including Pontecorvo and Bilenky [B76] (see Ref. [G07] for more details).

Neutrino oscillations explain experimental results by allowing neutrino flavor transitions. It is assumed that physically interacting (and observable) flavor eigenstates, like ν_e or ν_μ are combinations of mass eigenstates (usually denoted as ν_1, ν_2, etc.). Mass eigenstates propagate through space with different velocities, as they have different masses. This causes the change (oscillation) of neutrino flavor. In practical terms this means that if we produce at some point in space a pure beam of neutrinos of one flavor, the beam will no longer be pure after traveling some distance – the other flavors will appear. If we are sensitive only to a certain flavor, we will be seeing a deficit – some of the neutrinos will be invisible, as they have changed their flavor. This change has periodical character – and that is why it's called oscillation.

The probability of flavor switch depends on the type of initial and final neutrino, their energy and the distance they have traveled. Determining these probabilities are one of the main goals of modern neutrino oscillation experiments.

2.2 Neutrino oscillation formalism

First, for the sake of simplicity, let us consider vacuum oscillation of neutrinos of just two flavors, named ν_e and ν_μ [P00]. In the oscillation formalism they are treated as linear combination of two mass eigenstates ν_1 and ν_2:

$$\begin{pmatrix} \nu_\mu \\ \nu_e \end{pmatrix} = \begin{pmatrix} \cos\vartheta & \sin\vartheta \\ -\sin\vartheta & \cos\vartheta \end{pmatrix} \begin{pmatrix} \nu_1 \\ \nu_2 \end{pmatrix}$$

where ϑ is a mixing angle. The wave functions:

$$\nu_\mu = \nu_1 \cos\vartheta + \nu_2 \sin\vartheta$$
$$\nu_e = -\nu_1 \sin\vartheta + \nu_2 \cos\vartheta$$

are then orthonormal states. The mass eigenstates propagate in space, which is given by ($\hbar = c = 1$):

$$\nu_1(t) = \nu_1(0) e^{-iE_1 t}$$
$$\nu_2(t) = \nu_2(0) e^{-iE_2 t}$$

The mass eigenstates will have a fixed momentum p, so taking into account relativistic relation between energy and momentum

$$E^2 = p^2 + m^2$$

and assuming small neutrino masses $m_i << E_i$, we get:

$$E_i = p + \frac{m_i^2}{2p} \quad (*)$$

Let's consider the situation in which we start (t =0) with a pure muon neutrino beam, i.e.:

$$v_\mu(0) = 1$$
$$v_e(0) = 0$$

Then:

$$v_2(0) = v_\mu(0)\sin\vartheta$$
$$v_1(0) = v_\mu(0)\cos\vartheta$$

We would like to see what happens after time *t*:

$$v_\mu(t) = \cos\vartheta\, v_1(t) + \sin\vartheta\, v_2(t)$$

We can now obtain the amplitude:

$$A_\mu = \frac{v_\mu(t)}{v_\mu(0)} = \cos^2\vartheta e^{-iE_1 t} + \sin^2\vartheta e^{-iE_2 t}$$

and intensity:

$$\frac{I_\mu(t)}{I_\mu(0)} = A_\mu A_\mu^* = 1 - \sin^2 2\vartheta \sin^2\frac{(E_2 - E_1)t}{2}$$

If we reformulate the argument of the second sinus, keeping $\hbar$ and c omitted before, using $\Delta m^2 = m_2^2 - m_1^2$, $t = L/c$, expression (*) and assume E=p we'll get:

$$\frac{(E_2 - E_1)t}{2} \Rightarrow \frac{\Delta m^2 c^4}{4\hbar c}\frac{L}{E}$$

Expressing L (the distance traveled) in meters, $\Delta m^2 c^4$ in (eV)^2 and E in MeV enables us to find the familar expression:

$$\frac{\Delta m^2 c^4}{4\hbar c}\frac{L}{E} \Rightarrow \left(\frac{\Delta m^2 c^4}{4\cdot 197\, eV\cdot nm}\frac{L}{E}\right)\left(\frac{10^{-6}\, MeV/eV}{10^{-9}\, m/nm}\right) \Rightarrow 1.27\frac{\Delta m^2\left[eV^2\right]L[m]}{E[MeV]}$$

so the final expression for oscillation probability is:

$$P(\nu_\mu \to \nu_\mu) = 1 - \sin^2 2\vartheta \sin^2\left(\frac{1.27\,\Delta m^2 L}{E}\right)$$
$$P(\nu_\mu \to \nu_e) = 1 - P(\nu_\mu \to \nu_\mu)$$

In the above formulae two parameters are associated with a specific situation (oscillation distance and neutrino energy) and other two are global parameters governing the whole

oscillation process. These parameters, ϑ and $\Delta m^2 = m_2^2 - m_1^2$ are called oscillation parameters, where ϑ controls the strength of oscillations, Δm^2 - its periodicity.

In the three neutrino case, the situation is more complicated. The mixing is described by 3x3 unitary matrix , called Maki-Nakagawa-Sakata (MNS) matrix:

$$U = \begin{pmatrix} c_{13}c_{12} & c_{13}s_{12} & s_{13}e^{-i\delta} \\ -c_{23}s_{12} - s_{13}c_{12}s_{23}e^{+i\delta} & c_{23}c_{12} - s_{13}s_{12}s_{23}e^{+i\delta} & c_{13}s_{23} \\ s_{23}s_{12} - s_{13}c_{12}c_{23}e^{+i\delta} & -s_{23}c_{12} - s_{13}s_{12}c_{23}e^{+i\delta} & c_{13}c_{23} \end{pmatrix} \times \begin{pmatrix} 1 & & \\ & e^{i\alpha} & \\ & & e^{i\beta} \end{pmatrix}$$

where $c_{ij}=\cos\theta_{ij}$ and $s_{ij}=\sin\theta_{ij}$, δ is Dirac phase and α, β are Majorana phases. These phases are non-zero if CP violation occurs. If neutrinos are Dirac particles then Majorana phases vanish and we can disregard the matrix on the right hand side of the formula. We will make this assumption from now on, as Majorana phases do not affect neutrino oscillation process.
The MNS can be split into three factors describing rotations around three orthogonal axes:

$$U = \begin{pmatrix} 1 & & \\ & c_{23} & s_{23} \\ & -s_{23} & c_{23} \end{pmatrix} \begin{pmatrix} c_{13} & & s_{13}e^{-i\delta} \\ & 1 & \\ -s_{13}e^{i\delta} & & c_{13} \end{pmatrix} \begin{pmatrix} c_{12} & s_{12} & \\ -s_{12} & c_{12} & \\ & & 1 \end{pmatrix}$$

The probability of oscillations is given by the formula [A08]:

$$P(\nu_\alpha \to \nu_\beta) = \delta_{\alpha\beta} - 4\sum_{i>j} \mathrm{Re}\left(U^*_{\alpha i}U_{\beta i}U_{\alpha j}U^*_{\beta j}\right)\sin^2\Phi_{ij} + k\cdot 2\sum_{i>j} \mathrm{Im}\left(U^*_{\alpha i}U_{\beta i}U_{\alpha j}U^*_{\beta j}\right)\sin 2\Phi_{ij}$$

Here α, β are physically observable neutrino flavor states, e.g. e, μ, and

$$\Phi_{ij} = \Delta m^2_{ij} L \Big/ 4E_\nu = 1.27\Delta m^2_{ij}[eV^2]\frac{L[km]}{E_\nu[GeV]}$$

The third term provides CP violation, k=1 for neutrinos and –1 for antineutrinos. The oscillation parameters are now the following: three mass differences squared Δm^2_{12}, Δm^2_{13}, Δm^2_{23}, three mixing angles θ_{12}, θ_{13}, θ_{23}, and one CP violation phase (in Dirac case) δ. It's easy to notice that $\Delta m^2_{12} + \Delta m^2_{13} + \Delta m^2_{23} = 0$, meaning that we have 6 independent parameters (5 if CP is not violated).

The current best-fit values or limits on oscillation parameters obtained by the experiments described later in this chapter are summarized below [S08]:

$$\sin^2 \vartheta_{12} = 0.318^{+0.23}_{-0.18}$$
$$\sin^2 \vartheta_{23} = 0.50^{+0.12}_{-0.11}$$
$$\sin^2 \vartheta_{13} = 0.013^{+0.013}_{-0.009} \quad (\sin^2 \vartheta_{13} \le 0.034, CL = 90\%)$$
$$0 \le \delta \le 2\pi$$
$$\left|\Delta m^2_{31}\right| = (2.40^{+0.12}_{-0.11}) \times 10^{-3} eV^2$$
$$\Delta m^2_{21} = (7.59^{+0.23}_{-0.18}) \times 10^{-5} eV^2$$

Due to small value of θ_{13} the oscillations associated with Δm^2_{12} and Δm^2_{23} are almost decoupled and can be in a first approximation studied separately, as two flavor transitions. Δm^2_{12} is related to solar neutrino and long baseline reactor experiments (large L/E, dominant $\nu_e \to \nu_\mu, \nu_\tau$ transition – *solar sector*) and Δm^2_{23} to atmospheric neutrino and long baseline accelerator neutrino experiments (small L/E, dominant $\nu_\mu \to \nu_\tau$ transition – *atmospheric sector*).

For a long baseline experiment like T2K (and the whole atmospheric sector) we can neglect the contribution from Δm^2_{12} terms and the oscillation probabilities can be expressed in a simplified manner:

$$P(\nu_\mu \to \nu_e) = \sin^2 2\vartheta_{13} \sin^2 \vartheta_{23} \sin^2 \Phi_{23}$$
$$P(\nu_\mu \to \nu_\mu) = 1 - \sin^2 2\vartheta_{23} \cos^4 \vartheta_{13} \sin^2 \Phi_{23} - P(\nu_\mu \to \nu_e)$$
$$P(\nu_e \to \nu_\tau) = \sin^2 2\vartheta_{13} \cos^2 \vartheta_{23} \sin^2 \Phi_{23}$$
$$P(\nu_e \to \nu_e) = 1 - \sin^2 2\vartheta_{13} \sin^2 \Phi_{23}$$

Note that since θ_{13} is small, $\nu_\mu \to \nu_\tau$ transition dominates in this sector, and oscillation to electron neutrinos is subdominant (it may even not exist at all – θ_{13} may be as well equal to zero). The smallness of θ_{13} means also that in a first approximation the above formulae reduce to 2 flavor ones and "atmospheric" experiments can directly measure θ_{23} by studying $\nu_\mu \to \nu_\mu$ transition.

Using similar tricks one can also obtain oscillation probability for solar sector:

$$P(\nu_e \to \nu_{\mu\tau}) = \cos^2 \vartheta_{13} \sin^2 2\vartheta_{12} \sin^2 \Phi_{12} + 0.5 \sin^2 2\vartheta_{13}$$

Again, this reduces to a 2 flavor expression when small θ_{13} is assumed.

When oscillations happen in matter (and not in vacuum, as was assumed before) interactions of neutrinos with electrons in matter (elastic scattering) can lead to enhancement or

suppression of oscillations. This is called MSW (Mikhaev-Smirnov-Wolfenstein) effect. Widely accepted interpretation of solar neutrino experiments involve MSW oscillation enhancement as an explanation of observed electron neutrino deficit. It is worth to note that this effect is important only as long as electron neutrinos are involved (and is negligible for other flavors).

2.3 History and methods of measurement

Neutrinos are produced in many ways in nature, including:

- scattering of primary cosmic rays in Earth's atmosphere (atmospheric neutrinos)
- nuclear reactions in Sun's core (solar neutrinos)
- during a supernova collapse (supernova neutrinos).

They are also produced artificially, either on purpose, to measure their properties (neutrino beams in neutrino experiments) or as a byproduct in nuclear reactors (reactor neutrinos).

First hints suggesting the existence of oscillation phenomenon came from experiments measuring solar neutrinos. The Sun's core emits neutrinos in series of thermonuclear interactions, with the following dominating the total flux [P00]:

$$p + p \rightarrow d + e^{+} + \nu_e + 0.42MeV$$

This reaction is a first one in the pp chain (Fig. 1), one of two reaction chains in which solar neutrinos are produced. The other is the CNO chain (Fig. 2). These (and other) information has been combined into what is called Standard Solar Model (SSM) – a model able to predict solar neutrino fluxes on Earth (and many other observables related to solar activity). The most reliable model of this type, created in 1962 and improved from then on, is a result of work of John Bahcall and collaborators (see Ref. [B01]). The predicted fluxes are shown in Fig. 3. As can be seen, only electron neutrinos are produced in the Sun and their energy range up to 18 MeV. The dominating pp component however have energy of the order of 0.5 MeV and less. The solar neutrino flux on the Earth is about $6*10^{10}$ $cm^{-2}s^{-1}$ [G07].

Different parts of the spectrum have been studied by various neutrino experiments. The first experiment to observe solar neutrinos was the Homestake experiment in 1968, and it has monitored the solar neutrino flux for the next 24 years [C98]. It was a radiochemical experiment which detected neutrinos via inverse beta decay:

$$\nu_e + {}^{37}Cl \rightarrow {}^{37}Ar + e^{-}$$

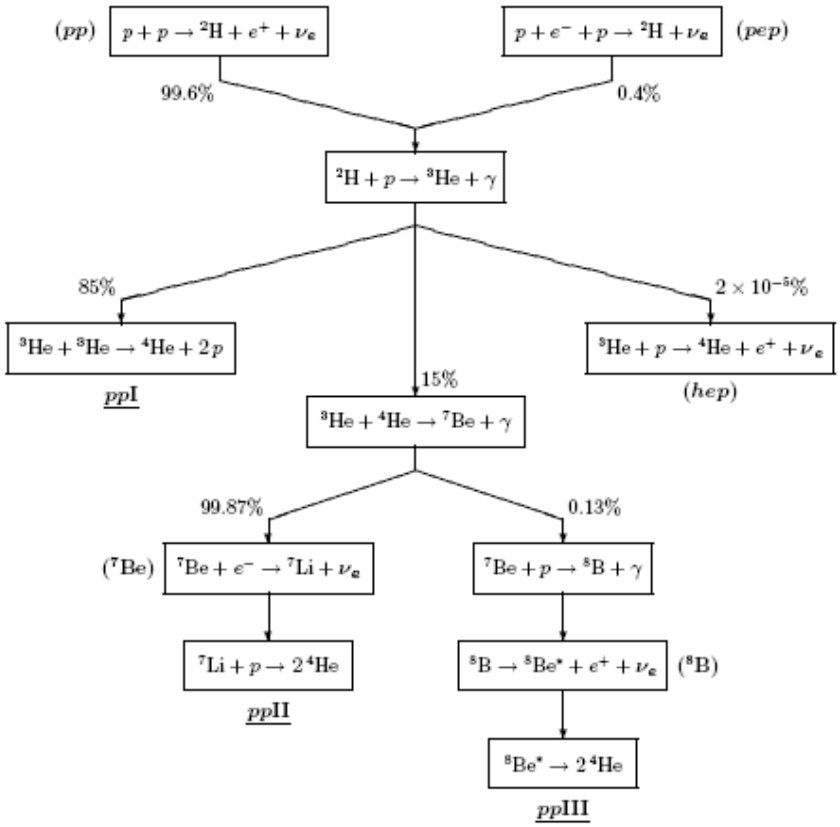

Fig. 1. Thermonuclear *pp* chain in the Sun's core. The traditional names of neutrino-producing reactions are given in parentheses. Corresponding relative neutrino fluxes are also indicated. The underlined labels indicate three main branches of the pp chain (from [G07]).

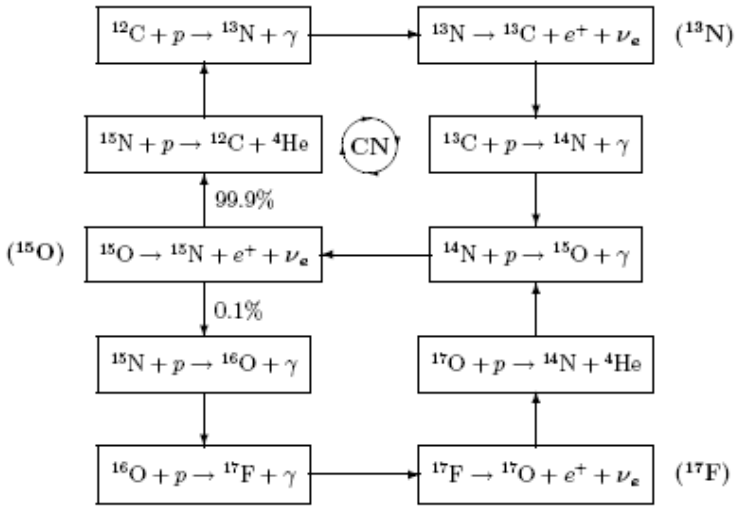

Fig. 2. CNO cycle in the Sun's core. The traditional names of neutrino-producing reactions and the corresponding neutrino fluxes are given in parentheses (from [G07]).

The energy threshold for the neutrino in this reaction is 0.8MeV, so experiment of this kind cannot see pp neutrinos. The reactions were taking place in a steel tank filled with tetrachloroethylene (C_2Cl_4, a washing liquid) located in an underground laboratory in Homestake in South Dakota, USA. Having the detector underground is important in most neutrino experiments – this gives a natural shielding of rocks that minimizes the number of secondary cosmic rays' interactions which otherwise would outnumber and dominate neutrino interactions one wants to spot.

About every two months the process of *extraction* was taking place: radioactive argon produced in neutrino interaction was pulled out from the tank through chemical methods and the argon atoms were counted using proportional counters. The results of the experiment were surprising: the number of recorded neutrino interactions was well below the rate expected by the SSM (about one third) with the discrepancy of more than 3σ. This was called a *solar*

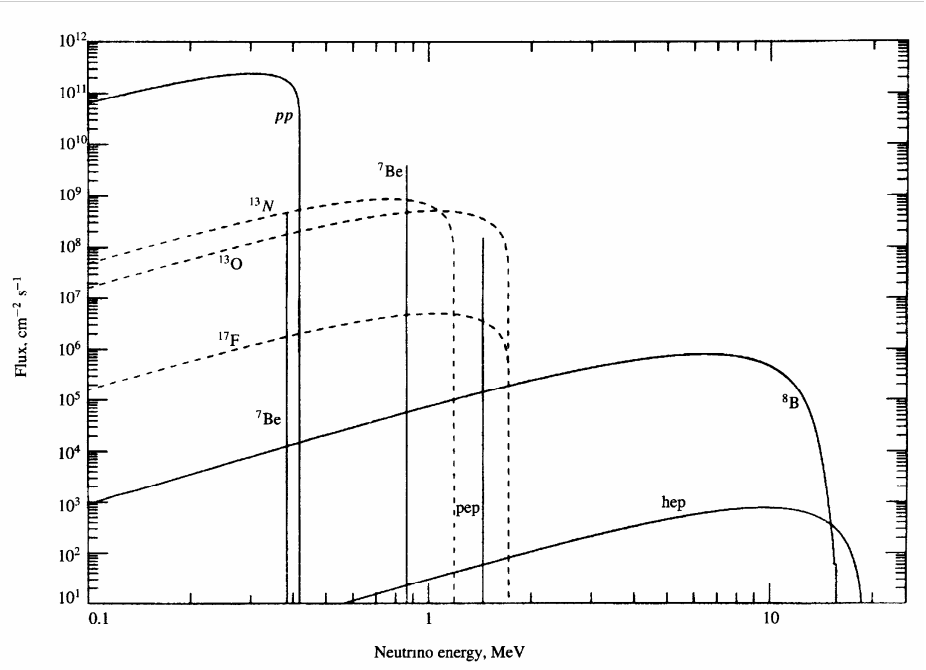

Fig. 3. Solar neutrino flux from different reactions at the Earth's surface (from [P00]).

neutrino problem, and it haunted neutrino physicists for the next 30 years, as all other solar experiments were also reporting a ν deficit.

SAGE [A98] and GALLEX [H99], two radiochemical experiments using gallium as a detector medium also observed neutrino event rate lower than expected. The threshold here was about 0.2 MeV, significantly lower than in the chlorine case. Finally, the Kamiokande and the Super-Kamiokande detectors [F96], using totally different observation technique,

have measured solar neutrino flux in the higher energy region. These detectors, both located in Kamioka mine in Japan, relied on Cherenkov effect to detect particles produced in neutrino interactions. When a relativistic charged particle propagates in some medium with velocity greater than the speed of light in this medium, the light is emitted in the cone around the direction of motion of the particle. If we detect this light (using photomultipliers installed on the walls of the detector), we can determine not only the energy of the particle (for particles that stop inside the detector) but also its direction (in real time – periodic extractions are not necessary). The detectors mentioned above utilize water as a detector medium. When a solar neutrino enters the water tank, it can interact via elastic scattering:

$$\nu_e + e^- \rightarrow \nu_e + e^-$$

and the recoil electron can be detected in the way described above. Its direction is highly correlated with the direction of incident neutrino – this way the Super-Kamiokande detector was able to produce the image of the Sun as seen from the Earth in neutrinos (analogously to the usual image we see in photons). One of the drawbacks of this method is however its high neutrino energy threshold – Kamiokande started with 9 MeV of neutrino energy to finally achieve 5 MeV (and recently even 4 MeV) in Super-Kamiokande case.

More information on Super-Kamiokande detector will follow in the next chapter, as it is one of the main elements of the T2K experiment.

The water Cherenkov experiments also observed massive deficit in number of detected solar neutrinos. This was accompanied by a directional plot showing that detected neutrinos were really coming from the Sun's direction.

The summary of all the results mentioned above are shown in Table 1. One can again see that all the experiments observe that the flux is smaller than expected by the SSM, and that the extent to which those observations differ from the theoretical predictions vary.

Experiment	Threshold	Observed/expected rate
Homestake	0.8 MeV	0.27±0.04
SAGE	0.2 MeV	0.56±0.07
GALLEX	0.2 MeV	0.53±0.08
(Super-)Kamiokande	5 MeV	0.39±0.06

Table 1. Solar neutrino experiments' results [P00]. Rate expectations are based on SSM predictions.

The possible explanations of these measurements included shortcomings of the SSM models or something that might have been happening to neutrinos on their way to the Earth, most probably oscillation phenomenon (favored by the data, from Super-Kamiokande in particular). The final resolution to this mystery was offered by the SNO collaboration. The Sudbury Neutrino Observatory (SNO) is an underground water Cherenkov experiment located in Creighton mine, Ontario, Canada [AH03]. It differs from Kamiokande experiments by the medium it uses – heavy water instead of normal. One kT of the medium is contained in a spherical acrylic vessel surrounded by photomultiplier tubes. The experiment sees solar neutrinos via three reactions:

$$CC: \nu_e + d \rightarrow p + p + e^-$$
$$NC: \nu_x + d \rightarrow p + n + \nu_x$$
$$ES: \nu_x + e^- \rightarrow \nu_x + e^-$$

where $x = e, \mu, \tau$. The first one (charged current exchange) is sensitive to electron neutrinos only (to produce a muon on the right-hand side of the equation, one would have to have neutrino of energies way too high for solar neutrinos). Other two channels – NC (neutral current exchange) and ES (elastic scattering on electrons) are available for all types of neutrinos. Each channel has different neutrino threshold energy, which makes them sensitive to different neutrino spectra. The elastic scattering (ES) of electrons by neutrinos is highly directional, and establishes the sun as the source of the detected neutrinos. The charged-current (CC) absorption of ν_e on deuterons produces an electron with an energy highly correlated with that of the neutrino. This reaction is sensitive to the energy spectrum of ν_e and hence to deviations from the parent spectrum. The neutral-current (NC) disintegration of the deuteron by neutrinos is independent of neutrino flavor and has a threshold of 2.2 MeV. To be detected, the resulting neutron must be absorbed, giving a 6.25 MeV photon for absorption on deuterium or photons totalling 8.6 MeV for absorption on ^{35}Cl with salt added to the D_2O (Phase 2 of the experiment, see below). The ability to measure the CC and NC reactions separately is unique to SNO and makes the interpretation of the results of the experiment independent of theoretical astrophysics calculations.

SNO started operating with pure heavy water (Phase 1). Then, the D_2O was doped with salt (Phase 2) to improve neutron detection capabilities. Finally, many proportional counter tubes have been placed inside the detector for efficient capturing of thermal neutrons resulting from NC process (Phase 3). The results from the first D_2O phase confirmed the deficit of solar electron neutrinos observed previously. Combination of results from the 3 channels showed

that about two electron solar neutrinos out of three change their flavor to ν_μ or ν_τ on their way to the Earth. These results have been confirmed by two later phases. The final plot showing the results is presented in Fig. 4. The results are the following [AH05]:

$$\Phi_{CC} = 1.68 \pm 0.06^{+0.08}_{-0.09} \times 10^6 \, cm^{-2} s^{-1}$$
$$\Phi_{NC} = 4.94 \pm 0.21^{+0.38}_{-0.34} \times 10^6 \, cm^{-2} s^{-1}$$
$$\Phi_{ES} = 2.35 \pm 0.22 \pm 0.15 \times 10^6 \, cm^{-2} s^{-1}$$

When compared with SSM, it appeared that Φ_{NC} agreed with expectations while Φ_{CC} and Φ_{ES} were significantly smaller than expected. This indicated the deficit in electron neutrino flux. This deficit is interpreted as a result of MSW-enhanced oscillation inside the Sun.

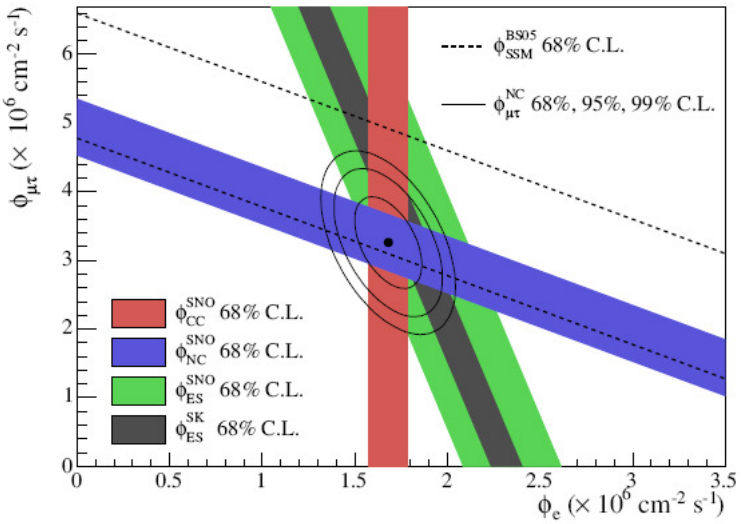

Fig. 4. SNO results after Phase 2. Three reactions give different contributions to electron neutrino flux (horizontal axis) and flux of neutrinos of other flavors (vertical axis). Black dot indicates the best fit point (from [AH05]).

KamLAND [E02] was another experiment built in the Kamioka mine, for studying low-energy electron antineutrinos coming from nuclear reactors in the region, i.e. from all nuclear power plants in Japan and some in Korea. The neutrinos have energy of the order of a few MeV, very similar to energies of solar neutrinos. Special detector – a spherical plastic balloon filled with oil mixed with scintillator and surrounded by photomultiplier tubes - was devised to detect neutrinos of such a low energy. Effective background rejection allowed the threshold for observing a neutrino to reach 1.8 MeV in the last phase of the experiment. Neutrinos were detected via inverse beta decay process:

$$\bar{\nu}_e + p \rightarrow e^+ + n$$

Electron antineutrinos were detected through the coincidence signature of positron annihilation followed by neutron capture on protons. The scintillation light from the prompt electron annihilation gave an estimate on neutrino energy.
KamLand studied electron antineutrino disappearance. It was the first experiment to observe reactor neutrino oscillation (by seeing a significant deficit in measured flux). It also provided the most precise constraint on Δm^2 in the solar sector up to now.

Other evidence suggesting oscillation were atmospheric neutrino observations. These neutrinos are produced in the high layers of Earth's atmosphere as a result of cosmic rays' interactions [G07]. The rays (mainly protons) are coming from outer space. When they collide with nuclei of atmosphere's gasses, mesons (mainly pions) are produced (see Fig. 5). These decay into muons:

$$\pi^+ \rightarrow \mu^+ + \nu_\mu$$
$$\mu^+ \rightarrow e^+ + \bar{\nu}_\mu + \nu_e$$
$$\pi^- \rightarrow \mu^- + \bar{\nu}_\mu$$
$$\mu^- \rightarrow e^- + \nu_\mu + \bar{\nu}_e$$

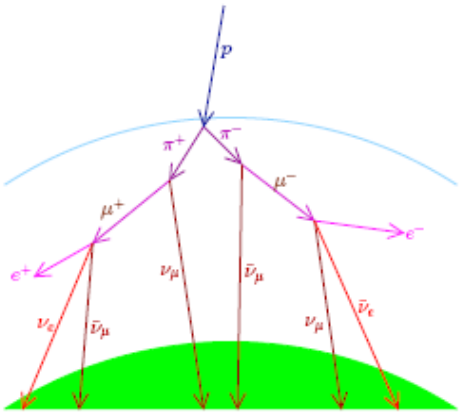

Fig. 5. Schematic view of neutrinos' creation in the atmosphere (from [G07]).

Energies of neutrinos produced in such a way range up to the order of TeV. If we assume that only pions are produced and all pions and muons decay before reaching Earth's surface, we can expect two muon neutrinos per one electron neutrino (an exact calculation gives a ratio of 2.1:1 [P00]). However, several experiments, starting in 1960s, reported lower fluxes of muon neutrinos than expected. These included Kamiokande and IMB water Cherenkov experiments. Other experiments based on fine-grained iron tracking detectors (NUSEX, Frejus) did not

measure anything suspicious, nevertheless the observed deficits prompted some people to call the problem the *atmospheric neutrino anomaly*. The anomaly could be finally confirmed and convincingly explained when the Super-Kamiokande collaboration published their data in 1998 [F98]. The Super-Kamiokande detector, as previously mentioned, is capable of measuring and determining the direction of solar neutrinos. The same is true for atmospheric neutrinos, however this time neutrinos scatter off nucleons rather than electrons (because they have higher energy than solar neutrinos; more on these interactions in the next chapters). This gives a unique possibility to measure the rate of neutrinos as a function of zenith angle (the angle between direction of a neutrino and the axis perpendicular to the Earth's surface).

Neutrinos coming from above have only about 15 km to travel from their creation point; however, those which come from below the detector have to cross the whole Earth, too. If a dependence of certain type on the zenith angle is observed, this could be a strong argument in favor of oscillation. Indeed, Super-Kamiokande data are best reproduced by a Monte Carlo taking into account oscillation effects (Fig. 6). The oscillations has been identified as a $\nu_\mu \to \nu_\tau$ transition (other hypotheses - $\nu_\mu \to \nu_e$ or a transition to sterile neutrinos - were strongly disfavored by the data). The result can be shown in a concise way as a value of up-

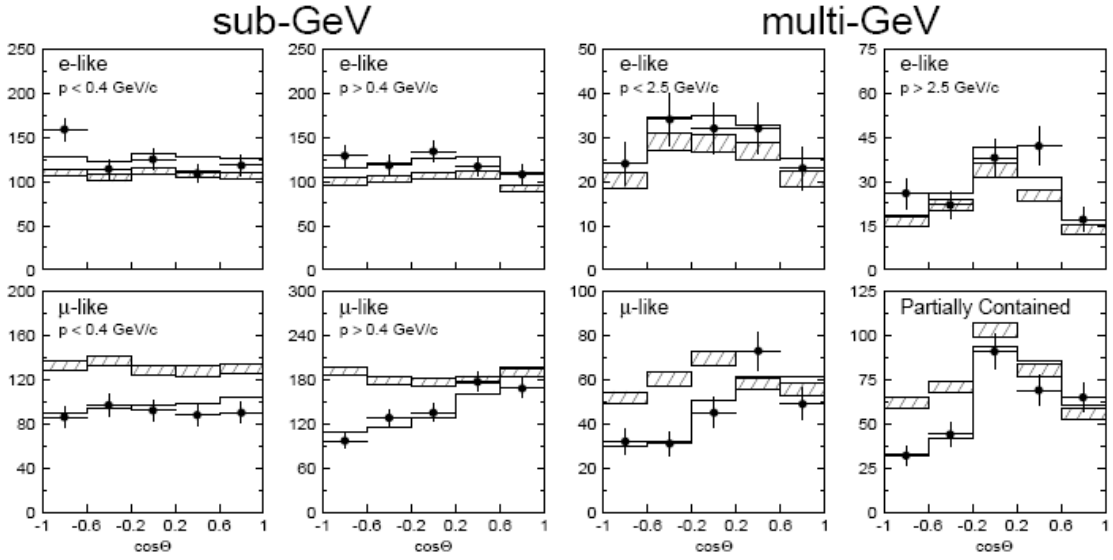

Fig. 6. Super-Kamiokande atmospheric results divided into two energy bins: sub-GeV (below 1.3GeV of visible energy) and multi-GeV (above 1.3GeV). Points with error bars are data, hatched boxes – Monte Carlo without oscillations, solid line – Monte Carlo with best-fitted oscillation effects. Regardless of the type of event considered (explanations in the next chapters) a clear oscillation pattern is visible. Picture taken from Ref. [F08].

down asymmetry [F98]:

$$A_{\mu}^{up-down} = -0.296 \pm 0.048 \pm 0.01$$
$$A_{e}^{up-down} = -0.036 \pm 0.067 \pm 0.02$$

This was considered as a 6σ model-independent evidence that part of the upward-going atmospheric muon neutrino flux disappears (the asymmetry for electron neutrinos is consistent with 0). Many other measurements done later by the Super-Kamiokande collaboration support these findings, among these a ratio of the data to Monte Carlo as a function of L/E (oscillation length divided by neutrino energy) [A04].

These results have been confirmed and made more precise by the first long baseline neutrino experiment with an artificial beam of muon neutrinos – K2K (KEK to Kamioka) [A01]. In this experiment the Super-Kamiokande detector was used as a far detector of the experiment – it was measuring neutrinos produced in KEK laboratory 290 km away. The near detectors (located in KEK near the production point) were measuring unoscillated flux; the far detector was aimed at detecting the oscillation effects. The L/E ratio for the experiment was chosen to be similar to the ratio for atmospheric experiments. K2K results confirm that $\nu_{\mu} \rightarrow \nu_{\tau}$ is the dominating transition. In the same time no evidence for existence of subdominant $\nu_{\mu} \rightarrow \nu_{e}$ channel was found (only the upper limit was set).

The similar experiment, but using steel-scintillator tracking calorimeter detectors – MINOS - is currently operating in the United States [M06]. The beam is produced at Fermilab and the neutrinos travel 735 km to reach far detector located in Soudan Mine, Minnesota. The experiment confirmed earlier results and keeps taking data to impose more stringent limits on oscillation parameters in atmospheric sector.

The long-baseline experiments mentioned above set limits on θ_{13} by looking at $\nu_{\mu} \rightarrow \nu_{e}$ transition (and not finding it). However, the best constraint was set by the reactor experiment operating at short baseline, thus being sensitive to atmospheric range of Δm^2 rather than solar. It was called Chooz and was located in the close vicinity of a nuclear power plant of the same name in France [AP03]. A scintillator detector was placed underground, 1 km from the reactor core. Like in similar Palo Verde reactor experiment in USA [BO01], no oscillations were observed. The search will be continued by Double-Chooz experiment in the same place [AR04].

We may add here that there also existed an experiment, which found an indication of oscillations in the region of $\Delta m^2/\theta$ different than those two just mentioned. It was called LSND and measured antineutrinos from predominantly muon antineutrino beam using scintillator detector. It has observed electron antineutrino appearance effect [AG01]. However, a recent experiment looking for oscillation in the same parameter region, called MiniBoone, did not observe any oscillation effects, either in neutrinos or antineutrinos, which exclude the LSND interpretation at the 98% confidence level [K09]. However, if LSND results turned out to be valid, it would mean that oscillation exists into some new kind of neutrino, possibly sterile one (directly undetectable), for three independent mass differences result in four

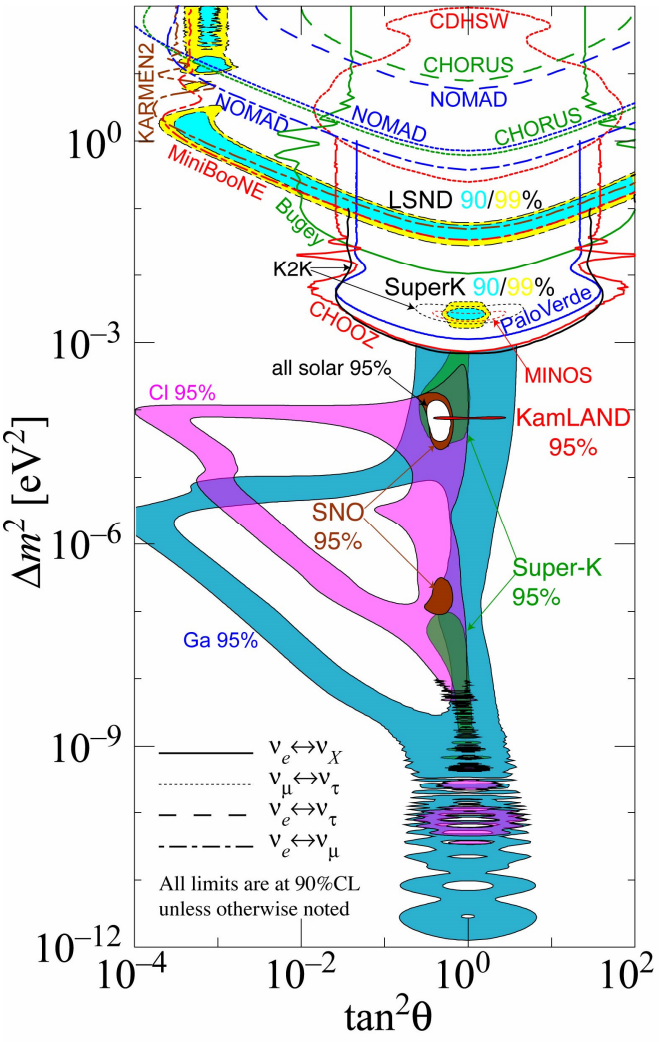

Fig. 7. Limits on oscillation parameters inferred from experimental data. One can see the allowed region for atmospheric sector (upper-middle part, conjunction of Super-Kamiokande, K2K and Minos allowed regions) and for solar sector (middle part, SNO and KamLand). LSND and MiniBoone results in the upper part of the plot. (from [A08])

different mass states.

Summarizing our present knowledge we can state, that [B04]:

- The solar electron neutrinos are transferred into muon and tau neutrinos inside the sun,
- In the KamLand range of L/E $\bar{\nu}_e \rightarrow \bar{\nu}_\mu, \bar{\nu}_\tau$ oscillations have been detected,
- In the atmospheric sector no $\nu_e \rightarrow \nu_\mu, \nu_\tau$ oscillation has been detected, just pure $\nu_\mu \rightarrow \nu_\tau$ transition,

All the results (along with results from experiments not discussed in this chapter) in the form of allowed regions in oscillation parameter space are presented in Fig. 7.

2.4 Main physical objectives of T2K experiment

The first stage of the Tokai2Kamioka (T2K) experiment is aimed at [H03]:

- discovering $\nu_\mu \rightarrow \nu_e$ transition, never observed before. This would allow us to determine that ϑ_{13} is larger than zero. The T2K experiment has the capability to estimate ϑ_{13} with a sensitivity better than 10 times larger over the present upper limit in 5 years of operation (see Fig. 8). Experimentally it boils down (simplifying a little) to observing electron neutrinos in the far detector, as the beam is composed of muon neutrinos (electron neutrino *appearance*).
- precise measurement of oscillation parameters in atmospheric region, i.e. ϑ_{23}, Δm_{23}. These parameters are known from previous experiments – the T2K goal is to reach the precision of 1% for $\sin^2 2\vartheta_{23}$ and 10^{-4} eV^2 for Δm^2_{23}. This is done by observing muon neutrino *dissapearance* in the beam.
- searching for sterile neutrinos in muon neutrino disappearance measurement by detecting the neutral current events.

For both measurements, main uncertainties will come from neutrino beam energy spectrum, cross-section and background measurement. These quantities will be measured before oscillation by a near detector and extrapolated at the far detector.

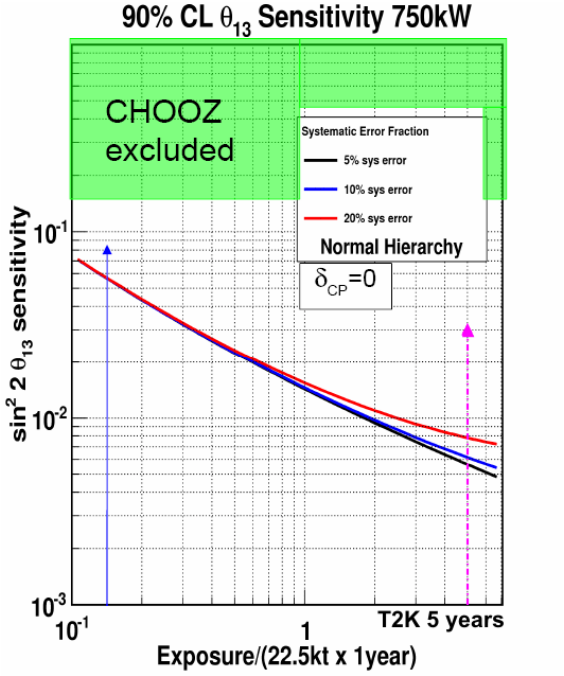

Fig. 8. Reaching the projected θ_{13} sensitivity through 5 years (violet arrow) of running of T2K experiment (from [KA09]).

The above measurements will be described in more detail in next chapters. Experimental signatures of electron neutrino appearance and muon neutrino disappearance are discussed in Chapter 3 (see Figs. 12 and 13).

Should the first stage of the experiment succeed, a second is envisaged, with a more powerful beam and a larger far detector. Such a setup will be capable of discovering CP violation in the lepton sector and an order of magnitude improvement in $\nu_\mu \rightarrow \nu_e$ sensitivity.

Chapter 3
Neutrino interactions

3.1 Physical processes

3.1.1 Neutrino interactions in matter

Neutrino interactions are described by the Standard Model. According to it, neutrinos interact only weakly with other particles. This means that interactions are very rare - typical cross-sections for neutrino interactions are 6 orders of magnitude smaller than for electromagnetic interactions.

Weak interactions take place between all quarks and leptons. $W^{\pm}$, Z^0 mediating bosons are interchanged in the course of reaction. Depending on the boson being exchanged, two types of interactions can be distinguished (see Fig. 9):

- charged current exchange (CC interactions) – when $W^{\pm}$ takes part in the reaction, and
- neutral current exchange (NC interactions) – when Z^0 takes part in the reaction.

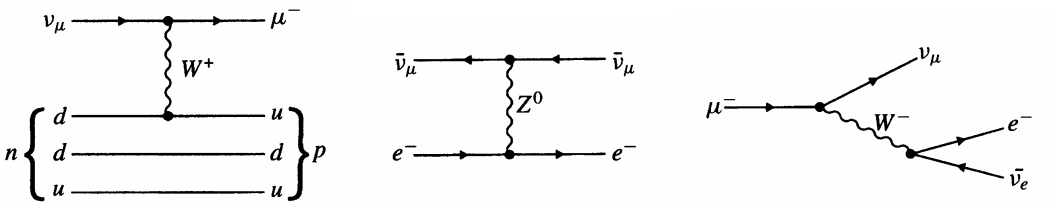

Fig. 9. Examples of neutrino involving interactions. From left to right: a) neutrino CC interaction with a nucleon's quark, b) neutrino NC interaction with an electron, c) muon decay.

For muon neutrino cross-sections on nucleons the following can be inferred from the data [P00] (cross-section on electrons are 3 orders of magnitude smaller and can usually be neglected):

- cross-section is proportional to energy of the neutrino for sufficiently large energies (in other words a value of σ/E_ν as a function of E_ν is constant),

- ratio of antineutrino to neutrino cross-section is approximately 0.5 (neutrino interactions are two times more frequent).

3.1.2 Significant processes regarding physical objectives of T2K experiment

In T2K energy range (neutrino energies around 1 GeV) the only processes that count are the ones similar to what is shown in Fig 9a, i.e. neutrino scattering off nuclei of detector medium. The media that have to be taken into account in the context of T2K are:

- for the far detector – water (hydrogen and oxygen)
- for the near detector – polystyrene (hydrogen and carbon) and water
- for the LAr TPC detector in a possible intermediate station – argon.

More details on detectors and detector materials are given in the next chapter.

Neutrino interactions with nuclei produce observable particles like charged leptons and hadrons, mainly pions. This depends on energy of the incoming neutrino and other factors. Several formalisms have been developed to describe these interactions, those important are listed below (see [W09] for more details).

Neutrino elastic NC scattering (NCE) is the simplest process, but in water Cherenkov detectors these interactions are usually undetectable (outgoing protons don't have a sufficient amount of momentum to be visible and neutrons are undetectable):

$$\nu + N \rightarrow \nu + N$$

where N is a nucleon. No energy threshold for neutrino exists for this reaction.

Quasi-elastic CC scattering (CCQE) is the most important and dominant channel for T2K energies. It is the easiest to reconstruct and for that reason is used in majority of measurements, like beam spectrum determination, cross section estimations and as a signal in oscillation measurements (see later in this chapter). It is a two-body neutrino reaction with a nucleon with production of a charged lepton:

$$\nu + N \rightarrow l + N'$$

where N is a nucleon and l is a lepton of the same flavor as the neutrino. Incoming neutrino energy in this reaction can be inferred from the sole properties of the measured outgoing lepton (its momentum and deviation from original neutrino flight direction). This process is usually calculated using Llewellyn Smith model [LS72] which parameterizes the cross section in terms of several form factors dependent on Q^2, the square of the four-momentum transferred to the nuclear system.

Neutrino scattering off nucleons with production of resonances (resonant production, RES) is a channel in which an intermediate particle – an excited baryon resonance – is produced. This resonance then decays into nucleon and one or more mesons:

$$NC: \nu + N \rightarrow \nu + r^* \rightarrow \nu + N' + meson(s)$$
$$CC: \nu + N \rightarrow l + r^* \rightarrow l + N' + meson(s)$$

where N is a nucleon, l a lepton and r^* is a resonance. This process is important for neutrino energies from around 1 to a few GeV . The most prominent resonance is Δ(1232), but a number of others can also contribute. Mesons are usually pions, charged or neutral; sometimes also kaons, rho mesons and other rare products. The most abundant class of resonant production events in T2K energy range is *single π production* with only one meson in the final state: a pion. Usually the resonant production is described by Rein-Sehgal model [R81], which incorporates several resonances up to hadronic invariant mass of 2 GeV/c^2. It describes all neutrino and antineutrino pion production processes in one uniform framework. Other approaches are also possible, including consideration of only Δ(1232) if the energy is sufficiently low and contribution from higher resonances is negligible – this is the case of Rarita-Schwinger formalism for the Δ(1232) excitation (see e.g. Ref. [G09]) used in NuWro generator [J05]. These models are also parameterized by form factors similar to the ones used in CCQE considerations. To fit the data, a non-resonant background have to be taken into account for some pion production channels.

Coherent scattering off whole nuclei (COH) is a situation in which neutrino interacts with a target nucleus as a whole leaving the nucleus in the initial ground state. It is associated with negligible energy transfer to the nucleus. This usually results in production of a forward-going lepton and a meson (most probably pion). Rein-Sehgal calculations [R83, R07] are a commonly used theoretical approach for cross-section calculation for this channel. From experimental point of view, coherent reactions are different from resonant single meson production for no nucleon is being "kicked out" of the nucleus. Another feature is that produced mesons are statistically less deviated from the direction of incident neutrino.

Both resonant and coherent processes are important as they are a source of pions, that constitute one of the main backgrounds to oscillation signal in water Cherenkov detectors.

Deep inelastic scattering (DIS) interactions are characteristic for neutrino energies of the order of several GeV and higher. For such high energies it is convenient to describe the interaction as a reaction between neutrino and partons (quarks and gluons) inside nucleons.

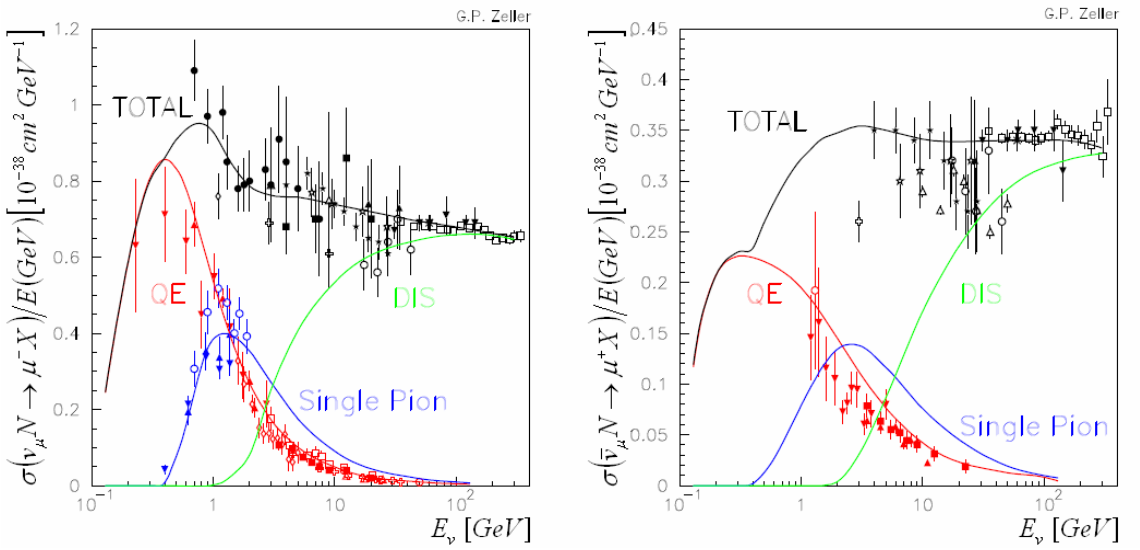

Fig 10. Cross-sections for ν_μ interaction on an average nucleon (p or n) split into different processes as a function of neutrino energy in GeV, left – neutrino interactions, right – antineutrino interactions (from [Z08]). These data come from old, mostly bubble-chamber experiments, utilizing deuterium as a target – in such a simple nucleus nuclear reinteractions are small. Single pion events constitute most of the resonant and coherent channels.

The energy dependence of cross-section for the three dominating channels is shown in Fig. 10 along with experimental data. Fig. 11 and Tab. 1 show number of events as a function of neutrino energy and interaction probabilities in different channel simulated for T2K experiment.

For each of the channels described above, neutrino interacts with a nucleon bound in the nucleus if interactions on nuclei (like oxygen in water) have to be taken into account. Thus nuclear environment has to be approximated and it is usually done according to relativistic Fermi gas model by Smith and Moniz [S75], assuming that nucleons are quasi-free, with an average binding energy and Fermi momentum, both specific for particular nuclei. Pauli blocking is also included in the model. An important role is also played by interactions between hadronic products of a primary reaction of neutrino with a nucleon and other nucleons in the nucleus. Many names are encountered in literature describing this phenomenon, including *reinteractions in nucleus*, *nuclear cascade* or *final state interactions*. In this thesis the last one will be used (or its abbreviated form – FSI). These interactions influence the number and momenta of hadrons (nucleons, pions) coming out from the nucleus and thus have an impact on observable features of events. Processes like pion absorption, charge exchange, etc. can occur in this stage of interaction. FSI depend on the number and

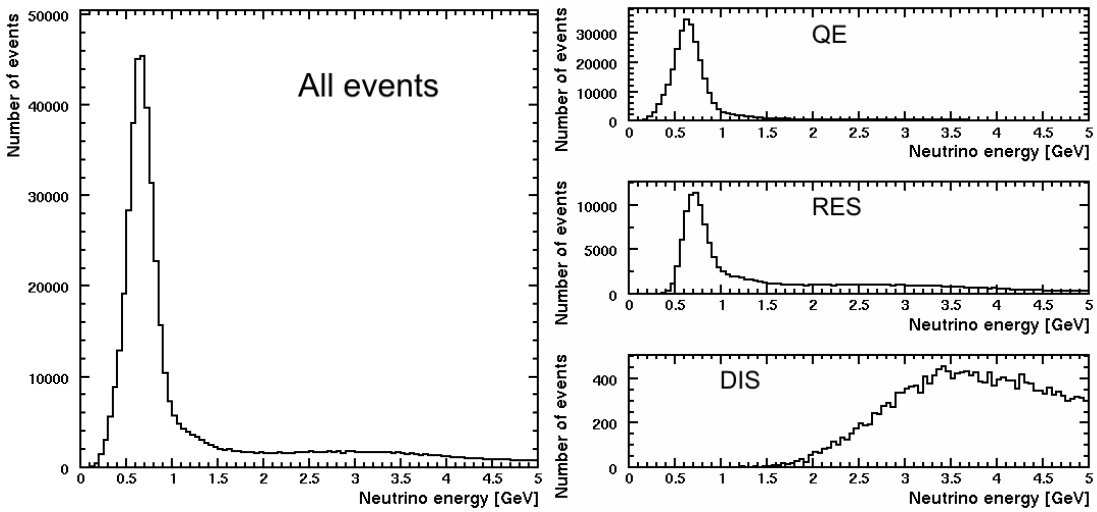

Fig. 11. Simulated number of interactions in near detector of T2K using T2K beam as a function of muon neutrino energy. Water was taken as a target material, 500,000 events were generated using Nuance. Left – all interactions, right – interactions split into three most significant production channels.

type of nucleons in the nucleus and therefore are different for different types of nuclei. The quality of FSI implementation is one of the crucial factors when choosing a neutrino generator.

	CC	**NC**	***All***
QE	42%	17%	**59%**
RES	22%	8%	**30%**
DIS	5%	2%	**7%**
Other	3%	1%	**4%**
All	**72%**	**28%**	**100%**

Table 1. Relative interaction probabilities in Nuance simulation for near off-axis detector of T2K using T2K beam. Water was taken as a target material.

In case of T2K experiment, two processes are particularly important, as they constitute *signal* in *electron neutrino appearance* and *muon neutrino disappearance* searches. These are:

- Electron neutrino charge current quasi-elastic interaction, leading to production of a single electron that tags electron neutrino interaction in Super-Kamiokande: $\nu_e + n \rightarrow e^- + p$

- Muon neutrino charge current quasi-elastic interaction, leading to production of a single muon that tags muon neutrino interaction in Super-Kamiokande: $\nu_\mu + n \to \mu^- + p$

CCQE processes are preferred, since they usually have only one observable product (lepton) and allow easy reconstruction of incoming neutrino energy by means of a simple formula (see Chapter 5). Lepton flavor is conserved in neutrino *interactions* - no flavor changing events have ever been observed (flavor conservation is broken in *oscillations* as we've seen in Chapter 2). This means that observation of a lepton of certain flavor in CCQE event indicates that a neutrino of the same flavor took part in the interaction. However, detectors are not ideal instruments and particle identification is not perfect. Certain other processes can mimic the signal by producing particles falsely identified as leptons. These interactions are called the *background.*

Electron neutrino appearance will be studied by measuring electrons from CCQE interactions in Super-Kamiokande. An appearance signal can appear if $\vartheta_{13} \neq 0$ (otherwise all ν_μ from the

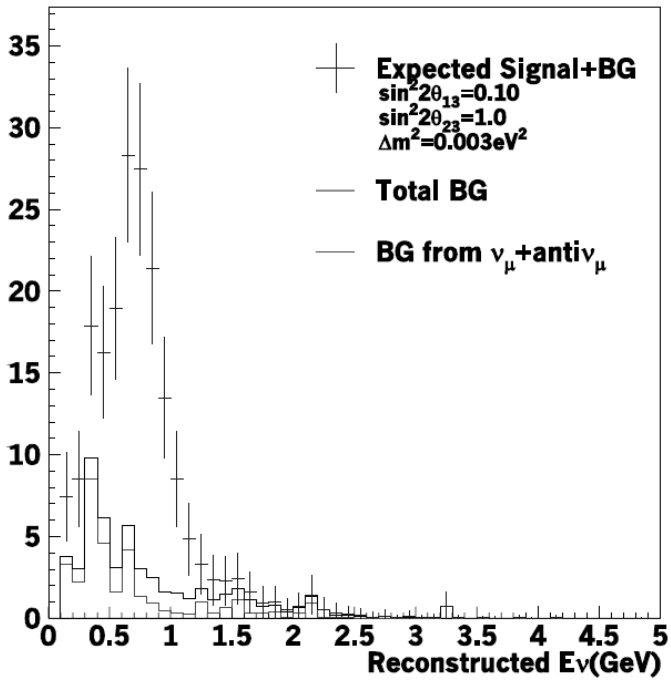

Fig. 12. Simulated energy spectrum of candidate electron appearance events for the oscillation parameters shown. The points with error bars show the spectrum from the expected signal plus background, the light grey histogram shows the background from the ν_μ (mostly from NC created π^0), while the black histogram shows the total background including the intrinsic contamination of the beam (from [T08]).

beam would oscillate into ν_τ) and allows for direct measurement of ϑ_{13}. However, it is known from other experiments that ϑ_{13} is small (see Chapter 2), and to measure such small values of ϑ_{13} one needs highest possible statistics and small systematic errors. The former is associated with high beam intensity, the latter with precise quantification of background. The background comes from two sources. First, the beam has an intrinsic ν_e component, which has to be measured by ND280 off-axis detector, before oscillations take place. Second, neutral pion production interactions can mimic CCQE electron production in SK (see next section). Fig. 12 shows how measured spectrum of electron neutrinos could look like for a certain set of values of oscillation parameters.

Muon neutrino dissappearance measurements will be done by means of observing muons

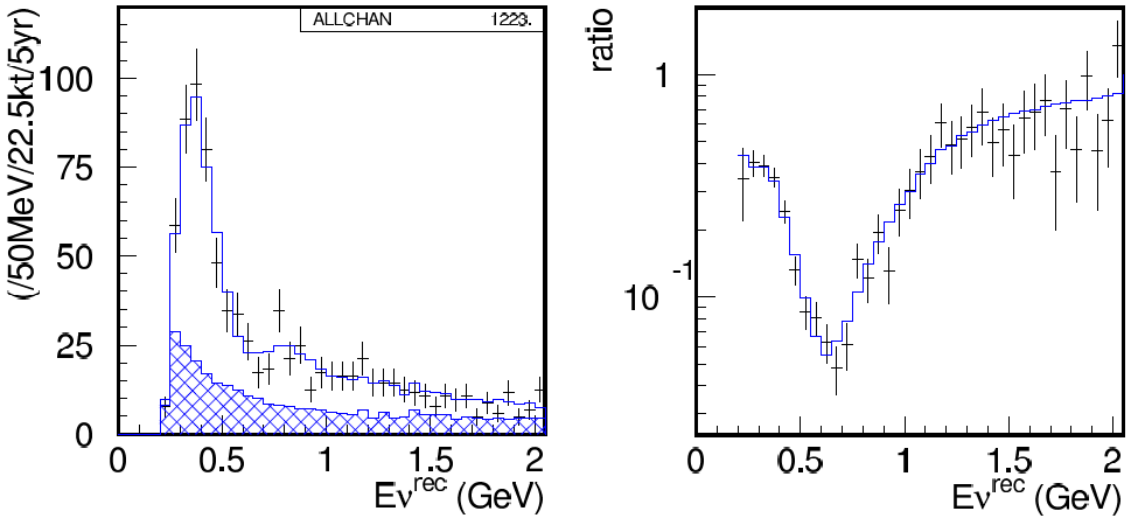

Fig. 13. Muon neutrino dissapearance in T2K. Left: the simulated reconstructed neutrino energy distribution. Oscillations with $\sin^2(2\vartheta_{23})=1$, $\Delta m^2_{32} = 2.7*10^{-3} eV^2$ have been taken into account. The solid histogram shows the expected spectrum at Super Kamiokande, after oscillations, but without statistical fluctuations. The points with error bars show a typical spectrum that can be expected from 5 years of running of the experiment. The hatched area shows the non-CCQE component. Right: the ratio of the expected reconstructed neutrino energy distribution with oscillations to the no-oscillation prediction (from [T08]).

from CCQE reactions in Super-Kamiokande. This way the flux of surviving muon neutrinos can be determined. This transition for T2K setup is dominated by oscillation in atmospheric sector, thus the measurement will allow accurate determination of ϑ_{23} and Δm_{23} oscillation

parameters. For the purpose of this measurements the reconstructed energy spectrum of ν_μ before and after oscillations must be precisely known, as oscillations produce a minimum (also called a dip) in the energy spectrum (see Fig. 13). In principle the depth of the minimum directly determines $\sin^2(2\vartheta_{23})$ and its position in energy determines Δm^2_{23}. However this dip is superposed on a spectrum which is strongly peaked in energy, so this spectrum before oscillations must be known with considerable precision before the actual properties of the dip can be inferred from the observed spectrum after oscillations. Careful understanding and rejection of non-CCQE background is necessary to this end.

3.1.3 Processes constituting the background

What processes constitute the background depend on the detection technique used. In T2K experiment the main measurements will be conducted in the far detector, so the background discussed here is mainly associated with Super-Kamiokande.

The main source of background for the electron neutrino appearance is muon neutrino neutral current scattering with neutral pion production (ν_μ NC π^0 production in short). The reaction looks like this:

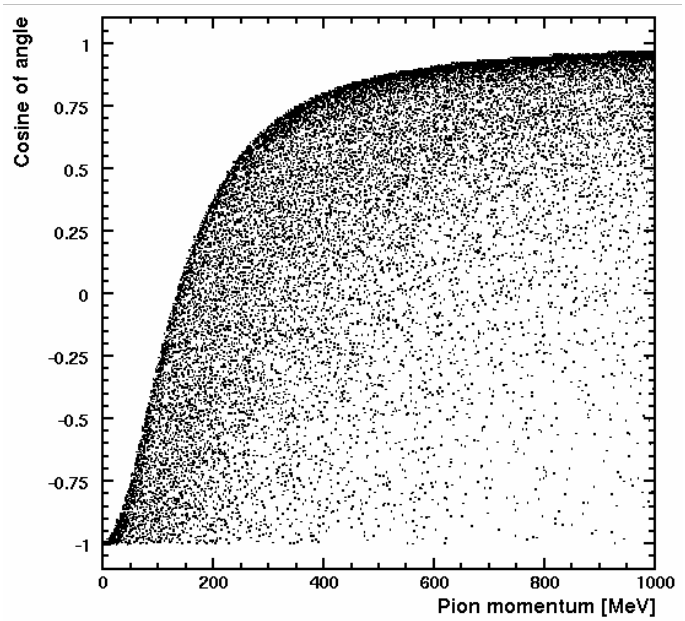

Fig. 14. Cosine of angle between two gammas from neutral pion decay as a function of its momentum. 100,000 pion decays have been simulated to create this plot.

$$\nu_\mu + N \rightarrow \nu_\mu + N + \pi^0$$

A π^0 in 99% of cases quickly decays into two gammas and these in turn initiate electromagnetic cascades. A similar cascade is created when an electron interacts in the detector medium. If, for some reason, one of the two gammas is invisible, or the two showers overlap, the event can easily be taken for a single electron.

The overlapping of showers (resulting in ring overlapping in Super-Kamiokande – see Chapter 4) happens when both gammas travel in similar directions, i.e. the angle between them is small. Fig. 14 shows how this angle depends on the momentum of decaying pion. It is seen that for pion momenta starting around 400 MeV/c, the gammas tend to be close to each other, with the angle lower than 40 degrees.

The background for muon neutrino detection is associated with a fact, that in water Cherenkov detectors muons and charged (mostly positive) pions are very difficult to tell apart. In effect, the following process:

$$\nu_\mu + p \rightarrow \nu_\mu + n + \pi^+$$

(ν_μ NC π^+ production) is a main source of background for muon neutrino disappearance signal. Muon identification can be aided by observing its characteristic decay into electron:

$$\mu \rightarrow e + \nu_e + \nu_\mu$$

This is especially useful in differentiating muons from negative pions which for the most part do not decay like positive pions:

$$\pi^+ \rightarrow \mu^+ + \nu_\mu$$

but rather get captured in the medium. Decay of positive pions makes them harder to tell apart, as they produce the same muon decay signature; however, at T2K energies, π^+s have much smaller energies than muons.

More details will be introduced in the next chapter, where design of the detectors is discussed.

3.2 Simulations

Simulation in particle physics is a computer-aided method of modeling particle interactions with an aim to predict results of experiment. Experiments are so complicated that analytical approach is impossible and one has to resort to statistical methods to calculate theoretical predictions for experimentally observable quantities. Simulations are used to evaluate the

feasibility and physics reach of proposed experiments, optimize the detector design, analyze the collected data samples and evaluate systematic errors [A09].

3.2.1 Generic algorithm of neutrino interactions' simulation

Simulation in a complicated neutrino experiment, such as T2K, has to take into account many factors that influence final result. Usually, flow chart of actions for a simulation looks like the following:

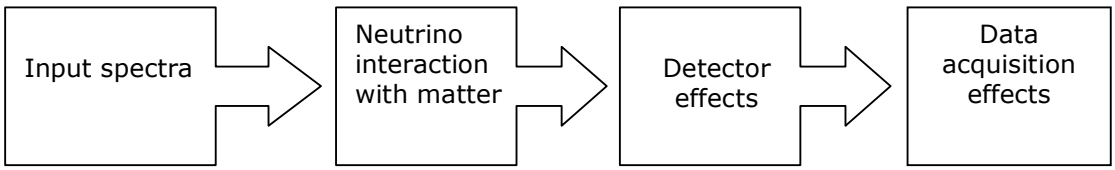

Neutrino generator takes spectra characteristics as an input. These spectra characteristics are usually a set of energy distribution histograms, one per each neutrino flavor considered. They are produced by input spectra simulation. Neutrino generator simulates primary interaction in the detector medium. The products of an interaction are then propagated further in the medium by detector simulation, which takes into account all the design subtleties of the detector. Then data acquisition effects (electronics noise, etc) are taken into account. Eventually an output is produced which is identical to the output of the real detector. This output is finally processed (noise subtraction, event reconstruction, etc.) by data analysis routines. Every step in the procedure should be carefully taken into account, as the aim is to produce samples that reproduce as closely as possible the real data samples that will be collected in the experiment. However, in many analyses (and this is the case for some of the studies described in this thesis) it is sufficient (and convenient) to use the neutrino generator only. This makes the considerations more generic (independent of the detection technique).

Let us now discuss the steps described above in more detail.

Input spectra simulation

Depending on the type of the experiment this part would amount to determining spectrum of neutrinos from a natural source (i.e. atmospheric neutrinos) or simulating beam spectra shapes (if there is an artificial neutrino beam). In each case a specialized simulation is needed to provide energy and angular distributions of incoming neutrinos of every flavor. Atmospheric neutrino simulation would have to deal with simulating extensive air showers initiated by cosmic rays in upper layers of the Earth's atmosphere. Beam simulation generates primary

interactions of accelerated protons in a target, and propagates the products through the decay pipe. T2K is an experiment that uses neutrinos from a beam. The beam simulation code is called *jnubeam* and is based on a simulation package GEANT3.

Neutrino interaction with matter

This is the most important stage of the simulation chain introduced above. Neutrino interaction simulation (sometimes also called *neutrino generator*) employed here takes care of simulating neutrino interactions with atoms of the detector medium. It determines needed cross-section values (for all the necessary energies and processes) – either by direct calculation or taking the precalculated values from files or tables – and generates required number of events. The event generation process is usually divided into two stages:

- Primary interaction - the primary neutrino-electron, neutrino-nucleus or neutrino-nucleon interaction is simulated, depending on the process being chosen (randomly, according to probabilities proportional to differential cross-sections)
- Secondary interactions of hadrons in nucleus (FSI simulation).

As a result one gets a list of particles coming out of the nucleus (along with their direction, momenta, etc.).

Detector simulation

Detector simulation takes care of propagation of the particles produced in the neutrino generation stage through the elements of the detector. Usually detector construction is complicated – e.g. the ND280 off-axis detector consists of several subdetectors, each with a sophisticated internal design. Detector simulation takes into account a detailed detector geometry and carefully tracks all the particles through multiple elements made of different materials, handling all possible physical effects between the particle and medium. Sensitive elements, providing detection signal (scintillation strips, photomultipliers), are also simulated. In case of Super-Kamiokande detector simulation tracks all the Cherenkov photons towards the detector walls, taking into account attenuation, reflections, etc. A list of tracks and hits (signals from sensitive elements) in the detector is the output of this stage of simulation. To view whole simulated events one usually uses dedicated *event viewers*, enabling to see the tracks and hits in a visual form (in 3 dimensions, from different points of view, etc.).

Simulation of electronics

In the experiment, signals from sensitive elements are collected and transformed into electronics' signals, then processed by electronics (amplification, noise subtraction, triggering) and passed onto a computer system, which writes the data to storage devices.

Simulation of this process is also important, as it can introduce certain distortions to the data. A package called *elecSim* handles this part in T2K experiments' simulation software.

3.2.2 Review of simulation packages used in the analyses

There are several neutrino generators and detector simulation packages available. The following were used in this thesis.

Nuance is an advanced and freely available neutrino generator written by Dave Casper of University of California, Irvine. Its source codes are publicly available. The technical details regarding physical models used in the program can be found in Ref. [C02]. The simulation was originally designed to handle neutrino interactions on water (the program was initially developed for IMB experiment and was later used in Super-Kamiokande and K2K experiments). In all the analyses, version 3.006 of Nuance was used. In this version, a user is allowed to choose target nucleus – this is important, because final state interactions (FSI) are strongly dependent on number of protons and neutrons in the nucleus (and other factors associated with the type of nucleus). Depending on the analysis, the target material was set to water, carbon or argon.

Nuance is a widely used tool, tested in experiments with water Cherenkov detectors like K2K. It is also used in MiniBoone experiment, where its FSI model was tuned to properly simulate interactions on carbon (MiniBoone uses mineral oil, CH_2, as a detector medium). It will be shown further in this chapter that its implementation of final state interactions (FSI) can be considered trustworthy.

NEUT [H09] is a Japanese neutrino generator developed over more than 20 years by many people and recently by a group led by Yoshinari Hayato. It was used in Kamiokande experiment and is presently used in Super-Kamiokande experiment. It was designed to simulate interactions in water and has a decent implementation of FSI for oxygen. This simulation package is one of the official simulations of the T2K experiment and was used in SMRD optimization study.

NuWro [J05] is a Polish neutrino generator developed by Wroclaw Neutrino Group led by Jan Sobczyk. It is a fairly new tool that has the advantage of possibility to change important parameters of theoretical models used in the generation. This feature was utilized in pion production uncertainty study. NuWro uses Rarita-Schwinger formalism for the Δ excitation for simulation of resonant pion production (differently from other generators which use Rein-

Sehgal model). NuWro can handle various materials and recently FSI have been implemented. It is a constantly developed tool and new features are still being added.

ND280MC simulation is an ND280 dedicated detector simulation tool based on GEANT4 [A03] and ROOT [B97], with all the detector geometry implemented. As an input it takes interactions generated by neutrino simulation (NEUT, Nuance or GENIE [A06]). It is a constantly developed large software package, with simulation and reconstruction routines bundled together, also suited for real data analysis. ND280MC was used in SMRD optimization study.

3.2.3 Nuance FSI implementation validity

Since Nuance is used extensively throughout this thesis, it is worth to evaluate its validity with regard to FSI implementation. The results are dependent on the nucleus chosen for a target.

For water (oxygen), Nuance has been tested in experiments with water Cherenkov detectors like K2K and Super-Kamiokande (SK). It appeared to be consistent with the measurements of CC π^0 production in 1KT near detector of K2K [M08] as well as atmospheric neutrinos in SK [A05]. Another test is also possible using results from Ref. [N05]. In this work a near detector of K2K experiment was used to measure a cross section for inclusive NC π^0 production normalized to cross section for all CC interactions. This cross-section was found to be equal to:

$$R = \frac{\sigma(NC\,\pi^0)}{\sigma(CC\,total)} = 0.064 \pm 0.001(stat) \pm 0.007(sys)$$

In order to find a corresponding result for Nuance, a sample consisting of 100,000 events for K2K beam was simulated. The obtained result is (statistical error is negligible):

$$R = 0.065$$

It agrees well with aforementioned K2K result (and NEUT result quoted in the article [N05])

As a conclusion, we can state that Nuance's implementation of nuclear effects in oxygen can be considered trustworthy.

Second validation was carried out for argon as Nuance was used in neutral pion study for liquid argon detector (Chapter 7). Nuance gives a possibility of specifying a target nucleus and has a generic procedure for handling FSI. However, it was only tested for water (and carbon in Nuance version used by MiniBoone experiment). We decided to focus on multiplicity and average momenta of nucleons and pions leaving the nucleus after interaction

(as these quantities have the largest impact on the results of our analysis) and compared the results with a second simulation package, NUX+Fluka. NUX [R01, B02] is a neutrino generator used in NOMAD and ICARUS experiments. Coupled with FLUKA [F05, B02], a widely used and thoroughly tested nuclear simulation package used here for FSI simulation, it constitutes a powerful tool for simulating neutrino interactions in various media. The main aim of the comparison was Nuance FSI validation for argon.

As the study dealt with neutral pion events, the comparison was carried out on resonant interactions only, with energy of incident neutrino set at 1750 MeV, which is an average neutrino energy for resonant channels in T2K. The results of the comparison in the form of number of particles (pions, nucleons) produced by both simulations per event are presented in the table below. Average momenta of the particles are also presented. Nuance without FSI is also shown for reference.

One can notice that there is a huge difference between Nuance samples with and without FSI in terms of number of nucleons (in contrast, total number of pions is similar). This is because Nuance creates a lot of low energy protons and neutrons during rescattering in nucleus. However, FLUKA does the same – number of nucleons is even slightly larger for this simulations. Number and average energies of pions are very similar. The conclusion is therefore that Nuance FSI implementation for argon is working reasonably well.

	Nuance no FSI (Ar)	**Nuance with FSI (Ar)**	**NUX+Fluka with FSI (Ar)**
π^0	0.36/evt 0.43 GeV/c	0.31/evt 0.35 GeV/c	0.32/evt 0.38 GeV/c
π^+	0.75/evt 0.44 GeV/c	0.52/evt 0.41 GeV/c	0.54/evt 0.41 GeV/c
π^-	0.06/evt 0.36 GeV/c	0.10/evt 0.26 GeV/c	0.06/evt 0.32 GeV/c
n	0.31/evt 0.81 GeV/c	2.27/evt 0.30 GeV/c	3.13/evt 0.21 GeV/c
p	0.84/evt 0.79 GeV/c	2.95/evt 0.36 GeV/c	2.34/evt 0.39 GeV/c

Table 2. Multiplicities and average momenta of pions (neutral, positive, negative) and nucleons (neutrons, protons) for Nuance (with and without FSI) and NUX+Fluka (with FSI). Samples of 100,000 events for Nuance and 35,500 events for NUX were used, 1750 MeV neutrinos were scattered on argon, only RES channels were taken into account. Statistical errors are negligible.

Chapter 4
T2K Experiment

T2K is a long baseline experiment aimed at measuring neutrino oscillation phenomenon using artificial neutrino beam. This means that neutrinos are produced at a certain location and shot towards a detector that is sufficiently far from the neutrino source to observe oscillation effects at their maximum. However, to control backgrounds, like beam contamination, one also has to measure beam neutrinos before oscillations can occur, i.e. at the close proximity of the beam source. This is a role of a second detector. It won't come as a surprise that those detectors are called, correspondingly, far and near. In T2K, ND280 plays a role of a near detector, and Super-Kamiokande (SK) is the far detector. The beam is formed by scattering accelerated protons off a graphite target and letting the products decay into neutrinos (mainly muon) in a decay pipe. The schematic view of the experiment is visible in Fig. 15.

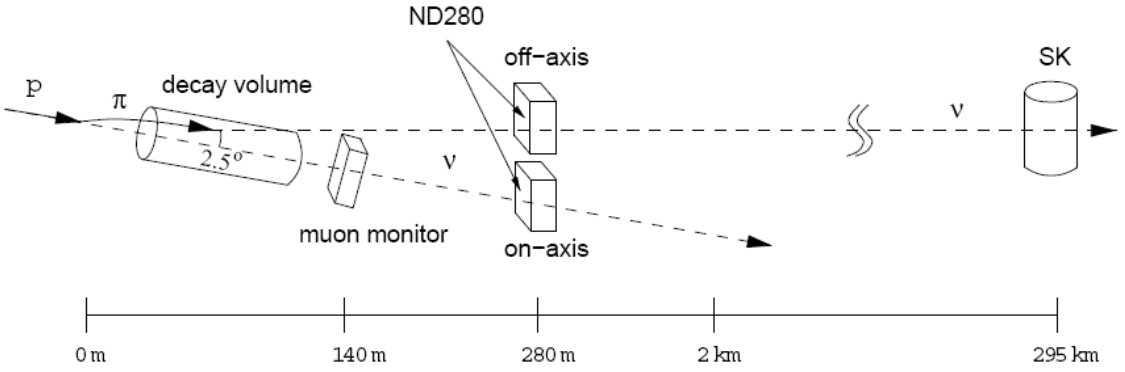

Fig. 15. Scheme of T2K experiment. At 2 km an intermediate station is possible in the later stage of the experiment. Picture taken from [V07].

Physically, the experiment is composed of two facilities located in Japan: J-PARC facility in Tōkai, Ibaraki prefecture with accelerator and near detector complexes and Kamioka mine underground facility near Mozumi in Gifu prefecture, 295 km away from Tōkai.

4.1 The beam and beam detectors

4.1.1 Beam production and monitors

The accelerator facility is designed to accelerate protons to 50 GeV of energy, however in the first years of experiment protons will have 30 GeV [T08]. Protons are accelerated first in linear accelerator (LINAC) and then injected into two proton synchrotrons (PS). The

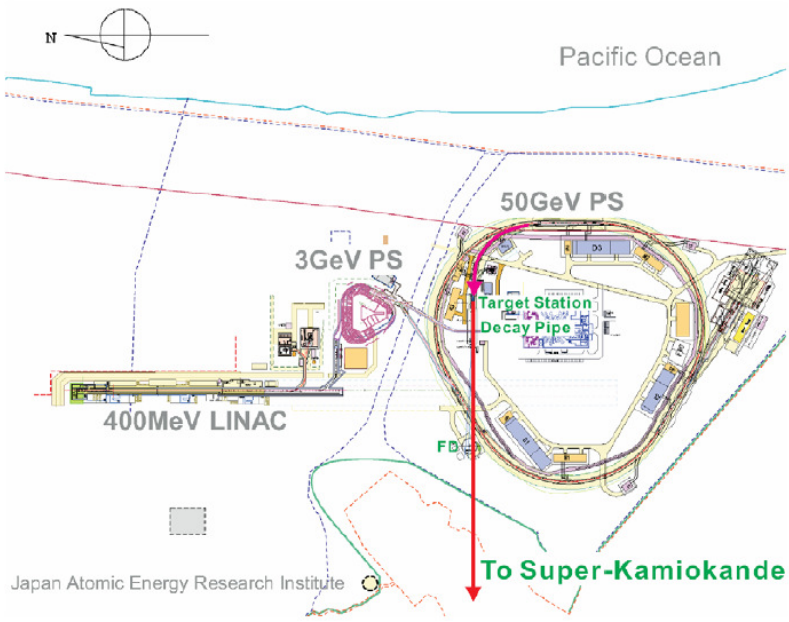

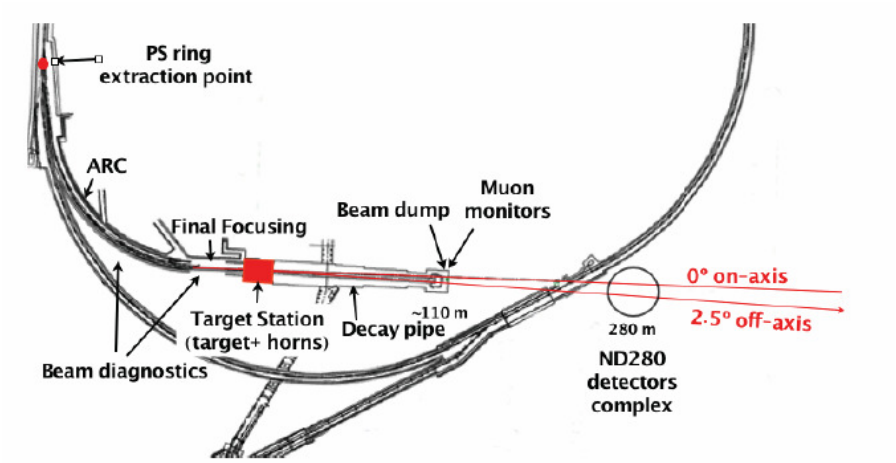

Fig. 16. T2K facilities in Tokai. Upper (from [H03]): J-PARC site map, lower (from [V07]): neutrino complex. The main accelerator, labeled '50 GeV PS' on the upper picture, will actually accelerate protons to 30 GeV in the first years of experiment.

accelerated particles are then extracted and bent inside the 30 GeV PS in the ARC section (see Fig. 16) using dual-function (dipole and quadrupole) superconducting magnets [V03].

Sufficiently focused beam is shot onto the target, a 90 cm long graphite rod cooled with high pressure helium. Produced positive hadrons, mainly pions, are collimated by a system of 3 horns. The horns are set to discard all the particles of negative charge which could be a source of unwanted antineutrinos (if the polarity of horns is flipped, one can get antineutrinos instead of neutrinos, which could be useful in later stages of experiment, when it will be looking for CP violation effects). To maximize the pion collection efficiency, the target is located inside the first horn magnet. The particles are directed into the decay pipe, 110 m long, helium filled tunnel [H03]. The pions decay into muons and muon neutrinos:

$$\pi^+ \rightarrow \mu^+ + \nu_\mu$$

Some of resulting muons can also decay producing muon antineutrinos and electron neutrinos:

$$\mu^+ \rightarrow e^+ + \bar{\nu}_\mu + \nu_e$$

Less numerous kaons also decay with production of electron neutrinos:

$$K^+ \rightarrow \pi^0 + e^+ + \nu_e$$

This way an intense 0.75 MW neutrino beam is created and directed towards the Super Kamiokande detector. Two last channels are a source of beam contamination, as our aim is to produce a pure muon neutrino beam.

At the end of the decay volume, a beam dump is located, absorbing any hadrons that reach the end of the tunnel. It is build of graphite blocks cooled with water in aluminum pipes.

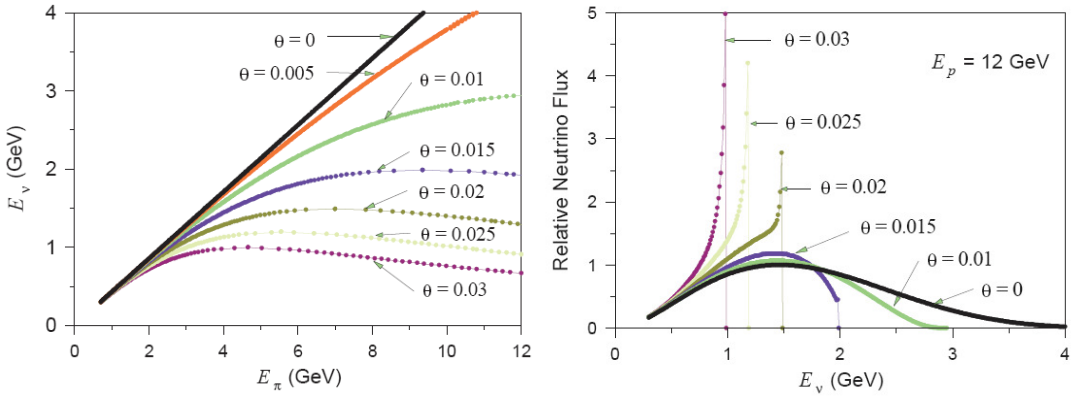

Fig. 17. Off-axis beam. Left: neutrino energy as a function of energy of decaying pions, right: Neutrino fluxes integrated over all pion energies. The plot was drawn for proton energy of 12 GeV. The angle θ is an angle between pion direction and neutrino direction (in radians), a good approximation of an off-axis angle. The larger the angle, the more peaked neutrino energy distribution one gets. From [M01].

Particles that pass the dump are, besides neutrinos of course, high energy muons. They are used by a muon monitor situated downstream the dump to keep an eye on the beam direction and possible unexpected things that can happen in the decay pipe. By means of this detector, consisting of solid state detectors and ionization chambers, the proton beam direction can be determined and monitored with an accuracy better than 1 mrad on a spill by spill basis [V03].

4.1.2 Energy spectrum and beam composition

Physical aims of the T2K experiment require the beam energy spectrum to be narrowly peaked around the energy of ~0.7 GeV which is optimal to observe electron neutrino appearance in the far detector. For this purpose an off-axis setup of the experiment has been chosen. The far detector is not situated on the axis of the beam – there is a certain non-zero angle between the beam axis and the axis connecting the beam source and SK. Fig. 17 illustrates why off-axis beam has a more favorable neutrino energy spectrum shape from the

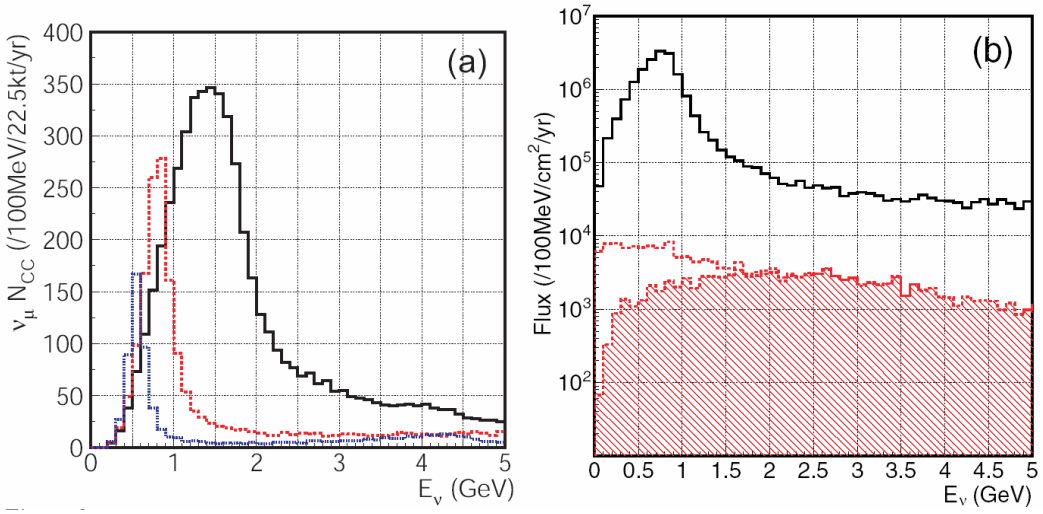

Fig. 18. Off-axis beam. Left: event energy spectrum in SK for three off-axis angles: black – 1 degree, red – 2 degrees, blue – 3 degrees off-axis. Right: Flux components for 2 degrees off-axis options; black line – total flux, red dashed region – electron neutrinos coming from kaon decays, empty region under the upper red line – electron neutrinos from muon decays. Plots taken from Ref. [H03].

T2K experiment's point of view. Let's consider pions decaying in the decay volume [M01]. In the pion rest frame, energy of the neutrino is constant and equals 29.8 MeV. Let's denote as θ the angle between the neutrino and the pion's direction of motion. The pion has spin zero, so the decay is isotropic in the pion rest frame. We can now transform the neutrino into laboratory frame and apply Lorentz boost to the neutrino's 4-vector:

$$(E_\nu, p_\nu) \equiv (E_\nu, E_\nu \sin\vartheta, 0, E_\nu \cos\vartheta) = \left(\gamma_\pi E_\nu^* (1+\beta_\pi \cos\vartheta^*), E_\nu^* \sin\vartheta^*, 0, \gamma_\pi E_\nu^* (\beta_\pi + \cos\vartheta^*)\right)$$

where quantities in pion frame of reference are labeled with an asterisk, and all others are in the lab frame, and get the formula for the angle in the laboratory frame:

$$\tan\vartheta = \frac{E_\nu^* \sin\vartheta^*}{\gamma_\pi E_\nu^* (\beta_\pi + \cos\vartheta^*)}$$

For relativistic neutrinos $E_\nu >> m_\pi$, then $E_\pi >> m_\pi$ also, so $\gamma_\pi >> 1$ and $\beta_\pi \approx 1$, and we can write (using the time component from the Lorentz boost above):

$$\tan\vartheta \approx \frac{E_\nu^* \sin\vartheta^*}{E_\nu}, \quad E_\nu^* = 29.8\,MeV$$

Since sin θ* cannot exceed unity, there is a maximum lab angle θ relative to the direction of the pion at which a neutrino of energy E_ν can be emitted. This also means that there is a maximal neutrino energy for a specified angle:

$$E_\nu \approx \frac{E_\nu^* \sin\vartheta^*}{\tan\vartheta} \le \frac{E_\nu^*}{\tan\vartheta}, \quad E_\nu^* = 29.8\,MeV$$

which is visible in Fig. 17 on the left. When translated into flux profiles, this gives peaked distributions, with energies at the peak and peak widths getting smaller as the angle

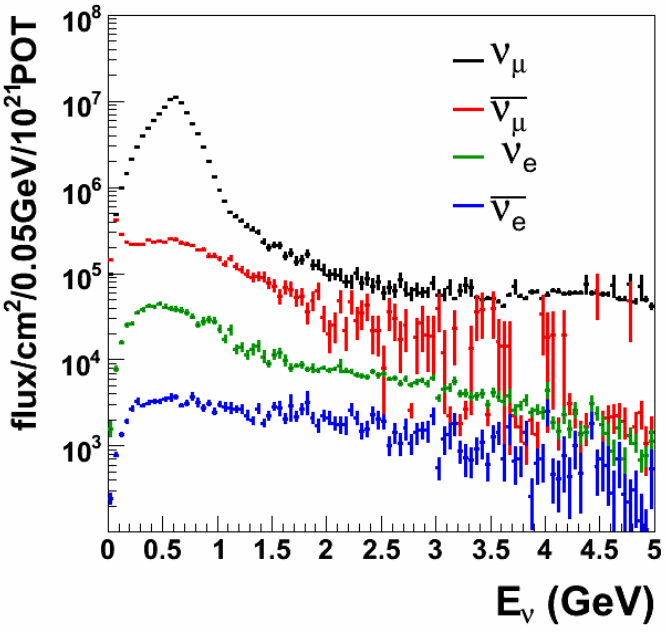

Fig. 19. Simulated T2K beam flux at the Super-Kamiokande site (2.5 degrees off-axis). Black points – muon neutrinos, red – muon antineutrinos, green – electron neutrinos, blue – electron antineutrinos. Plot obtained by Magdalena Posiadała [P10] using *jnubeam*.

grows larger (Fig. 17, right).

How this situation looks in the case of T2K experimental setup is shown in Fig. 18, left. Three energy profiles are shown for three off-axis angles. It is worth to notice that one cannot increase the off-axis angle too much – numbers of events recorded in detectors are smaller for larger angles.

As it was mentioned, beam will be contaminated with $\bar{\nu}_\mu$ and ν_e. Muon antineutrinos' abundance is expected to be at the level of a few percent. Electron neutrinos, though less numerous (they consist 1% of the whole beam neutrinos and 0.2% at the peak energy around 0.7 GeV [H03]), are much more dangerous, as they constitute a background to neutrino appearance measurements. Fig. 18, right shows the beam energy profile for 2 deg. off-axis angle and contribution from electron neutrino background originating from kaon and muon decays.

Ultimately the angle of 2.5 degrees was chosen and the Super-Kamiokande flux for this option is presented in Fig. 19.

4.1.3 T2K beam structure

The design intensity of the PS is 3.3×10^{14} protons/pulse at a repetition rate of 0.285 Hz (3.5 second period), resulting in a beam power of 0.75 MW (2.64 MJ/pulse). The spill structure is shown in Fig. 20. A typical one-year operation is 10^{21} protons on target (POT), which corresponds to about 130 days of operation [H03].

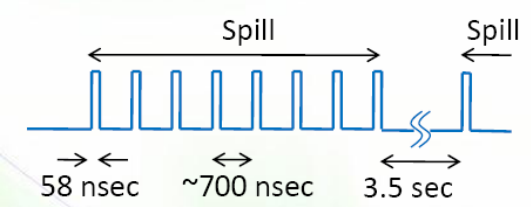

Fig. 20. T2K beam time structure. A spill contains 8 bunches. From [M09].

4.2 Near detectors - 280m station

The near detector complex is a three-floor pit, a 36 m deep concrete structure in the ground. It is located 280m away from the beam source and consists of two parts: on-axis and off-axis. On-axis part is a collection of detectors monitoring stability of the beam; off-axis detector will

be used for cross-section, flux and background measurements.

4.2.1 On-axis detectors

On-axis detectors occupy lower part of the pit (second and third floor) and are collectively called *INGRID – Interactive Neutrino Grid.* It consists of 14 detector modules aligned in a form of a cross (see Fig. 21) perpendicular to the beam direction. Two others are placed at the bottom-left and top-right parts of the cross. Every module (1m × 1 m × 1 m) is composed of 11 alternated planes of scintillating plastic and thick iron layers. Four veto planes are installed on the sides of each module [D06].

INGRID measures neutrino interactions and determines beam direction, intensity and mean energy. The spatial distribution of modules allows to measure beam shape and asymmetries in every direction. The grid has been designed to provide sufficient statistics to determine on a day-to-day basis, the beam direction within 1 mrad corresponding to a 2% (14 MeV) shift in the off-axis beam spectrum. It will be able to notice beam shifts of the order of 1 mm at the target [V07].

4.2.2 Off-axis detectors

The off-axis detector (hereinafter called ND280oa, Fig. 21, right) is placed on the first floor of

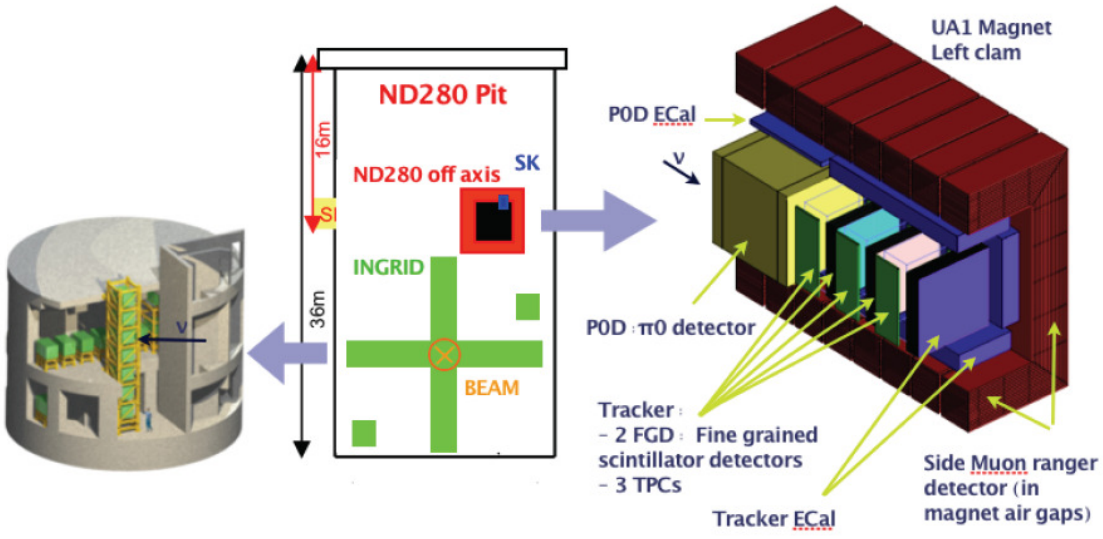

Fig. 21. 280 m station. Center: station's pit cross-section, left: lower floors with INGRID installed, right: ND280oa detector. From [V07].

the 280 m pit. It is a set of subdetectors arranged in the following way [D06]:

- the internal part of dimensions 3.5 m x 3.6 m x 7 m, usually referred to as *the basket*, containing:
  - P0D – detector aimed at measuring pizero mesons,
  - Tracker, consisting of two FGDs – Fine Grain Detectors, used mainly to reconstruct proton tracks and three TPCs – gas Time Projection Chambers,
- several electromagnetic calorimeters (ECALs) around the basket,
- the magnet, consisting of:
  - a coil (in form of a belt surrounding the basket and ECALs from upper, lower, downstream and upstream side), and
  - a magnet yoke, encompassing the basket from two sides. Each side part is divided into eight independent parts, of a C-letter-like shape (the so-called 'Cs'). SMRD detector is installed in the magnet to measure high energy muons exiting the basket.

A magnetic field of 0.2 T will be provided by the magnet to enable momentum measurement and particle sign determination by curvature of tracks.

P0D and FGDs will also be used as target material for neutrino interactions that are to be observed by ND280. To measure cross-sections also on water, the medium used in the far detector, parts of P0D and second FGD are instrumented with water tanks.

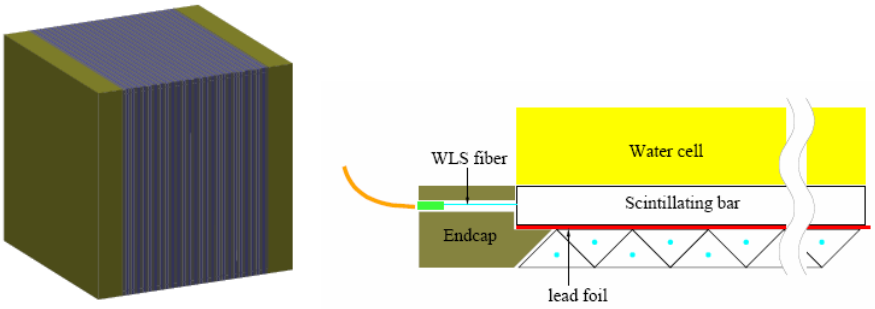

Fig. 22. P0D (left – blue region is the area equipped with water tanks) and cross-section of a P0D module (right - two scintillator planes and a water tank are visible). From [D06].

P0D (π^0 *detector,* 220 x 233 x 242 cm^3, 6T of fiducial mass, Fig. 22), placed upstream, is a specialized detector for measuring π^0 mesons from neutral current interactions, an important background for electron neutrino appearance search [D06]. Neutral pions are tagged via

observation of two electromagnetic showers initiated by gammas from neutral pion decay.
P0D consists of P0D modules (P0Dules) - scintillator tracking planes alternated with lead plates (in the front and rear parts) or water tanks (in the central part). A scintillator plane consists of two layers, so called *X* and *Y*, each composed of extruded polystyrene bars doped with a scintillator and oriented perpendicularly on the two consecutive layers. Layers are separated with lead foil which is used as a radiator, accelerating gamma conversion process. A particle has to traverse one plane (two layers - one X, one Y) to have its position determined in three dimensions. The number of traversed double X-Y planes is the number of tracking points recorded in the detector.
Scintillator bars are equipped with wavelength shifting (WLS) fiber which transports the light signal towards two ends of a bar. On one end the light is detected by MPPC (Multi-Pixel Photon Counter) sensors and transformed into electric signals; the other is mirrored.
The bars are triangular in cross-section to ensure better coverage – a particle traversing a layer will typically leave a trace in at least two bars and a better spatial resolution can be achieved.
On the four sides of P0D electric calorimeters are installed to detect particles leaving the detector (like escaping gammas).

Tracker is a set of detectors devoted to measuring longer tracks of neutrino interaction products, mainly muons and pions (for precise reconstruction of CCQE and single charged pion events) [D06]. The reconstruction of muon neutrino CCQE interactions should give a precise measurement of the beam energy spectrum. This subdetector is composed of 2 FGDs and 3 TPCs, with FGDs serving also as target for interactions. TPCs are in front and at the back of each FGD, so the more energetic particles are very likely to be measured in one of the TPCs.
FGDs (Fine Grained Detectors) are two units utilizing layered design similar to P0D. In case of a first, upstream FGD, the target is the scintillator itself (doped polystyrene) organized in 30 X-Y planes. Second FGD contains water as the target – there are 7 sensitive planes alternated with water tanks. Scintillating bars (0.96 x 0.96 x 184.3 cm^3, Fig. 23, left) with WLS fibers are used, with one-end MPPC readout (the other end of a fiber is mirrored). Two target materials make it possible to determine cross-sections on carbon and oxygen separately. Each FGD has outer dimensions of 230 cm (width) x 240 cm (height) x 36.5 cm (depth in beam direction), and contains 1 ton of target material. FGDs aim at measuring short-range particles, like recoil protons (essential for CCQE tagging). All others (muons, pions) will

usually reach one of the *TPCs (Time Projection Chambers),* three metal cages (2.5 x 2.5 x 1 m^3, Fig. 23, right) filled with gas (argon with small admixtures). Principle of operation for such a detector is discussed later in this chapter when discussing intermediate station's TPC. An electric field of 200V/cm is sustained inside to force ionization electrons to move towards the sidewalls, where MICROMEGAS modules (36 x 48 grids of 6.8 mm x 9.7 mm sensitive pads) record them and the signal is digitized. TPCs will allow to measure momentum with 10% precision around 1 GeV basing on curvature of tracks and identify particles by studying their energy loss pattern. Measurement of momentum is possible if the track in TPC is at least 60 cm long.

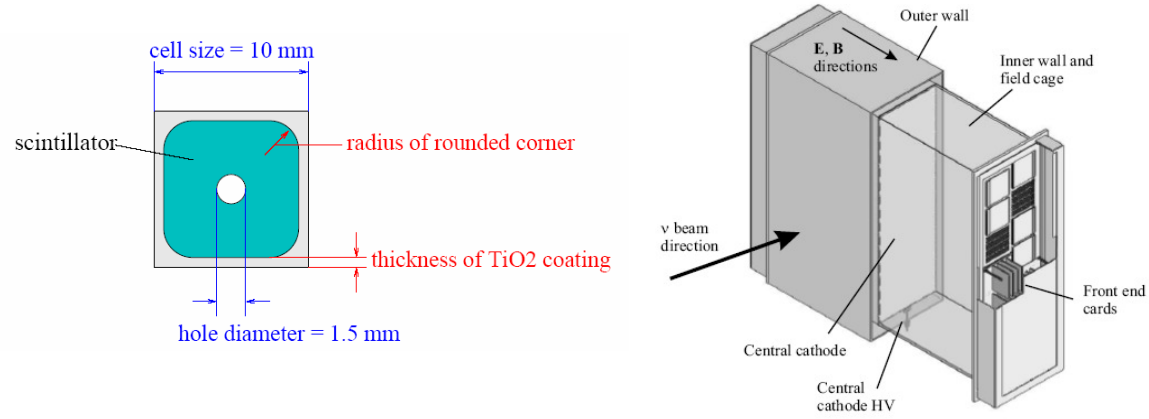

Fig. 23. Left: A cross-section of FGD's scintillator bar, right: tracker's TPC scheme (from [D06]).

Electromagnetic calorimeter (ECAL) comprises two sections [V07]. A fine grained Tracker ECAL (TECAL) surrounds the FGDs and TPCs. It takes care of particles exiting the tracking volume reconstructing and identifying them. Its main aim is to aid the tracker in measuring neutrino interactions from the beam, which is particularly important when the muon does not traverse any of the TPCs or its track in TPCs is too short. It can also track showers from π^0 decays (this measurement is less efficient than the P0D measurements, but has different systematic errors). A coarse P0D ECAL (around the P0D section of ND280oa) will be catching gammas leaving the P0D and tagging exiting muons. Both ECALs are lead-scintillator sandwiches; TECAL is made of 4 cm wide, 1 cm thick plastic scintillator bars separated by layers of 1.75mm-thick lead sheets, P0DECAL scintillator layers are made of 20 cm wide, 2 cm thick slabs alternated with 5 mm thick lead converter. There are 6 units around the Tracker plus one downstream and 12 around the P0D; the upper, bottom and side units are

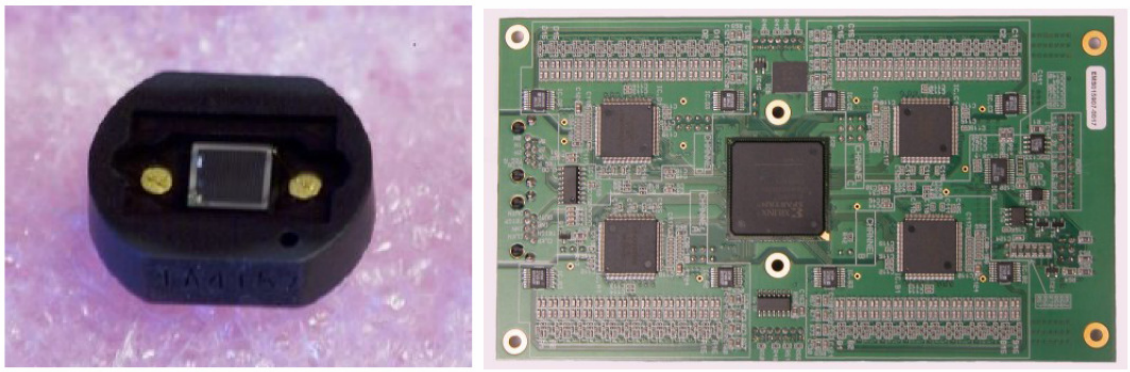

Fig. 24. Left: a Multi-Pixel Photon Counter (MPPC). Right: a Trip-t board. Images taken from [L09].

mounted to the magnet.

All light signals from scintillator detectors are transported by WLS fibers and transformed into electric signals by MPPC photodiode sensors [L09]. A *Multi-Pixel Photon Counter* (Fig. 24, left) is an array of photodiode pixels. Each pixel operates above its breakdown voltage (approximately 70V) and can produce an avalanche of electrons if struck by a photon. An MPPC therefore provides the single photon counting capability and electronic gain of a traditional photomultiplier, and is less expensive and can operate in an environment where magnetic field is present. ND280oa will use around 50.000 MPPCs in total. These sensors will be read out by suitable electronics – in case of most subdetectors *Trip-t boards* will be used (Fig. 24, right). The Trip-t chip provides time and charge for any discriminated pulses, with nominal time resolution of 2.5 ns [D06]. The boards provide also high voltage current required for proper MPPC functioning.

4.3 Configuration optimization of SMRD detector in off-axis part of 280m station

4.3.1 SMRD construction and role

Magnet yoke for ND280oa is a reused unit from UA1/NOMAD experiment (donated by CERN). The *SMRD (Side Muon Range Detector)* is a scintillator detector making use of the presence of slits in this yoke [D06]. Every slit can be equipped with a scintillation sensor. The detector, consisting of the sensors, accompanying WLS fibers, photo detectors and electronics is aimed at measuring high energy particles that do not stop inside the basket and therefore cannot be well reconstructed using inner detectors only. The most important class of these

particles are muons that do not travel sufficiently long distance in the TPCs.

A single scintillator unit consists of:

- A plastic scintillator slab (870x170x0.7mm^3) covered with a reflective material
- A wavelength shifting (WLS) fiber glued into a sinusoidally shaped groove on slab
- A photodetector – MPPC – that transforms optical signal to electric one that is then processed by electronics.

Units in groups of 4 or 5 are attached to themselves and form modules. Each module resides in a single slit.

4.3.2 Physical role of SMRD

There are three main purposes of the SMRD detector:

- measurement of muons produced in neutrino interactions that cannot be well reconstructed by tracker detectors,
- cosmic ray muons detection for calibration triggering,
- veto for muons that come from the outside.

Measurement of muons

The most important tracks to be measured by ND280 detectors are muons, since the neutrino energy reconstruction relies mostly on muon reconstruction (the reconstruction for the most abundant CCQE events is based only on reconstruction of momentum of outgoing muon). TPC gas chambers in the tracker are the best for this purpose, as they offer good tracking capabilities and momentum reconstruction via track curvature measurement. It was estimated (see Ref. [D06]) that one needs to have the track at least 60cm long in TPC to effectively reconstruct a muon's momentum. This suggests that there is a class of tracks that has to be handled by other subdetectors; that's where SMRD comes into play. These tracks are mainly the ones that are almost perpendicular to the beam axis – they traverse the FGD they were created in, cross one of the ECals and enter the SMRD.

SMRD can roughly measure momentum (using range information) and direction of muon track (direction estimation needs at least two hits left by the muon). SMRD precision is worse than the precision of TPC measurements, but still provides useful information. SMRD measurements can also supplement measurements in the TPCs.

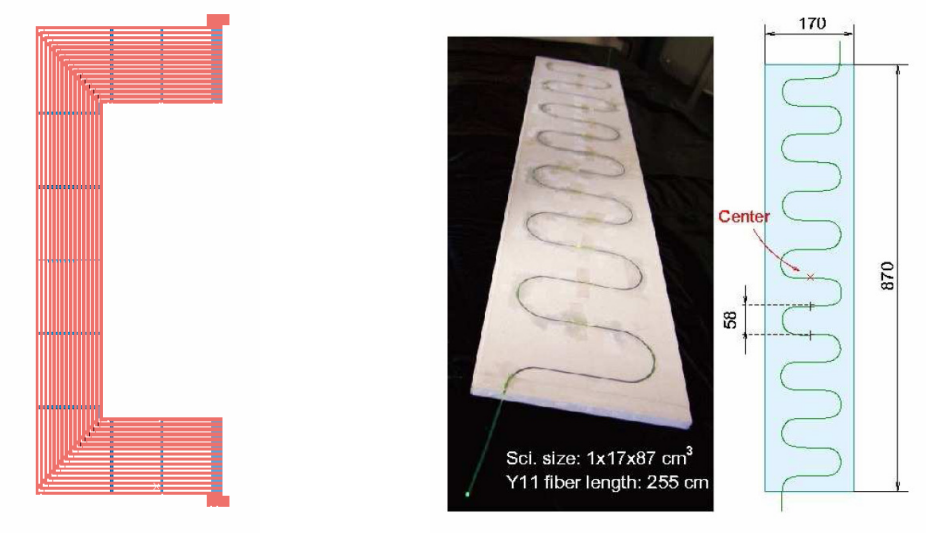

Fig. 25. On the left: one "C" of magnet yoke, vertical and horizontal slits are visible. On the right: a scintillator unit.

Calibration and monitoring role

One of the methods of the ND280oa detector calibration makes use of cosmic ray muons. It utilizes the fact that neutrino interactions in the detector occur only when beam spills arrive – no neutrino measurements are conducted between the consecutive spills. This allows us to perform other measurements in this in-between time.

The calibration measurements described here use cosmic ray muons as the calibration signal. The muons, produced in atmosphere as a result of cosmic ray interactions, cross the detector giving signal in SMRD at an average rate of 4600 counts per second [LA09]. One can verify operation of all subdetectors looking at the signals produced by traversing muons.

SMRD plays a role of a trigger in this procedure. A signal detected in scintillators in two different sides of the magnet (be it upper and bottom or left and right) indicates a passing muon. One can now verify if all the sensitive parts of the subdetectors in the basket on its way gave appropriate response. If some deviation from the expected response is observed, the element should be tuned to eliminate it. Detector efficiencies can also be determined this way.

The calibration is done once before the start of the experiment. Then, during its operation, the same procedure is used to monitor all the elements of the detector and to recalibrate or signal a necessary replacement of some of them when needed.

Veto role

When the spill arrives it is important to have the possibility to measure neutrino interactions only and to discard all other tracks that can possibly enter the detector from outside. As the SMRD is the outermost subdetector in ND280 complex, it is the most convenient tool for ruling out the unwanted 'garbage' tracks coming from cosmic ray muons and various products of interactions in the rock surrounding the 280m station pit. The exclusion procedure can be based on time relations between signals – the hits in SMRD will have earlier timestamps than hits in the inner detectors in the basket. The time resolution for SMRD is less than 2 ns, taking into account two signals from both ends of a scintillator [S10].

4.3.3 Configuration optimization

The spatial configuration of scintillators is limited by the yoke design. The yoke consists of two parts, left and right, each part is divided into 8 sections in the shape of a C letter (therefore called "The Cs"). One such "C" is presented in Fig. 25. The slits are arranged in columns called *towers*. Each tower has 15 layers of slits in it. Four towers are located in lateral parts; another four in upper and bottom parts. There are additional slits in the corners but these differ in dimensions from the others and are difficult to equip. Taking into account the above information, one can potentially have 120 modules per single "C" and 960 in the whole detector.

Due to financial constraints however, one cannot provide such a large number of scintillators. It is therefore necessary to optimize the scintillators' layout to maximize the detection capability while keeping the number of scintillators at a reasonably low level.

By the detection capability we mean:

- A capability that allows good reconstruction of muons produced in neutrino interactions, particularly those that cannot be reconstructed elsewhere,
- A capability enabling the detector to efficiently trigger calibration events (this amounts to the ability to see cosmic ray muons in the yoke), and
- A capability to veto tracks coming from the outside of the off-axis detector.

To answer the question how many scintillator modules should be installed in various parts of the detector, simulations of particle interactions in the detector have to be employed.

In this analysis we used NEUT neutrino generator and ND280MC simulation package. We assumed the detector is located 2.5 degrees off-axis and used suitable neutrino spectra for this off-axis angle. Since the electronics of the detector were not fully designed at the time the

analysis was conducted, we did not simulate electronics.

The signals induced by particles passing through scintillator units were carefully studied. The histogram of energies deposited by passing particles in each recorded hit is shown in Fig. 26. The peak for very small deposits is caused mainly by very short tracks of protons emerging from the iron, induced by neutrons coming from neutrino interactions. The neutrons can travel long distances (of a few meters) before interacting and creating a proton. Such small tracks wouldn't give a signal above a discriminator threshold (which will be optimized to get rid of dark noise) and they were excluded from further analysis (a deposit of 0.5 MeV was used as a threshold). One might also add here that the efficiency to get a signal from muon crossing the counter is close to 100%.

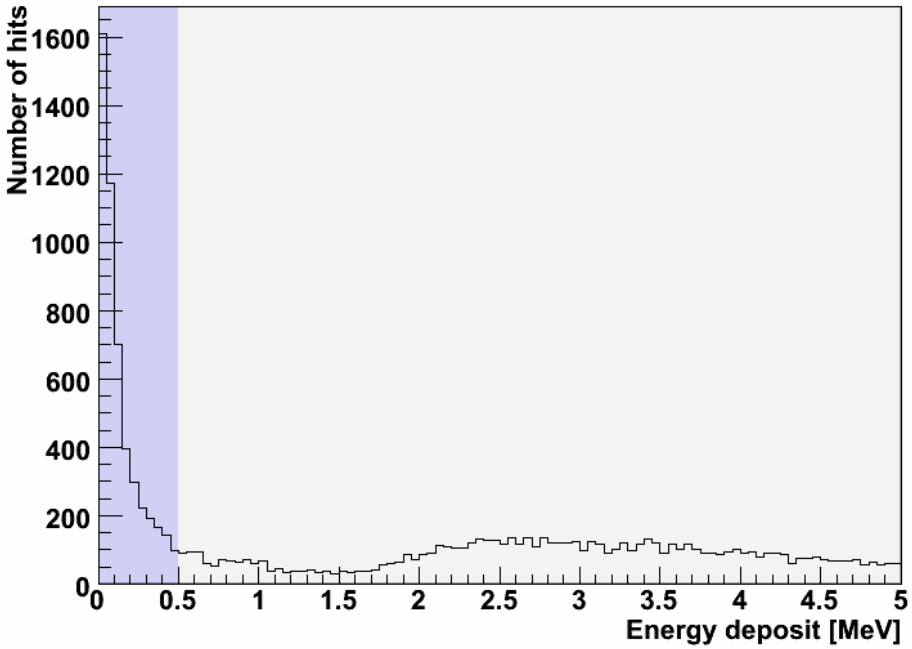

Fig. 26. Energy deposits per hit in the SMRD. A sample of 20,000 interactions in the basket was used to create this histogram. Hits in the shaded area (below 0.5 MeV) were discarded from the analysis (see the text).

As the ability to reconstruct muons coming from neutrino interactions is by far the most important role of the SMRD this was the main subject of optimization. To find out which regions of the subdetector are the most crucial for muon detection, one has to look at the number and energy of muons entering SMRD. As a convenient measure of the latter, we've chosen the *outermost layer* variable, i.e. we will simply check which layer of modules is reached by muon tracks, depending on ring and tower. This will give us an indication how

many layers are needed to reconstruct majority of tracks. The layers are numbered outwards: layer #1 is the innermost, closest to the basket.

4.3.4 Results

Some tendencies have been observed in distributions of outermost layer reached by muons. Three of them are significant:

- Forward – backward asymmetry – more muons are collected in the downstream parts of the detector,
- Lateral – horizontal asymmetry – more muons reach lateral parts of the magnet yoke,
- Up – down asymmetry – bottom parts are more populated than upper ones.

Forward – backward asymmetry

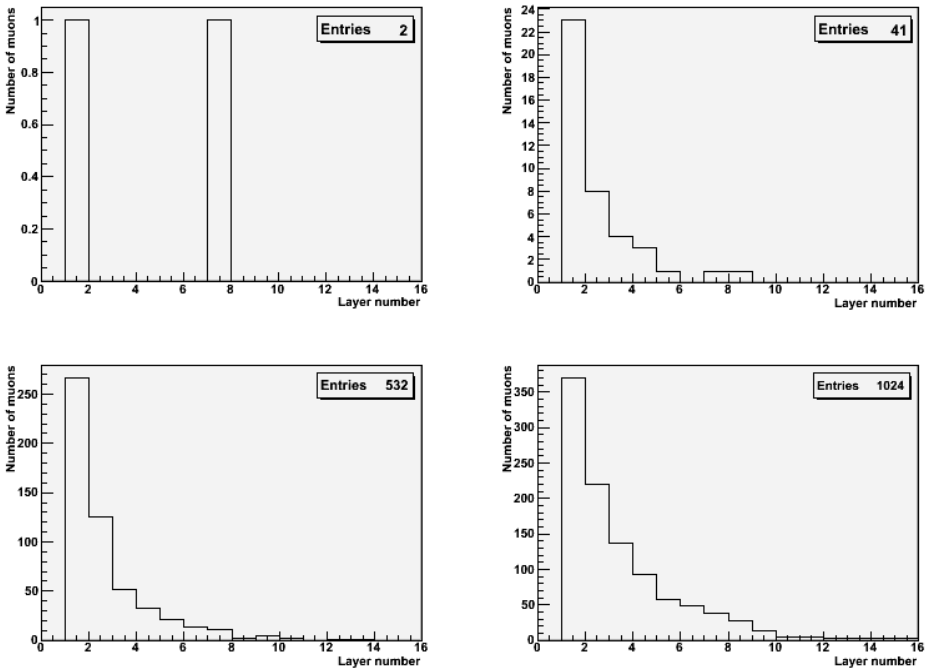

Fig. 27. Outermost layer distributions for a) rings 1 and 2 (most upstream), b) rings 3 and 4, c) rings 5 and 6, d) rings 7 and 8 (most downstream). The more downstream the ring is, the more abundant and energetic the muons are. Only QE events with muons that traveled less than 60cm in TPCs were taken into account.

This is the most obvious asymmetry, which is the result of total momentum conservation. A simple observation that a total momentum is dominated by momentum of incoming neutrino (directed along the axis of the detector) as compared with Fermi momentum of a target

nucleon leads to a conclusion that measured muons are more likely to go forwards than backwards – and indeed this is the case, as shown in Fig 27. One should keep in mind that the figure was plotted only for muons that come from interactions in FGDs, and not POD (which is situated upstream and therefore producing muons that are more populated in upstream rings of the magnet). However, SMRD plays no role in P0D measurements as the P0D is not designed for muon reconstruction; that is why only muons from tracker should be taken into account here.

The tendency in the number of events is coupled with the tendency in maximum outermost layer. One can see that muons are reaching farther layers in downstream rings of the yoke – the most energetic tracks will in vast majority be directed forwards.

Since in principle there should be no difference in number and energy of the tracks in left and right parts and upper and bottom parts, one can take advantage of the absence of the coil in the lateral parts and fully reconstruct only tracks there without loosing generality. This of course means some loss in term of statistics.

Lateral – horizontal asymmetry

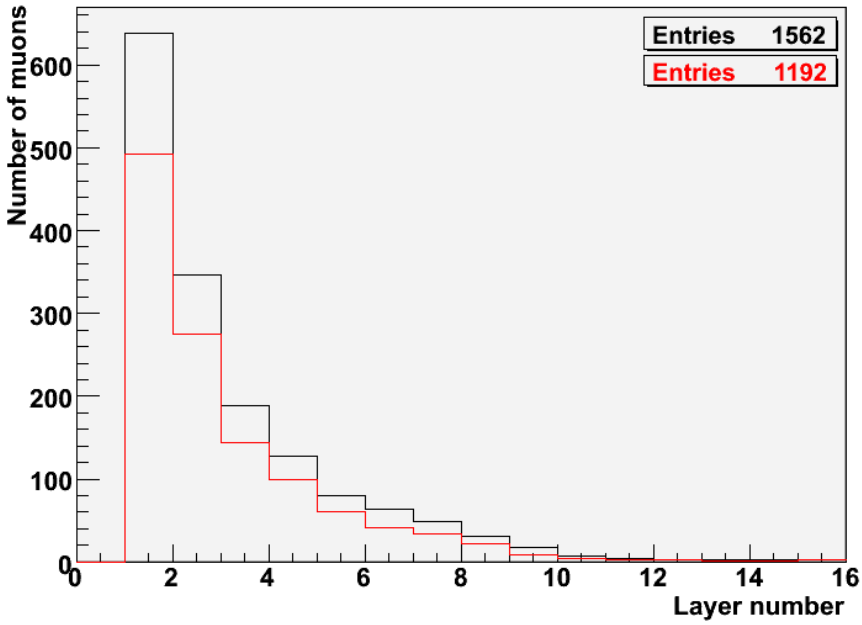

Fig. 28. Lateral – horizontal asymmetry in outermost layer distribution. Red histogram – muons in the lateral part of the yoke, black – all muons (the difference shows the contribution from top and bottom part events). Only QE events with muons that traveled less than 60cm in TPCs were taken into account.

As already described, the magnet coil separates the basket from the yoke from top and bottom sides. Aluminum shielding provided this way will slow down the muons, causing some of them to stop inside the coil, which will be reflected in less tracks collected and lower energy of those tracks in upper and bottom parts of the detector. This asymmetry is shown in Fig. 28. One can predict that more scintillator modules will be needed in lateral parts of the yoke to handle muons of higher energy there.

Up – down asymmetry

The last asymmetry is caused by the magnetic field present in the detector. The field strength is set at 0.2T and is directed along left-right axis. It is therefore bending positive tracks upwards, and negative ones downwards. Since the beam consists mainly of neutrinos (and not antineutrinos), and the tracks that reach SMRD are mainly muons, this causes most of the outgoing tracks to go towards the bottom part of the yoke (Fig. 29).

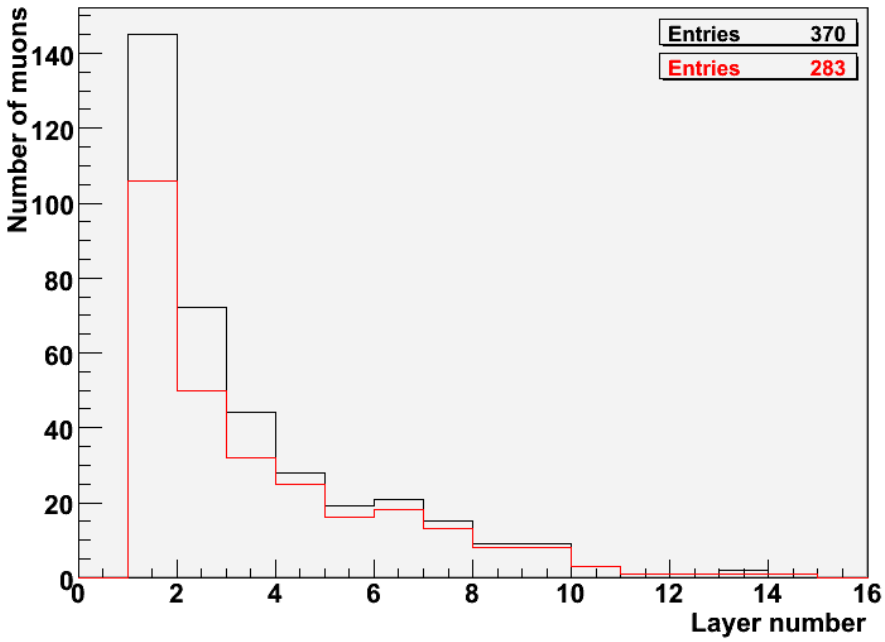

Fig. 29. Up – down asymmetry in outermost layer distribution. Red histogram – muons in the bottom part of the yoke, black – all muons (the difference shows the contribution from top part events). Only QE events with muons that traveled less than 60cm in TPCs were taken into account.

As stated before, SMRD will be used as a trigger for calibration and monitoring purposes. To trigger a calibration event, a muon has to be detected in two different sides (upper, bottom, left, right) of the yoke (see above). In order to maximize reliability of triggering a so called

2/3 logic has been devised:

- To give a subtrigger (a trigger in one part of the yoke), a muon has to light up at least two of three (or more) scintillator layers in a single tower located in that part
- Two subtriggers in different parts of the yoke add up to a calibration trigger discussed here.

For this method to work we have to have at least three layers of scintillators at hand in each side of the yoke.

Efficient veto operation requires at least one layer of scintillators in all the parts of SMRD.

All the requirements that follow from the above considerations can be summarized as follows:

- More scintillator layers are necessary in the downstream rings of the magnet, in particular rings 5-8 have to be equipped to serve the tracker,
- More scintillator layers are needed in the lateral parts of the yoke,
- More layers are needed in the bottom part
- All regions of the yoke should be equipped with at least three layers of modules.

How many layers is enough? To answer this question, let's look at the fraction of tracks reaching certain layers for all ν_μ CC events and QE ν_μ CC events (tables below).

All ν_μ CC	**Outermost over 4**	**Outermost over 5**	**Outermost over 6**
all	2.9%	2.1%	1.5%
With 60cm TPC distance cut applied	2.0%	1.4%	1.0%
With distance cut applied, only rings 7 and 8	1.6%	1.2%	0.9%

Table 3. Percentages of muons for given outermost layer thresholds. In this table data for all ν_μ CC events are shown.

Quasielastics are the most important class of events as they are relatively simple in reconstruction and will be used in majority of measurements. Percentages shown in the tables relate to total number of muon tracks produced in neutrino interactions (all and QE,

respectively). We've decided that a muon containment at a level of 99% for all events is acceptable. By choosing the number of layers at 6 in the forward part, only 0.7% of muons coming from CCQE events do not stop within the covered region of the magnet.

CC ν_μ, QE only	**Outermost over 4**	**Outermost over 5**	**Outermost over 6**
all	2.2%	1.4%	0.9%
With 60cm TPC distance cut applied	1.5%	1.0%	0.7%
With distance cut applied, only rings 7 and 8	1.2%	0.8%	0.6%

Table 4. Percentages of muons for given outermost layer thresholds. In this table data for ν_μ CCQE events are shown.

The final detector setup, taking into account all the above suggestions and financial constraints, is presented in the table below.

	Left/right		**Top/bottom**		**# of modules**
	layers	modules	layers	modules	
Ring 8	6	48	3	24	**72**
Ring 7	6	48	3	24	**72**
Ring 6	4	32	3	24	**56**
Ring 5	3	24	3	24	**48**
Ring 4	3	24	3	24	**48**
Ring 3	3	24	3	24	**48**
Ring 2	3	24	3	24	**48**
Ring 1	3	24	3	24	**48**
Total		**248**		**192**	**440**

Table 5. Final SMRD layout resulting from the optimization procedure described in the text.

The suggested layout of the scintillators has been accepted by T2K SMRD group and 440 modules were installed in the summer of 2009.

4.4 Intermediate detectors – 2km station

A proposed intermediate station would contain 3 detectors that are designed to supplement measurements carried out in the near detectors [H03]. It is not yet decided whether this station will be built – the experiment will start with near station only. In the course of T2K operation it will become clear whether this additional station is necessary.

The following arguments support the idea of 2km detectors [K05]:

- Intermediate station will be dealing with almost exactly the same beam profile as the Super-Kamiokande (see Fig. 30) - the spectrum at 280 m is distorted due to its proximity to the beam source (the source is not point-like from the 280 m perspective). This allows for various detector systematics to cancel by taking the far-near ratio.
- Systematics can be further limited, if the experimental technique is identical to the one used in far detector, i.e. water Cherenkov imaging. Intermediate station allows construction of small water Cherenkov detector, which would be impossible in 280 m station (event rates would be too high for a large Cherenkov device).

The intermediate station will be helpful in measuring beam profile and various cross-sections. According to a proposal (see Ref. [K05]) the station will consist of three detectors (Fig. 31). The biggest, 1 kT water Cherenkov, is designed to match Super-Kamiokande resolution. Its size is driven by two factors. It should be large enough to contain most muons which interact

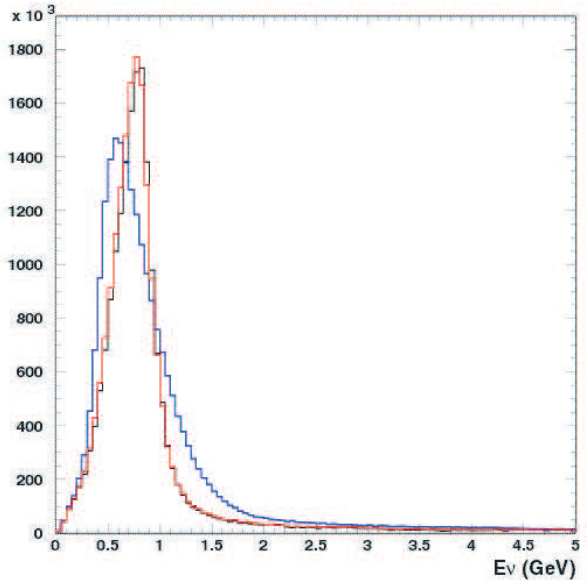

Fig. 30. The expected shape T2K neutrino spectrum at 280 m (blue line), 2 km (red line), and SK (black line). Figure taken from [K05].

inside the fiducial volume. At the same time it should be small enough to make sure there is no more than one neutrino interaction per spill on average (Cherenkov photons need some time to reach photomultipliers before next neutrino interaction occurs). The chosen size of the detector - 13.8 m long and 9.3 m in diameter – fulfils these requirements. The tank will be equipped with 5660 phototubes.

Muons that exit the water detector will be measured by a muon range detector situated downstream. This will increase accuracy of incident neutrino energy reconstruction. The proposed size of this detector is 7.6m x 7.6m x 5m. It will consist of 22 steel planes interchanged with sensitive elements – scintillator planes. In order to maintain a relatively constant energy resolution over the entire range of energies considered, the steel plane thickness increases as muon penetration increases.

Liquid argon imaging chamber is used in one of the studies described further in this thesis and so its construction is discussed in detail below.

4.4.1 Liquid argon TPC

A proposed liquid argon tracking detector is a time projection chamber (TPC) contained in a cylinder-shaped vessel approximately 8 m long and 7 m in diameter (Fig. 31) [K05]. The active tank, filled with liquid argon, is rectangular in cross-section; inside an uniform electric

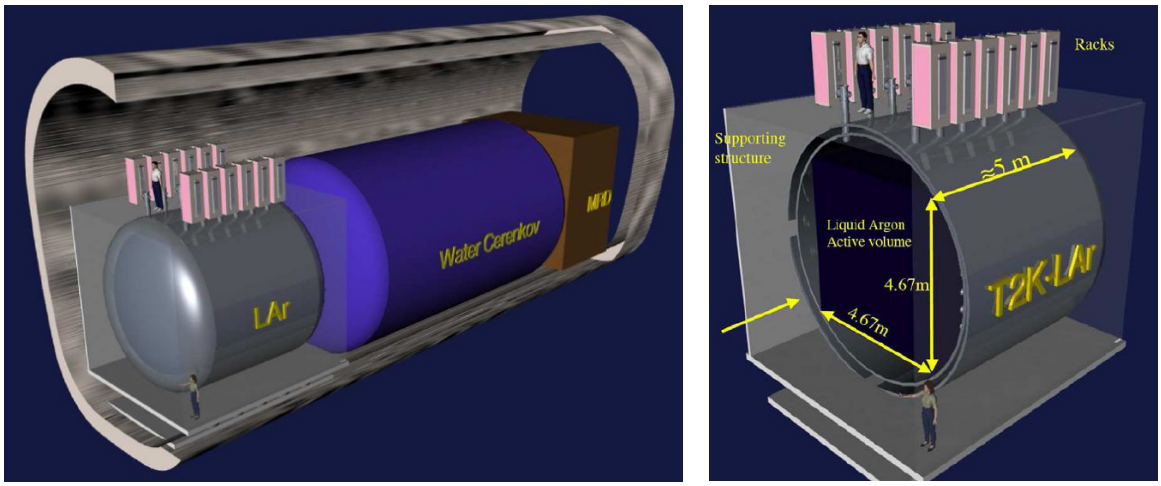

Fig. 31. Design of a) proposed 2km station (left) and b) its liquid argon detector (right) (from [K05]).

field is sustained between a cathode (in the middle) and walls. An option is considered to put a certain amount of frozen water into the cathode to provide a target material similar to the one in far detector. Two sidewalls are equipped with two or three wire planes with different wire orientations, constituting the read-out anodes. The detector is capable of recording tracks

of charged particles traversing the active liquid argon volume. Every such particle ionizes the medium and produces electron-ion pairs. The electrons are then transported towards the walls by the field present inside the detector. Electrons reaching the wires are recorded by all planes - they induce signals on the *induction planes* and are collected on the *collection plane*. Signal from wires in each plane can be presented as a two-dimensional image with one dimension being the wire number, and the other the time of flight of ionization electrons. Since the wires on each plane are oriented in different directions, the images obtained are different projections of events inside the detector. This allows for spatial reconstruction: one can take advantage of having two/three different views of the same event. The first step of the procedure is the hit identification on 2D images. A hit is a point of a track on 2D image. Then adjacent hits are grouped into larger structures, called clusters. Reconstruction ends with finding corresponding clusters on three projections and this way obtaining their position in space. Information from the collection plane is also used for calorimetric reconstruction; the charge of collected electrons is proportional to the ionization energy loss of the particle traversing the detector. This is of course only valid if the track in question is fully contained in the volume of the detector; for long tracks exiting the detector, a more suitable method utilizes multiple scattering analysis. The particle identification is based on examining the energy loss pattern of a particle.

Liquid argon TPC technique was first used and tested in ICARUS experiment [I04]. It has a lot of advantages: very good spatial resolution, possibility for precise reconstruction of event topology, particle type recognition capability and good calorimetric features. These allow for precise reconstruction of events and can lead to a good estimation of electron neutrino component in the beam and pion background estimation. It can also supplement measurements carried out using other detectors in the 2km station. The detector is also continuously sensitive which is important when rates are high.

4.5 Far detector – Super-Kamiokande

The Super-Kamiokande detector (SK in short) is the largest water Cherenkov detector in the world. It is located in Kamioka mine under Ike mountain in western Japan. A stainless steel cylindrical tank is placed inside a cavern made especially for this purpose (see Fig. 32). The tank is 41.4 m high and has a diameter of 39.3 m and during normal detector operation is filled with ultra-pure water. Inside there is a steel structure that supports photomultiplier tubes (PMTs) and splits the detector into two parts: outer (*outer detector*, OD) and inner (*inner*

detector, ID). These parts are optically separated by plastic sheets: black from inside, white from outside. Two kinds of photomultipliers are installed. The bigger ones, 20 inch in diameter, are facing inwards and serve the ID. There is 11,146 of them. The smaller ones, facing outwards, equip the OD. There is 1885 of them, each one of 8 inch in diameter. At the top of the detector, electronics are installed. There are two control rooms: one inside the mine and other in Mozumi village nearby.

The detection takes place in the ID. When a high energy charged particle propagates through a dielectric medium (water in this case) with its speed larger than the speed of light in this medium, Cherenkov effect occurs, and light is emitted by atoms excited by the passage of the particle. The photons form a cone around the particle's direction of motion. The opening angle of this cone can be determined by the following formula [P00]:

$$\cos \vartheta = \frac{1}{\beta n}, \ \beta > \frac{1}{n}$$

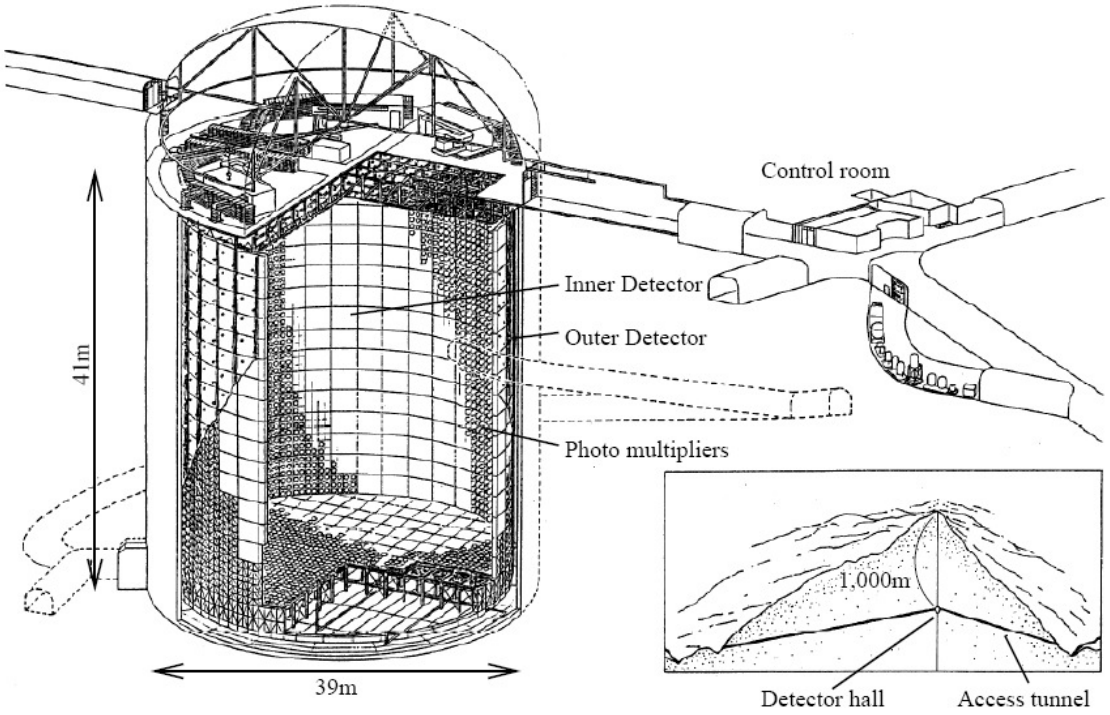

Fig.32. Super-Kamiokande detector, picture taken from Ref. [H03]

where n is the refractive index of the medium and β is velocity of the particle expressed in the units of speed of light in vacuum. For water (n=1.34) and relativistic particles the angle is about 42 degrees.

Light cones are detected by photomultipliers on the walls of ID in form of rings (circles). The

shape of a ring identifies a particle. Two classes of particles can be recognized in SK:

- *e-like* particles – electrons and gamma rays, and
- *μ-like* particles – muons and charged pions.

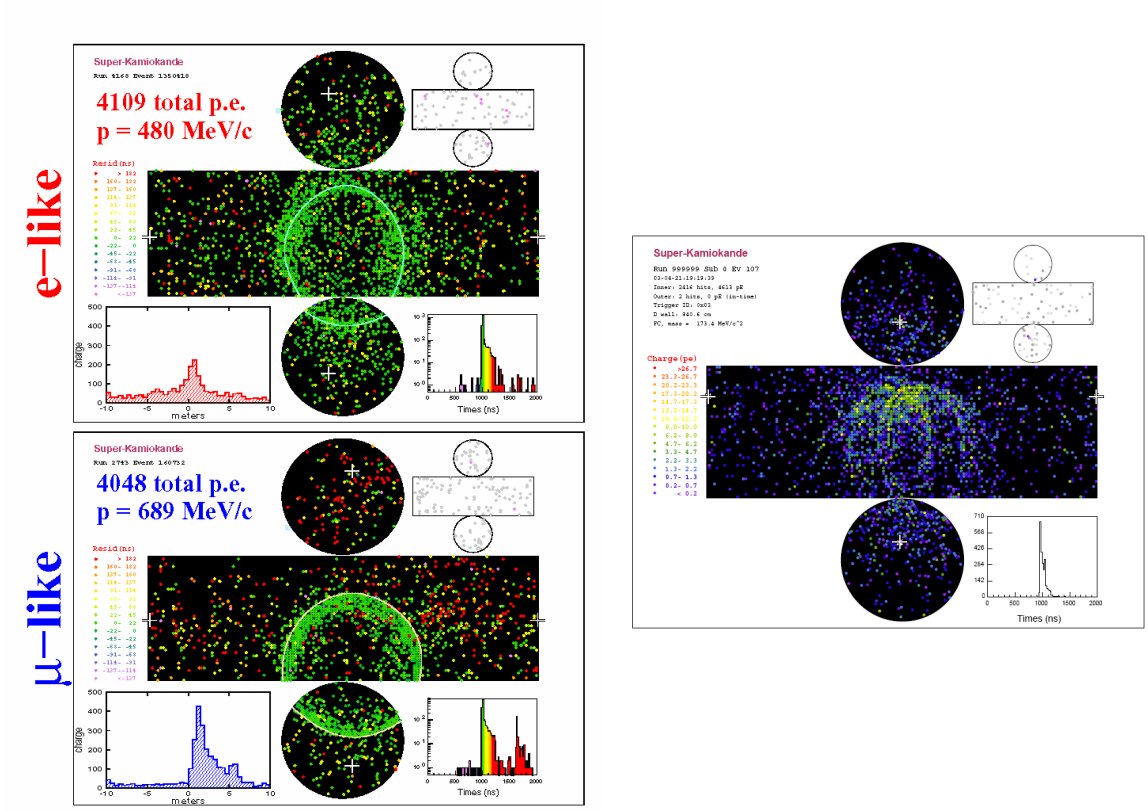

Fig. 33. Events in Super-Kamiokande detector. Left: two types of rings recognized in the detector . Right: an example of a neutral pion signature [K05].

The difference is visualized in Fig. 33. E-like rings are blurred at both edges (inner and outer) due to electromagnetic cascades initiated by a propagating electron. High energy γ quanta convert into electron-positron pair – in this case also cascades develop. The outer edge for μ-like rings is sharp, the inner is fuzzy, as the muon/pion after loosing a large amount of its kinetic energy is subject to Coulomb scattering which changes its direction. Topological information about rings is supplemented by timing information – this makes it possible to recognize muon decay events, in which a ring belonging to decay electron is recorded later than the main muon ring. For muons thickness of a ring is proportional to energy loss of the particle while it emits Cherenkov light (so called *visible energy*).

Particles emit Cherenkov light in water when their total energy is larger than roughly 1.5

times their mass. The threshold momenta are: for electrons – 0.57 MeV/c, muons – 118 MeV/c, pions – 156 MeV/c, protons – 1049 MeV/c. Neutrinos are tagged by observation of particles that are produced in their interactions with water, usually leptons (muon or electron). Most of the protons produced by neutrinos of the considered energies are below the Cherenkov threshold, so usually the only visible particle is the lepton. Such situation is an example of a *single ring event*, the most numerous and easiest to reconstruct class of events in SK.

Neutral pions are recognized by their decay into two gammas. Those convert and create showers, visible as e-like rings in the detector (see Fig. 33, right). For energetic pions, those two showers are close to each other and the rings overlap, making them hard to distinguish from a single electron ring.

If the particle exits the detector while emitting light, its total energy cannot be determined (it leaves a ring without inner border) – such events are called *partially contained* (PC). If all particles stop inside the detector, the event is called *fully contained* (FC).

To eliminate interactions that happen outside of the inner detector, the OD is used. If a track is visible in the OD before it is seen in the ID, it is a sign that the particle entered the detector rather than was produced inside. Additionally, a fiducial cut is applied, restricting the fiducial volume of the detector to 22.5 kiloton of water to discard events caused by radioactivity of surrounding rock and cosmic muons. However, thanks to being situated at the depth of 2700 m water equivalent, the detector is shielded from most of unwanted cosmic ray background.

Super-Kamiokande started working in 1996 as a standalone experiment, detecting solar and atmospheric neutrinos. It discovered neutrino oscillations in its atmospheric neutrino data in 1998 [F98]. It was also used as a far detector in long baseline neutrino oscillation experiment K2K. It is a well studied detection device, with very well understood backgrounds. As such it is an ideal far detector for T2K experiment.

In 2001 Super-Kamiokande suffered a massive PMT loss due to an accident during refilling after reconstruction works [D04]. In 2004 data taking was resumed with half of the photomultipliers installed. In 2006 the rest of the PMTs was put again in place and the detector returned to its original form.

Reconstruction works are performed every couple of years to replace defective PMTs, provide new plastic insulation between ID and OD, etc. Two people from Warsaw Neutrino Group (including the author of this thesis) took part in 2006 refurbishment, when aside from normal

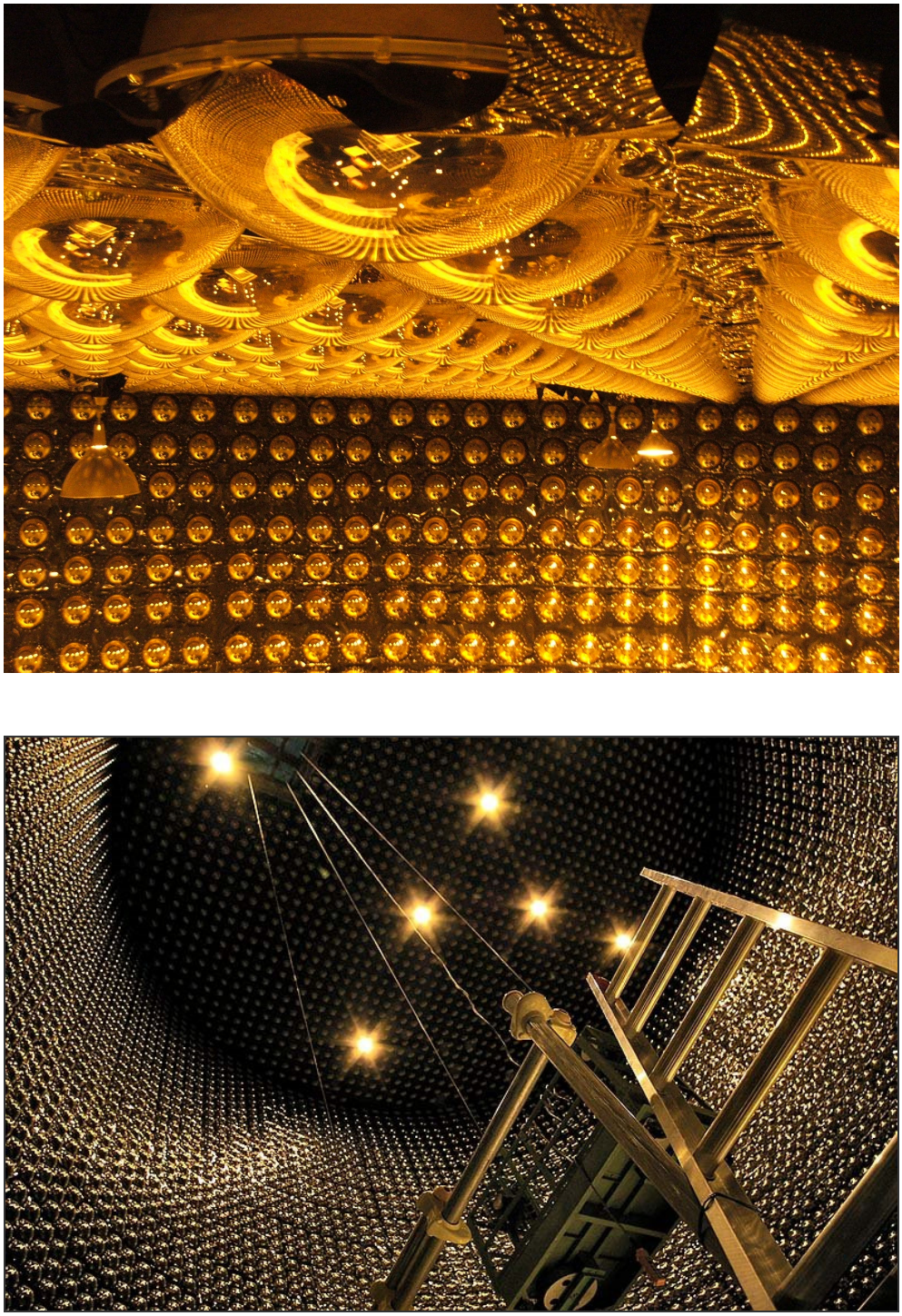

Fig. 34. SK detector during reconstruction in 2006 (water is drained from the detector volume). Photomultipliers and black plastic insulation is visible. Upper photo by Paweł Przewłocki, lower photo by Piotr Mijakowski.

reconstruction works the PMT coverage was restored to its original level from before the accident. Two photos of the detector during these works are shown in Fig. 34.

Chapter 5
On reconstruction of some kinematic variables

After data have been collected and stored, the process of reconstruction has to take place. In case of ND280oa detector it consists of several steps, including translation of electronics' signals into hits (the smallest units of detection), organization of the hits into tracks, obtaining energy, momentum and other quantities for those tracks, and inferring information about features of the whole event.

Reconstruction hinges heavily on precise knowledge of detector response settings, which is why calibration is a necessary prerequisite of reconstruction. The response will be carefully monitored in the course of experiment, and reconstruction software will be aware of any changes reported by the monitoring tools.

In ND280oa, the oaRecon package (bundled with the ND280MC official simulation) is responsible for reconstruction. First, reconstruction is made for all subdetectors separately; then, the results are combined using methods available in RECPACK, a toolkit developed for reconstruction in High Energy Physics [C04].

5.1 Neutrino energy reconstruction

5.1.1 Introduction

T2K detectors deal with neutrinos from the beam. In case of neutrino interaction, one can observe only some products (electrons, muons, hadrons), not the neutrino itself. Properties of incident neutrino have to be therefore inferred from the available observables – directions, momenta and energies of observed particles. As incident neutrinos are coming from the beam, their direction is known and the only quantity necessary to reconstruct is the energy (or momentum - neutrino mass can be neglected).

Detection techniques differ from near to far detectors – different particle types are visible in the detectors, the accuracy of determining momentum and energy is not the same. In this chapter we will focus on neutrino energy reconstruction in ND280oa detector, though many remarks below can also be applied to Super-Kamiokande.

Neutrino energy reconstruction will be used in beam spectrum determination and cross-section measurements in the Tracker. Such measurements are based on CC interactions and mainly CCQE events, which are numerous and the easiest to reconstruct precisely, thus introducing small systematic errors. For T2K energy range, protons in such reactions are frequently impossible to reconstruct as they carry too little energy.

Two methods of neutrino energy reconstruction were taken into account:

- Neutrino energy reconstruction using total momentum of outgoing interaction products – *total momentum method.* Since the total momentum is conserved in an interaction, one can calculate total momentum of products which will be (with some assumptions) equal to the momentum of neutrino. It is the simplest method, but to be precise it requires the target nucleon to be at rest (no Fermi motion) and all particles to be visible and their momenta reconstructable.
- For CCQE events, one can propose another method of neutrino energy reconstruction - *QE method*, treating the interaction as a two-body process. Value of momentum and direction of outgoing muon only determines the final state; using these properties one can calculate energy of incoming neutrino according to the following formula:

$$E_\nu = \frac{m_N E_\mu - m_\mu^2 / 2}{m_N - E_\mu + p_\mu \cos\theta_\mu}$$

  assuming that the nucleon in the initial state is at rest (m_N is the target nucleon mass, m_μ, E_μ, p_μ are mass, energy and momentum of the outgoing muon respectively. θ_μ is the angle between muon track direction and beam axis). Binding energy is not taken into account in this formula, but it does not affect the results significantly. This method is applicable only to CCQE events for which the muon is correctly tagged and reconstructed. This (in conjunction with proper identification of the event as CCQE) is, however, usually easier than reconstructing all of the products as it is needed in the total momentum approach.

To verify the extent to which both methods are reliable and applicable for T2K beam and in ND280oa, simulations of neutrino interactions have been performed using Nuance 3.006 neutrino generator. Water was used as a target as significant fraction of events studied in the Tracker is an effect of interactions in water tanks in second FGD.

A total of 500.000 events were generated in two samples: with and without FSI. Samples without FSI are easier to study and are a main tool in verifying reconstruction methods here, but real-life reconstruction has to take into account events with FSI. FSI influence the number

(due to absorption and other processes) and momenta of hadrons exiting the nucleus and thus usually degrade reconstruction quality in the total momentum method.

5.1.2 Reconstruction quality

For quality evaluation let's introduce here a scatter plot which we will be using throughout this chapter. Two examples of such a plot are visible in Fig. 35. True value of neutrino energy (known from the simulation) is shown on the horizontal axis, the reconstructed value – on the vertical axis. Ideal reconstruction would amount to the points evenly aligned on the diagonal line across the plot. The larger the distance from the diagonal is, the worse is the reconstruction.

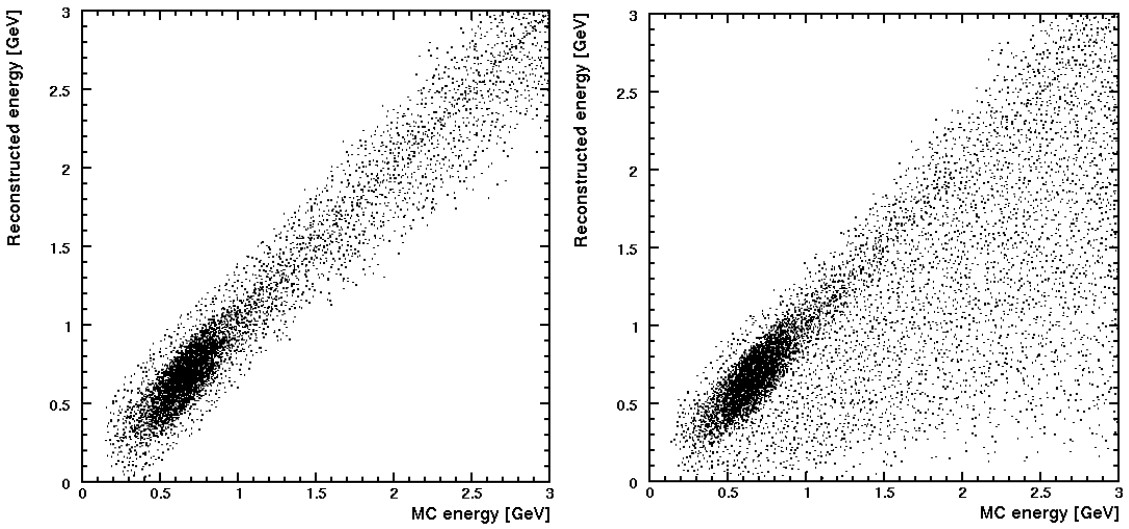

Fig. 35. Quality of reconstruction of total momentum method, CC events. Left – all final state particles considered visible, right – with simple visibility criteria as described in the text.

Fig. 35, left shows the quality of reconstruction using total momentum method, when all the particles are assumed visible and ideally reconstructable. Even with these strong assumptions one can see some smearing of the energy – this is due to Fermi motion of the target nucleon.

To make the situation more realistic, we introduced simple visibility criterion by narrowing the list of visible particles to muons, electrons, protons, neutral and charged pions. Muons (and to smaller extent charged pions) have usually long tracks and are easily tagged and measured in the tracker, electrons produce electromagnetic showers; neutral pions in most cases decay into two gammas, each of them resulting in the similar electromagnetic shower.

Some protons can be reconstructed in FGD. To keep the criteria simple, we do not use cuts on particles' range.

Invisibility of some particles deteriorate the reconstruction quality – this is clearly visible in Fig. 35, right. This effect is mainly caused by the fact that neutrons are not visible under the criteria described above. Neutrino energy for a large fraction of events is underestimated, because of the invisible momentum in the final state.

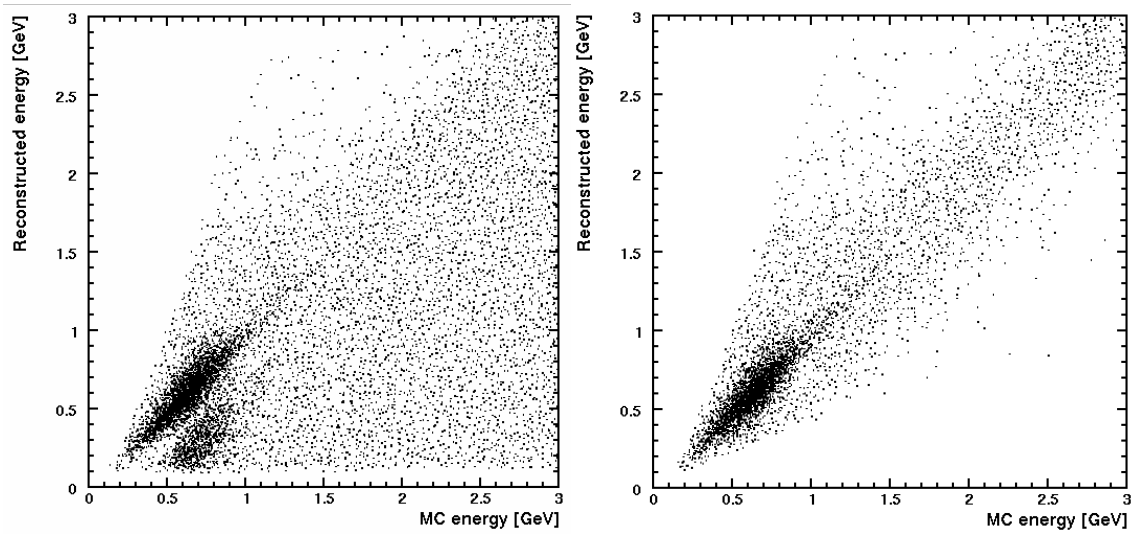

Fig. 36. Quality of reconstruction of QE method, CC events. Left – all CC events, right – CCQE events. Visibility criteria play no role for QE method (as long as the muon is considered reconstructable).

Reconstruction results with the QE method are shown in Fig. 36. It relies solely on muon reconstruction, so in some cases it may turn out to be better than the total momentum method. In particular it is totally independent of visibility assumptions introduced before, as it influences only hadrons. It would be ideal to use this method only for CCQE events, but problems with visibility of low energy protons and pions make it difficult to select a pure sample, so the results are shown here both for all and CCQE events. Left-hand side of Fig. 36 presents the overall result, similar in some degree to the plot for total momentum method (many events with underestimated energy). One can see a cluster of events in lower energy range just below the diagonal – these events' energy was miscalculated because they were non-QE events (the plot for QE events only is shown on the right-hand side). The best reconstruction is achieved for CCQE events, however one observes smearing that can be again attributed to existence of the Fermi motion of target nucleon (the impact of the Fermi motion is not as straightforward as in the previous case though – see next section).

To finalize this stage of analysis, we will compare both methods using distributions of a measure defined as a relative difference between real and reconstructed energy:

$$\delta E = \frac{E_{reco} - E_{true}}{E_{true}}$$

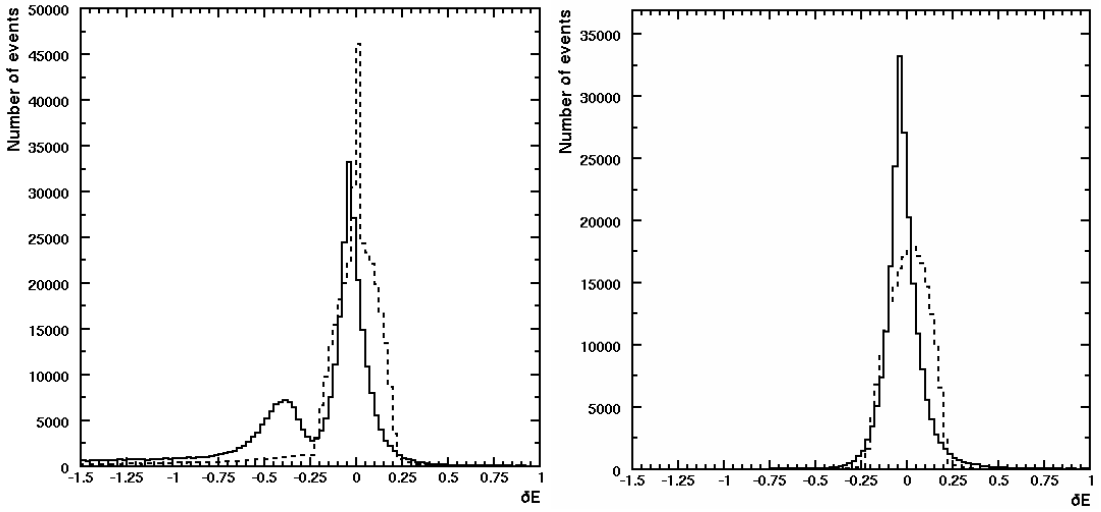

Fig. 37. Reconstruction quality comparison – distribution of δE variable described in the text. Solid line – QE formula, dotted line – total momentum formula. Left – comparison for CC events, right – comparison for CCQE events.

Fig. 37 compares both discussed methods in two event classes: CC events (left-hand side) and CCQE events (right-hand side). Wider shape for QE method (solid line) in the CC case suggests inferiority of this method to the total momentum one. On the contrary, in the CCQE event domain, the QE method unsurprisingly takes the lead over the total momentum, as it the best suited for this type of events.

One should keep in mind that in the above analysis it was assumed that all visible particles can be perfectly reconstructed, in terms of their energy and direction. If they are not, it is more likely to worsen the total momentum results, as it is dependent on reconstructability of different types of particles; QE method relies only on reconstruction of muons, and these are relatively easy to handle and the reconstruction errors should be relatively small.

Taking into account all the advantages and drawbacks of the two methods described above one can try to set up an optimal reconstruction procedure that could look like the following:

- if an event can be qualified as CCQE (one muon, one proton), then use QE method,
- for all other CC events, use total-momentum method.

If one is able to separate CCQE and CCnonQE events efficiently, it makes no sense to use total momentum method in the CCQE class.

5.1.3 Errors in the QE method

When looking at the Fig. 37, right one can notice that errors of QE method for CCQE events are sometimes much larger than for total momentum method with ideal particle visibility assumption – δE for QE method easily exceeds ±25% while there are almost no points for total momentum method in this region. It is also visible in comparison of Fig. 35, left and 36, right (the spread of points in Fig. 36, right is significantly larger). The inaccuracy of total momentum reconstruction is caused by the Fermi momentum of target nucleon that is not taken into account. Below we will study intricacies of the QE method to a greater detail to see what causes the large discrepancies in this case. In order to do this, a simple CCQE neutrino simulator was created. A neutrino, with a given momentum was scattered off a nucleon. Two simulations were made: one without and one with inclusion of Fermi motion. For a second sample Fermi momenta were chosen at random from a flat distribution ranging from 0 to 250MeV. The distribution of muon production angle in the center-of-mass frame was assumed to be flat for simplicity. For each interaction, properties of outgoing muon and proton were calculated.

The QE method formula:

$$E_\nu = \frac{m_N E_\mu - m_\mu^2 / 2}{m_N - E_\mu + p_\mu \cos\theta_\mu}$$

depends on two independent variables, momentum and cosine of the deviation angle (θ) of the muon. It can be also formulated as a function momentum and its z component. Fig. 38 shows curves for different incoming neutrino energies in those two variable spaces (Fermi motion is not included here). Each point on those plots corresponds unambiguously to a certain neutrino energy. One can also note that only points within grey areas correspond to physical neutrino energy values. Fig. 39 presents the curve for 3 GeV but with Fermi motion included – this results with a large smear. One can notice (comparing the plots), that some smeared points are close to the region boundary, corresponding to infinite reconstructed energy. This boundary is a singularity, and a gradient of neutrino energy values is very high in the region close to it. This explains why the discrepancies are so large (smear towards the opposite direction doesn't create such large errors, as the reconstructed energy decreases, and cannot be lower than zero).

The region on the left of the right plot in Fig. 38 is forbidden because absolute value of the longitudinal, z component must be lower or equal to the total momentum. Furthermore, transversal momentum of the muon has the maximal value that depends on the energy available in the center-of-mass system – Lorentz boost cannot change it, as it goes along the longitudinal axis. If transversal momentum has the maximum value, the z component of momentum has to have a minimal value for a given total momentum of the muon, hence the second constraint to the right of the allowed area on both plots.

Approaching this problem in a different way, we can once again look again at the QE method formula and find an equation for infinite neutrino energy by requiring its denominator to be equal to zero:

$$m_N - E_\mu + p_\mu \cos\theta_\mu = 0$$

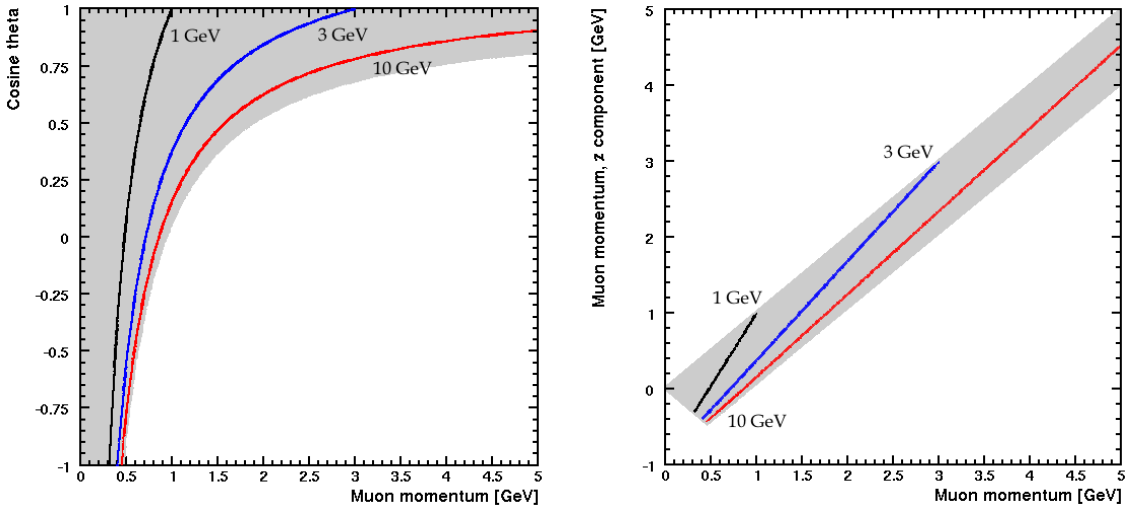

Fig. 38. Neutrino isoenergetic curves in two variable spaces: left – muon momentum vs. cosine of muon deviation angle, right – muon momentum vs. its z component. Lines denote variable values for specified incoming neutrino energies: black - 1 GeV, blue – 3 GeV, red – 10 GeV. Fermi motion is not included in this simulation. Grey area shows the physical region. Combinations of values corresponding to the points inside the white region are impossible.

Assuming relativistic correspondence between energy and momentum:

$$E^2 = m^2 + p^2$$

one can see that the solution can be presented as a line on the plots shown above. Indeed, reformulating it as a function of cos θ gives

$$\left[1-\cos^2\theta\right]p^2 - 2m_N\cos\theta\, p + \left[m_\mu^2 - m_N^2\right] = 0$$

Solving this quadratic equation leads to the following result:

$$p(\cos\theta) = \frac{m_N \cos\theta \pm \sqrt{m_N^2 - m_\mu^2(1-\cos^2\theta)}}{1-\cos^2\theta}$$

One result of the two can be discarded as belonging to the non-physical region (negative value of momentum).

The above consideration can be further extended to find $p(p_z)$ by noticing that:

$$\cos\theta = \frac{p_z}{p}$$

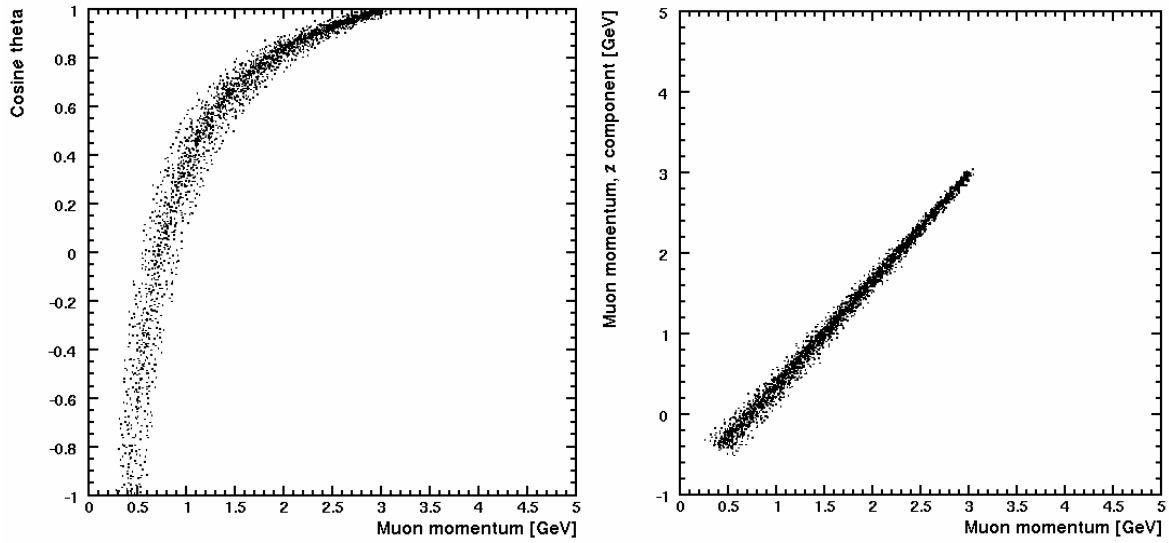

Fig. 39. Effect of Fermi motion inclusion on the isoenergetic curves. The plots show reconstructed neutrino energy in the two variable spaces (see Fig. 38). This simulation was carried out for incident neutrino energy of 3 GeV (corresponding to the blue curves in Fig. 38).

Then:

$$p(p_z) = \sqrt{(m_N + p_z)^2 - m_\mu^2}$$

and taking into account that m_μ^2 is small in comparison to all other quantities in this formula, we can get an approximate linear relation:

$$p(p_z) = m_N + p_z$$

The curves resulting from these calculations are constraining gray areas in Fig. 38. from the right. As it can be seen (and was already said), they form a singularity, and in its vicinity the neutrino energy gradient is large and introduces large errors when Fermi motion smear is taken into account.

As a conclusion we should state that it is advisable not to take into account the events lying close to the infinite neutrino energy curves. Such events should probably be reconstructed using total momentum method.

5.2 Four-momentum transfer (Q^2) reconstruction

5.2.1 Introduction

Q^2 variable – four-momentum transfer squared – plays a significant role in modeling neutrino interactions. Cross-sections for neutrino interactions on nucleons depend on model-dependent form factors which are functions of Q^2. Weak form factors can be measured only in neutrino interactions. Cross-section measurements are also usually presented as a function of Q^2. Therefore, in this section we will study the possibilities for accurate Q^2 reconstruction and try to find potential problems associated with it.

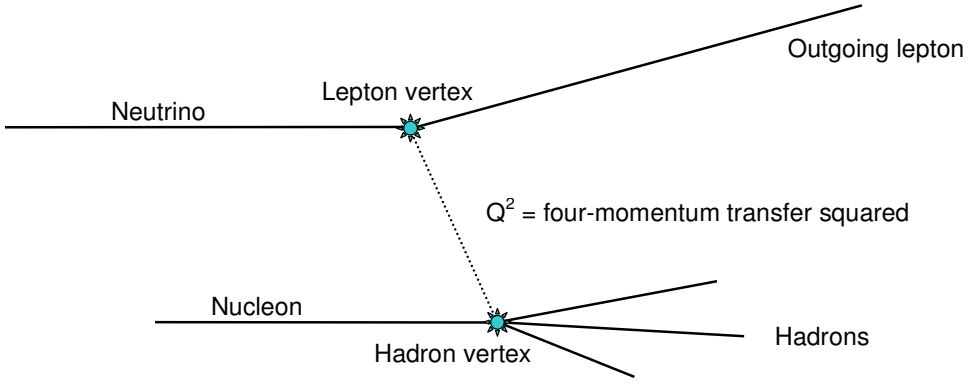

Fig. 40. Scheme of neutrino interaction with hadron and lepton vertices indicated.

To define Q^2 let's look at the simplest picture of neutrino interaction (see Fig. 40). A neutrino scatters off a nucleon producing a charged lepton and some hadrons. Q^2 is defined as a squared four-momentum transfer between *lepton vertex* and *hadron vertex*. If all properties of initial and final states are known, Q^2 can be calculated in two ways, one utilizing particles in lepton and one in hadron vertex.

To be more specific, a four momentum transfer squared is defined as squared length of four-momentum vector in question:

$$Q^2 = E^2 - \left(p_x^2 + p_y^2 + p_z^2 \right)$$

One can write the formula using lepton vertex variables:

$$Q^2 = (E_\nu - E_{lep})^2 - \sum_{i=1,2,3} (p_{i\,\nu} - p_{i\,lep})^2$$

or hadron vertex variables:

$$Q^2 = (E_N - E_{had})^2 - \sum_{i=1,2,3} (p_{i\,N} - p_{i\,had})^2$$

where *N* index denotes nucleon, *had* index denotes hadronic (i.e. coming out of hadron vertex, e.g. p_{had} is total momentum of all particles coming out of this vertex) and *lep* index - leptonic. Neutrino goes along the beam line, so it has only one momentum component, p_z. Initial momentum of nucleon is its Fermi momentum.

In a real physical experiment, neutrino energy (equal to momentum) and Fermi motion of target nucleon are unknown. In order to reconstruct Q^2 one has to either reconstruct neutrino energy (and take into account errors emerging in the reconstruction process) for lepton vertex reconstruction, or assume that Fermi motion is negligible (as the values are in low hundreds of MeV, which is small in comparison with neutrino energies typically around 1GeV) and try to reconstruct the variable using hadron vertex. We will pursue the latter approach and compare obtained results with values calculated for lepton vertex utilizing variables available in the Monte Carlo. NUANCE 3.006 neutrino generator was used in the analysis. Two 500.000 muon neutrino event samples for T2K beam were created, with and without FSI. Let us emphasize that the generator always takes into account Fermi motion of target nucleons.

5.2.2 Q^2 reconstruction quality

To start verifying reconstruction quality, one has to assume certain detector capabilities in determining various properties of particles. We will now assume perfect reconstructability of all particles to evaluate impact of neglecting target's Fermi momentum. We'll revise this assumption later to take into account more realistic situations.

Fig. 41, left presents a comparison of reconstructed values of Q^2 (FSI not included). Solid line represents lepton vertex calculations. These include values that can be known only from simulations – we'll therefore call it *ideal* Q^2. The dashed line on the other hand refers to hadron vertex calculations, where Fermi momentum has been neglected. This is an *observable* Q^2. The comparison shows some effect of the absence of Fermi motion in calculations (Fermi motion was included in the simulation) – the observable Q^2 is visibly smeared, with some of the events even falling below zero.

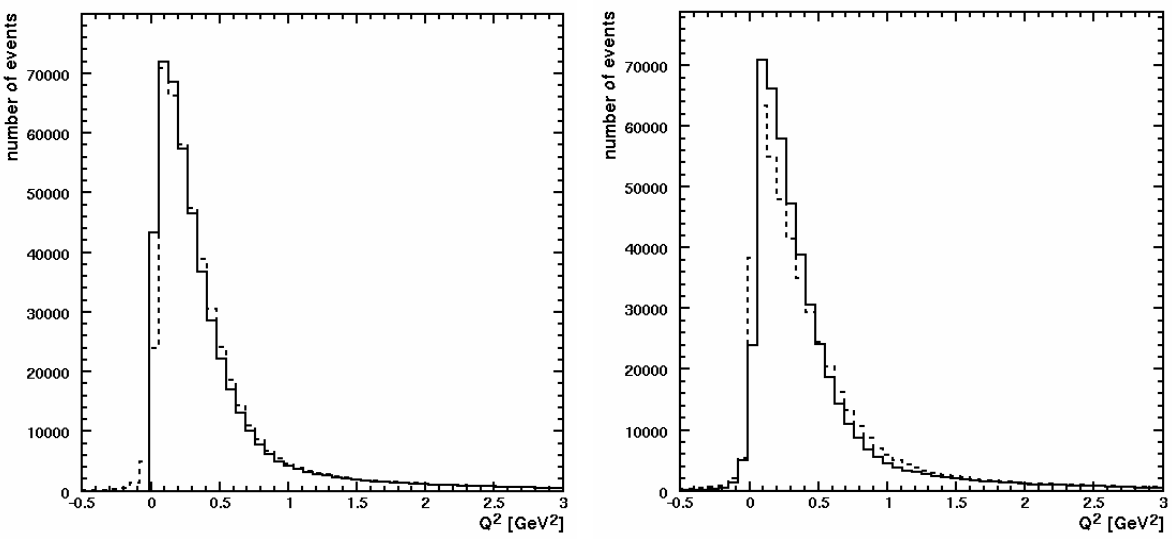

Fig. 41. Comparisons of Q^2 distributions for all neutrino interactions. Left: Ideal (solid line) and observable (dashed line) Q^2 for all events in the 'no FSI' sample. Right: Effects of FSI - observable Q^2 for 'no FSI' (solid line) and 'FSI' (dashed line) samples.

Inclusion of final state interactions adds another smearing factor which is visible in Fig. 41, right. It presents observable Q^2 for 'no FSI' and 'FSI' samples. The smear introduced by FSI is comparable with the impact of neglecting Fermi motion. It is probably caused by vanishing of some momentum in the reinteractions (pion absorption, etc).

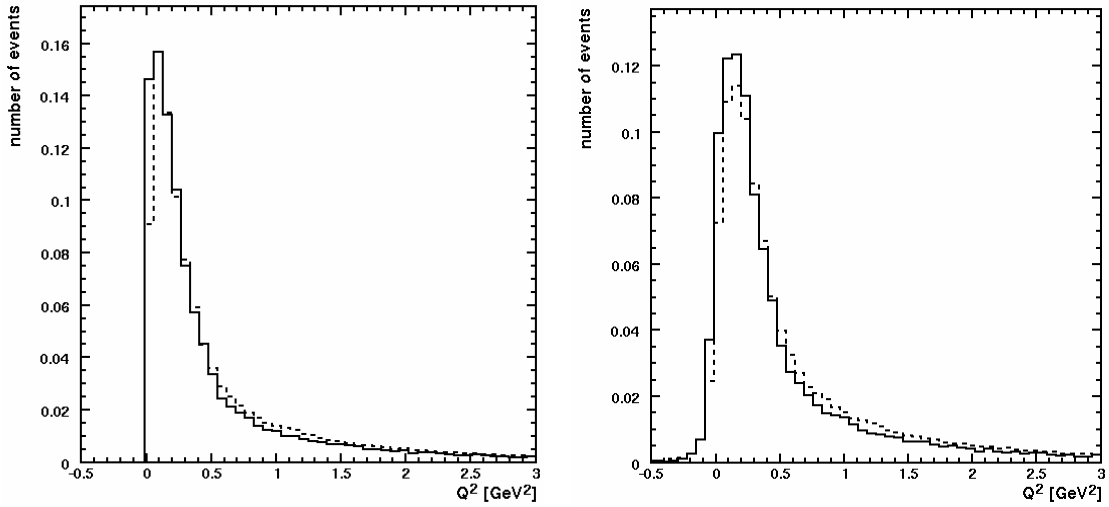

Fig 42. Shape comparison of Q^2 distributions of NC π^0 production (solid line) and CC π^+ production (dashed line) events for 'no FSI' sample. Left – ideal Q^2, right – observable Q^2. Distributions are normalized to 1.

Another objective was to study differences in Q^2 distributions for different pion production channels. We studied two channels:

- $\nu_\mu + p \to \mu^- + p + \pi^+$, $\nu_\mu + n \to \mu^- + n + \pi^+$ (CC π^+ production), and
- $\nu_\mu + p \to \nu_\mu + p + \pi^0$, $\nu_\mu + n \to \nu_\mu + n + \pi^0$ (NC π^0 production).

The results are presented in Figs. 42 and 43. Fig. 42 presents results for 'no FSI' sample. The distributions are very similar, with CC events having a little larger average. Inclusion of FSI changes the situation, because some of the pions get absorbed in the nucleus (causing many events to be classified as belonging to different channels than in the 'no FSI' case). This changes the normalization of both distributions, causing the number of events to decrease significantly which is visible on both plots in Fig. 43. We also observe further smearing of both distribution shapes.

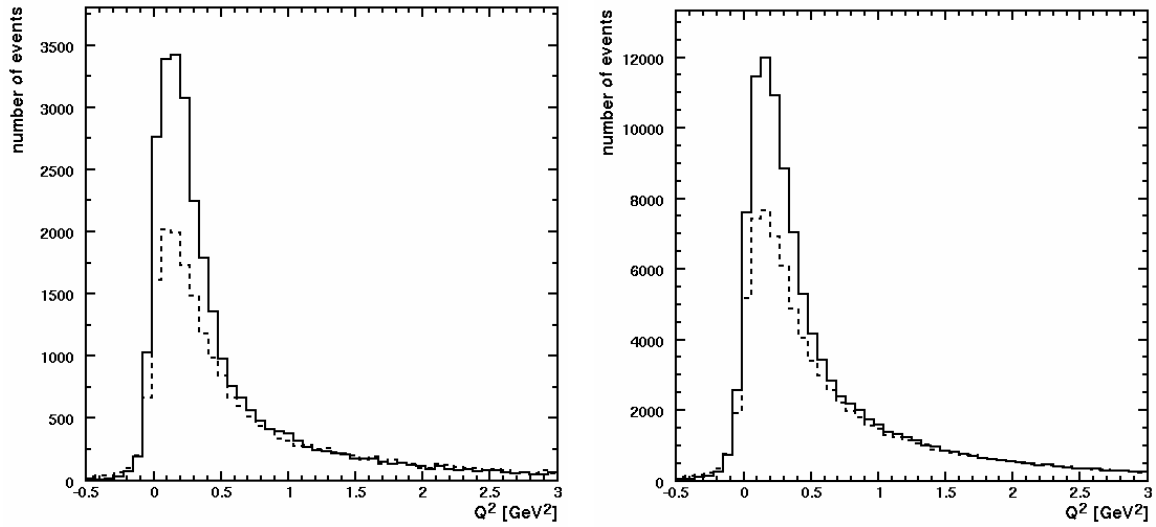

Fig 43. Q^2 comparisons for 'no FSI' (solid line) and 'FSI' (dashed line) samples. Left – NC π^0 production, right – CC π^+ production. Most of the events we lose when going from 'no FSI' to 'FSI' case are identified as QE, due to pion absorption.

Summarizing this section, one can say that we observe small differences between two reconstruction methods and samples with and without FSI if we take into account all events. If only pion production interactions are selected, the main impact on normalization and shape of the Q^2 distributions has selection rather than reconstruction methods. Q^2 distributions for both pion production channels are similar, regardless of reconstruction method. Number of

events however change, when comparing samples with and without FSI. It is important to note that all these considerations do not take into account detector visibility effects, which can have a dramatic impact on observable values. We will consider these effects in the next section.

5.2.3 Visibility analysis

We have already seen what problems we face when reconstructing Q^2. Now we will take into account detector effects and find out how they change observed Q^2 distributions. We will focus on modern high-precision scintillator detectors like P0D and FGD used in ND280oa. To make our considerations generic, we will not use any specific detector simulation. Instead, some cuts will be imposed on data to mimic behavior of scintillation detectors. This will enable us to determine which tracks are visible in the detectors.

Subdetectors in question consist of scintillator planes and (in some parts) water layers (used as a principal target). Each scintillator plane consists of several polystyrene bars aligned in the same direction (see Chapter 4 for details). A particle has to traverse two perpendicular planes to have its position determined in three dimensions. The number of traversed double X-Y planes is the number of tracking points recorded in the detector. The higher the number of points, the better identification and reconstruction of a particle track. In general one needs at least two points to say something about a track (usually it has to be more).

Track length	**Proton momentum cut**	**Charged pion momentum cut**
6cm	400 MeV/c	110 MeV/c
10cm	450 MeV/c	120 MeV/c
14cm	500 MeV/c	130 MeV/c
18cm	550 MeV/c	140 MeV/c

Table 6. Track length cuts and corresponding momenta for protons and charged pions. Momentum values are approximate. See description in the text for details.

Let's consider P0D and FGD as an example. These two detectors differ in thicknesses of the layers. In P0D one scintillator – water layer (a P0Dule) is 6.5 cm thick; in case of FGD this thickness amounts to 4.5 cm. Since the minimum track length depends on the detector, we have chosen to take into account several possible cuts, each for different length of track. The

above table presents the cuts, along with the associated momenta for pions and protons in water. They were calculated using range-energy curves from [A08].

The cuts are performed on the z component of momentum which goes along the longitudinal axis of the detector, as the layers are oriented perpendicularly to this axis. Neutral pions and leptons were considered always visible in this analysis. All cuts were imposed on the 'FSI' sample.

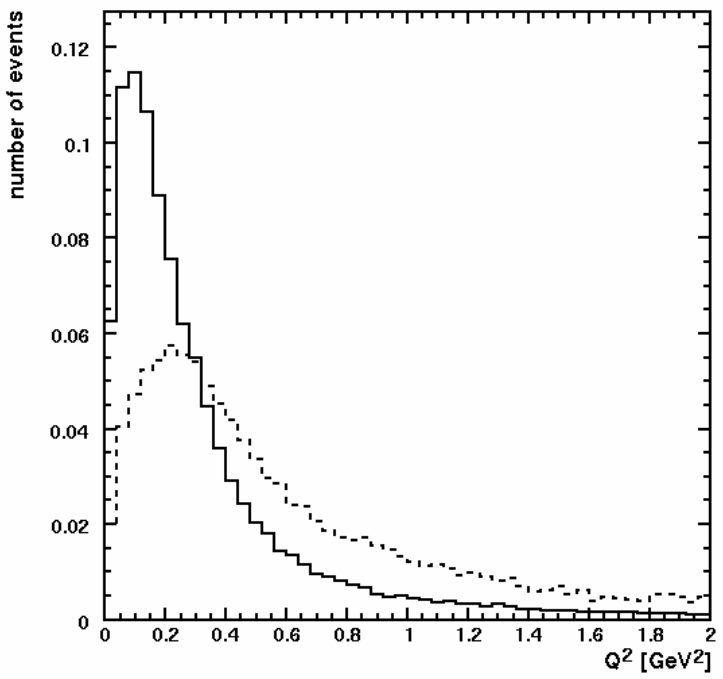

Fig. 44. Ideal Q^2 distributions for $\nu\, p \rightarrow \mu^- \pi^+ p$ reaction. Solid line – ideal selection, dashed line – with visibility cuts applied (6 cm track length) on the 'FSI' sample. All curves are normalized to enable shape comparison.

The reaction considered in the visibility analysis was $\nu_\mu + p \rightarrow \mu^- + p + \pi^+$ (CC π^+ production with a proton in the final state). We've chosen CC interaction with a proton in the final state as this is the only reaction that can be efficiently tagged for exclusive analysis and for which the Q^2 can be reconstructed in the real detector environment. First, Q^2 distributions for this reaction were examined to check what regions of Q^2 are hidden to an experimentalist because of inability of the detectors to see all the tracks. It appears (Fig. 44) that this is the case for low Q^2 events. One can see that the most of events lie in the low Q^2 region; however, when the visibility cuts are applied, most of these events are simply not classified as CC π^+

production with a proton in the final state, because of invisible proton and/or pion. Thus we lose a significant number of events in the region where cross-sections are very poorly known. Next, a comparison of different track length cuts in terms of number of visible events was made. The percentage values are calculated with true number of events, i.e. the number one gets when no cuts are imposed, considered as 100% . The results are shown in Table. 7.

Track length cut	**Number of events identified as CC π^+ production with a proton in the final state**
no cut (true number of events)	61964 (100%)
6 cm cut	16793 (27%)
10 cm cut	14044 (23%)
14 cm cut	11743 (19%)
18 cm cut	9990 (16%)

Table 7. Fractions of events identified as CC π^+ production with a proton in the final state interactions when different track length cuts are in effect. See the text for details.

One can see that, unsurprisingly, the longer the required track lengths, the smaller the number of events identified. It may be also noticed that regardless of a cut being imposed, the number of observed events is quite low. This is due to cut on protons and charged pions in the same time The pions tend to be created with lower momenta than protons – this is due to Pauli blocking, which forces most of the nucleons to have larger momentum (as lower energy levels are already occupied). This phenomenon is absent in case of pions. Additionally, pions produced in the resonant interactions tend to have a large transversal momentum (hence smaller longitudinal momentum, on which the cut is imposed). This is why most of events with charged pions get discarded when the cut is applied.

To summarize, detector effects have a large impact on Q^2 shape for the $\nu_\mu + p \to \mu^- + p + \pi^+$ channel. For neutral pions such effects are less important (π^0 quickly decays into two gammas, which do not interact in nucleus; gammas are also easier to reconstruct in the detectors in questions). We can then conclude that it is impossible to precisely reconstruct Q^2 distribution for single pion production (via delta resonance), even by using potentially optimal channel, i.e. CC π^+ production with a proton in the final state. It will be necessary to have a support of theoretical models for neutral pion production. Those models of pion production will be discussed in the next chapter.

Chapter 6
Estimation of π^0 background prediction uncertainty in T2K experiment

Large uncertainties exist in predicting π meson production cross sections for neutrino energy range of the order of 1 GeV that is most important for new long baseline experiments like T2K. The problem is particularly eminent for single neutral pion production. Consequently, there are many different theoretical expectations based on different parameterizations of the resonance model that is used to describe pion production in this energy range. The T2K experiment will enable to verify them to greater extent. However, those predictions are valuable also in the preliminary stage of the experiment - differences in the π^0 production affect background predictions in Super-Kamiokande and therefore estimations of the expected precision of electron neutrino appearance measurements in T2K.

This study presents a new way of dealing with old bubble chamber neutrino data that takes into account systematic errors related to neutrino beam flux uncertainties. This results in a fit in which two parameters of form factors are determined: M_A and $C_5^A(0)$. One sigma contours of the fit are then used to obtain uncertainty in cross-section for pion production via simulations of neutrino interactions. The results are important for systematic error calculations in T2K experiment.

Theoretical analysis and the fit was done by Krzysztof Graczyk and Jan Sobczyk. Uncertainty estimation is a part carried out by the author of this thesis. The whole study was made in collaboration with Danuta Kiełczewska. Full description can be found in Ref. [G09].

6.1 Bubble chamber experiments

Two experiments provided data in the energy region that is of interest here. These were ANL (Argonne National Laboratories) and BNL (Brookhaven National Laboratories) bubble chamber experiments. Both experiments utilized wide-band muon neutrino beams peaked at the energy of 0.5 GeV and 1.2 GeV, respectively. Bubble chambers filled with hydrogen or

deuterium were used as detectors. Data were collected using analog cameras, the film was then processed and analyzed manually. More details about these experiments can be found in Ref. [B77, B81].

Using a target composed of light nuclei has its advantages. When using deuterium it enables us to see not only products of the interaction itself but also the spectator proton. This, coupled with a capability of bubble chamber to reconstruct low energy protons (protons of momentum as low as 100MeV/c could be observed) gives a unique possibility of full reconstruction of kinematics.

Targets used in the experiments described above allow to study the interactions on primary vertex - the impact of FSI is very small. This needs to be taken into account when one wants to extrapolate these results to detectors filled with water or carbon compounds, like Tracker subdetectors in ND280 off axis detector. For such materials FSI play a significant role; to predict cross-sections for specified channels one has to rely also on predictions of FSI model used by the Monte Carlo software.

6.2 Theory and fit

Dominant channels of pion production in T2K energy region are resonant and are usually described by Rein-Sehgal model [R81], which takes into account several resonances. However, in low energy region (around 1 GeV) a different model, taking into account only Δ resonances, can be applied with satisfying results. This approach, called Rarita-Schwinger formalism for the $\Delta(1232)$ excitation, was used in this study (for more details, see Ref. [G09]). Variants of resonance models are usually different in the way the structure functions are parameterized. The vector part of form factors is well known from electron scattering experiments; axial form factors can only be studied in neutrino interactions and hence their form is much less certain. There exist several parameterizations of axial form factors, some of them being results of fitting to the available data from ANL and BNL experiments. The main contribution to the axial current comes from the $C_5^A(Q^2)$ and in this analysis it was assumed to have a dipole form (a simplest possible functional form):

$$C_5^A(Q^2) = \frac{C_5^A(0)}{\left(1+\frac{Q^2}{M_A^2}\right)^2}$$

where Q^2 is four-momentum transfer and M_A is axial mass. M_A and $C_5^A(0)$ are the fitted parameters.

We look for a simultaneous fit to both ANL and BNL experiments' data by applying the χ^2 method. The best fit is obtained by minimizing a function $\chi^2 = \chi^2_{ANL} + \chi^2_{BNL}$. In both cases the χ^2 is given by the standard formula with the additional quadratic term which comes from the total systematic uncertainty for the flux (see the Appendix for details):

$$\chi^2 = \sum_{i=1}^{n} \left(\frac{\sigma_{th}^{diff}(Q_i^2) - p\sigma_{\exp}^{diff}(Q_i^2)}{p\,\Delta\sigma_i} \right) + \left(\frac{p-1}{r} \right)^2$$

$$p \equiv \frac{\sigma_{tot-th} N_{\exp}}{\sigma_{tot-\exp} N_{th}}$$

where $\sigma_{th}^{diff}(Q_i^2)$ and $\sigma_{\exp}^{diff}(Q_i^2)$ are experimental results and theoretical predictions for the differential cross section in i-th bin of Q^2, $\Delta\sigma_i$ is the experimental result uncertainty (statistical and uncorrelated systematic), σ_{tot-th} and $\sigma_{tot-\exp}$ are the experimental and theoretical flux averaged cross sections measured and calculated with the same cuts and *r* is

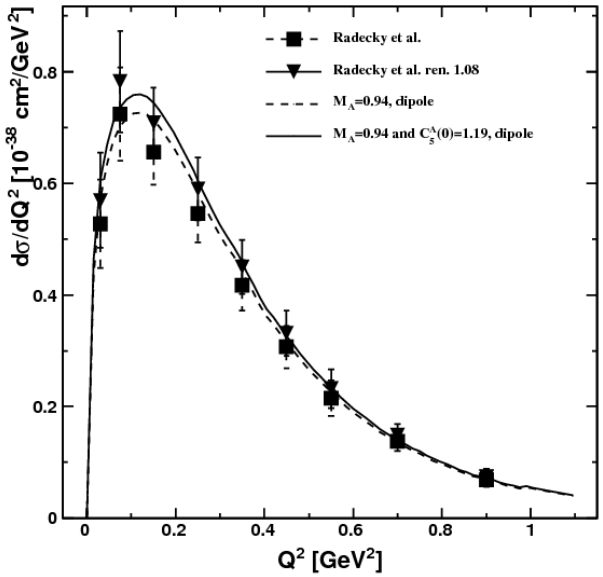

Fig. 45. Fit results for ANL data. The solid/dashed lines denote the best fit obtained with $C_5^A(0)$ fitted/fixed (second option refers to a fixed value of 1.15, the option not discussed in this thesis – see Ref. [G09] for details). Black squares - experimental data [R81], black triangles - experimental data multiplied by the re-normalization factor p_{ANL} obtained from the fit.

the flux uncertainty. This uncertainty has to be taken into account as the beam flux was not very well controlled in the bubble chamber experiments and it was not included in the experimental results' uncertainties $\Delta\sigma_i$.

Estimation of flux uncertainties is a complicated task. General problem of neutrino experiments is a determination of the neutrino beam flux and energy spectrum. Neutrino detectors measure rates of events $N(E_\nu)$, which depend on a product of flux $\Phi(E_\nu)$ and $\sigma(E_\nu)$ in the following way:

$$\frac{dN(E_\nu)}{dE_\nu} = \Phi(E_\nu)\cdot\sigma(E_\nu)$$

We then have to know $\Phi(E_\nu)$ in order to calculate $\sigma(E_\nu)$ or vice versa.

One approach to this problem is to simulate the neutrino beam on the basis of a known intensity and energy of the primary proton beam and known (with a certain accuracy) differential cross-section for meson (mainly pion) production. A separate experiment can be set up to measure those cross-sections for a specific target.

Another approach is to measure precisely CCQE interactions. In this case there is essentially only one unknown theoretical parameter: axial mass, M_A^{QE}. One can determine quite precisely M_A^{QE} from the shape of Q^2 distribution and use it to determine $\sigma_{CCQE}(E_\nu)$. In bubble chamber experiments one can reconstruct fairly well the neutrino energy for CCQE events (see Section 6.1) and therefore get $dN(E_\nu)/dE_\nu$, hence making it possible to obtain $\Phi(E_\nu)$. This method however depends somewhat on model description for the CCQE interactions and should be confronted with the beam simulation method.

Having all that said, we can now estimate the flux uncertainties as follows:

- 20% for ANL data ($r_{ANL} = 0.20$). The data from Ref. [R82] are used. The authors state that the overall normalization uncertainty is ±15% in the energy range 0.5 do 1.5 GeV and 25% elsewhere. This comes from the flux calculation on the basis of the measured pion production by 12.4 GeV protons on beryllium in a separate experiment [C71]. The calculation is described in Ref. [B77]. Most of Δ^{++} production events happen between 0.5 and 1.5 GeV; however, in Ref. [B77] a comparison of fluxes calculated from pion production with fluxes derived from ANL's measurements of QE interactions was made and it was concluded that the latter flux was 21% lower. That's why the approximate value of 20% was used.

- 10% for BNL data ($r_{BNL} = 0.10$). Refs. [B81, K86] were used. The uncertainties of axial mass determination from QE analysis in these papers suggest the error on absolute flux of less than 10%. One can also add that another beam study was done using scintillator detector [A86] and the comparison showed that both estimates differed by 10% (with good spectrum shape agreement). It is an indirect indication that 10% uncertainty on the BNL flux derived from QE events is reasonable.

In the paper [G09] the fits were repeated also for other assumptions about *r*. It has been found that the results have changed only slightly (and agree with the original results within statistical errors), with larger difference for $C_5^A(0)$.

Data that were used in the fit were taken from Refs. [R82, K86]. In the analysis deuteron nuclear effects were taken into account.

The two sets of data (from ANL and BNL) turned out to be consistent. The fit yielded the following result:

$$M_A = 0.94 \pm 0.03$$
$$C_5^A(0) = 1.19 \pm 0.08$$
$$p_{ANL} = 1.08 \pm 0.10$$
$$p_{BNL} = 0.98 \pm 0.03$$

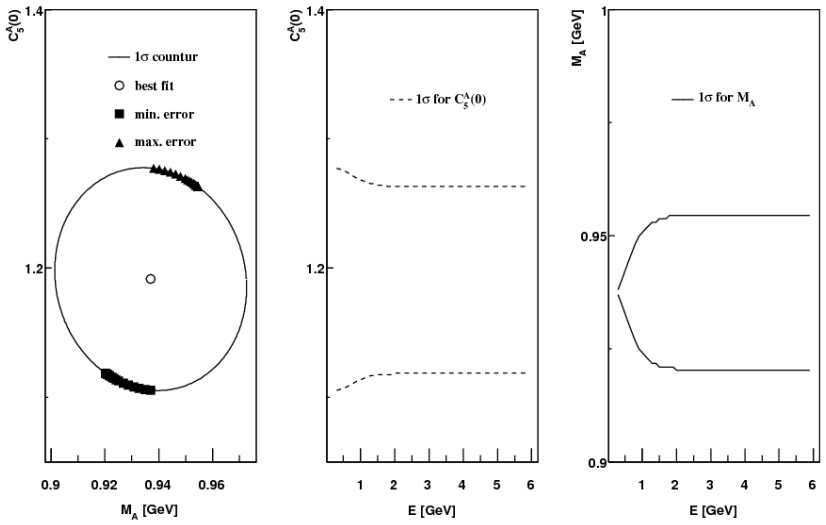

Fig. 46. Error ellipse. Black squares and triangles denote the points with maximal and minimal errors for total cross section for $\nu + p \to \mu^- + p + \pi^+$ at different values of neutrino energy E (from 0 to 6 GeV). The obtained points are then mapped in the form of $C_5^A(0)$ and M_A dependence on E (middle and right figures).

Fit result for ANL data is visible in Fig. 45, the error ellipse is presented in Fig. 46. This ellipse is a result of the fit and it demonstrates correlation between the two fitted parameters. For further analysis, the 1σ values for specific energies for NC π^0 production (see below) were calculated and are shown as points on this ellipse.

6.3 Uncertainty estimation

It is interesting to investigate how the 1σ error contours look like for different pion production channels in terms of cross sections. In particular, one might study two channels that are most important in modern neutrino experiments, i.e.:

- $\nu_\mu + p \to \mu^- + p + \pi^+$, $\nu_\mu + n \to \mu^- + n + \pi^+$ (CC π^+ production), and
- $\nu_\mu + p \to \nu_\mu + p + \pi^0$, $\nu_\mu + n \to \nu_\mu + n + \pi^0$ (NC π^0 production).

The π^0 production is the main source of background in water Cherenkov far detectors of long baseline neutrino experiments searching for ν_e appearance, like T2K. The NC π^0 interactions are however difficult to study exclusively, because the reaction kinematics are not constrained enough to reconstruct neutrino energy. One can try to study them by measuring π^+ production and extrapolating the results to π^0 production.

We will now use fit results described above to estimate cross-section uncertainty for pion production channels in the context of T2K experiment. For this purpose two software packages for simulation of neutrino interactions are used. The main simulation package used in this analysis was NuWro Monte Carlo generator of events. For resonant pion production it uses the Adler-Rarita-Schwinger formalism for the Δ excitation (the same model was used in the fitting procedure). The non-resonant part is described with a fraction of DIS contribution, applying the algorithm described in Ref. [S04]. NuWro is a generator in which many parameters can be specified manually, including axial form factor parameters, which are of interest in this analysis. Nuclear effects in oxygen (FSI) have been recently implemented in NuWro and were used in this study. As a reference, Nuance neutrino generator was used. This generator has an implementation of FSI in oxygen which was verified by the data (see Chapter 3). Resonant pion production in this generator is calculated according to Rein-Sehgal model.

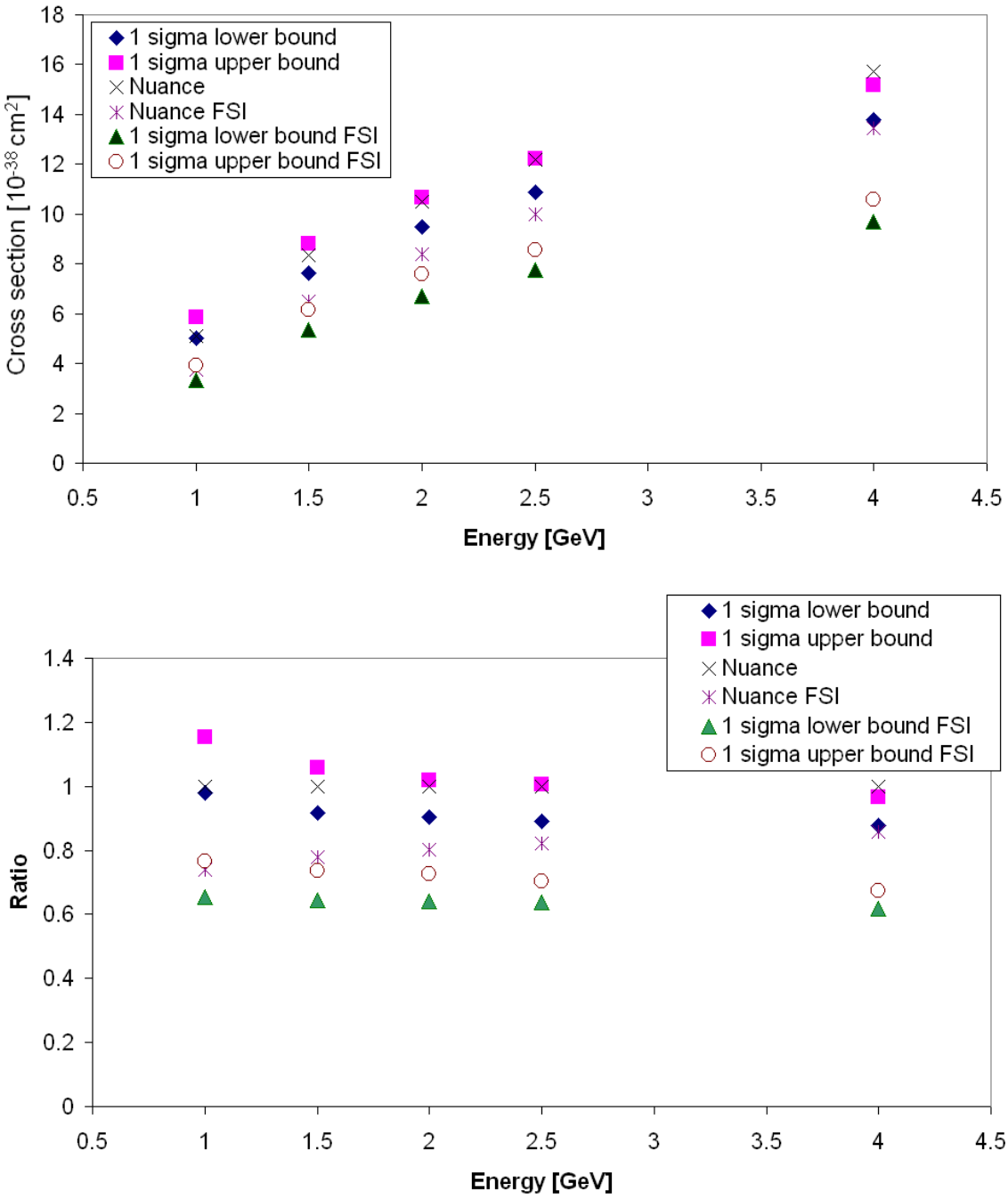

Fig. 47. Cross sections per nucleon of pion production on water - CC π^+ channel. Upper figure - CC π^+ production absolute cross-section, lower figure - CC π^+ production cross-section normalized to Nuance results without FSI. NuWro points show 1σ error ranges, Nuance points are shown here for reference.

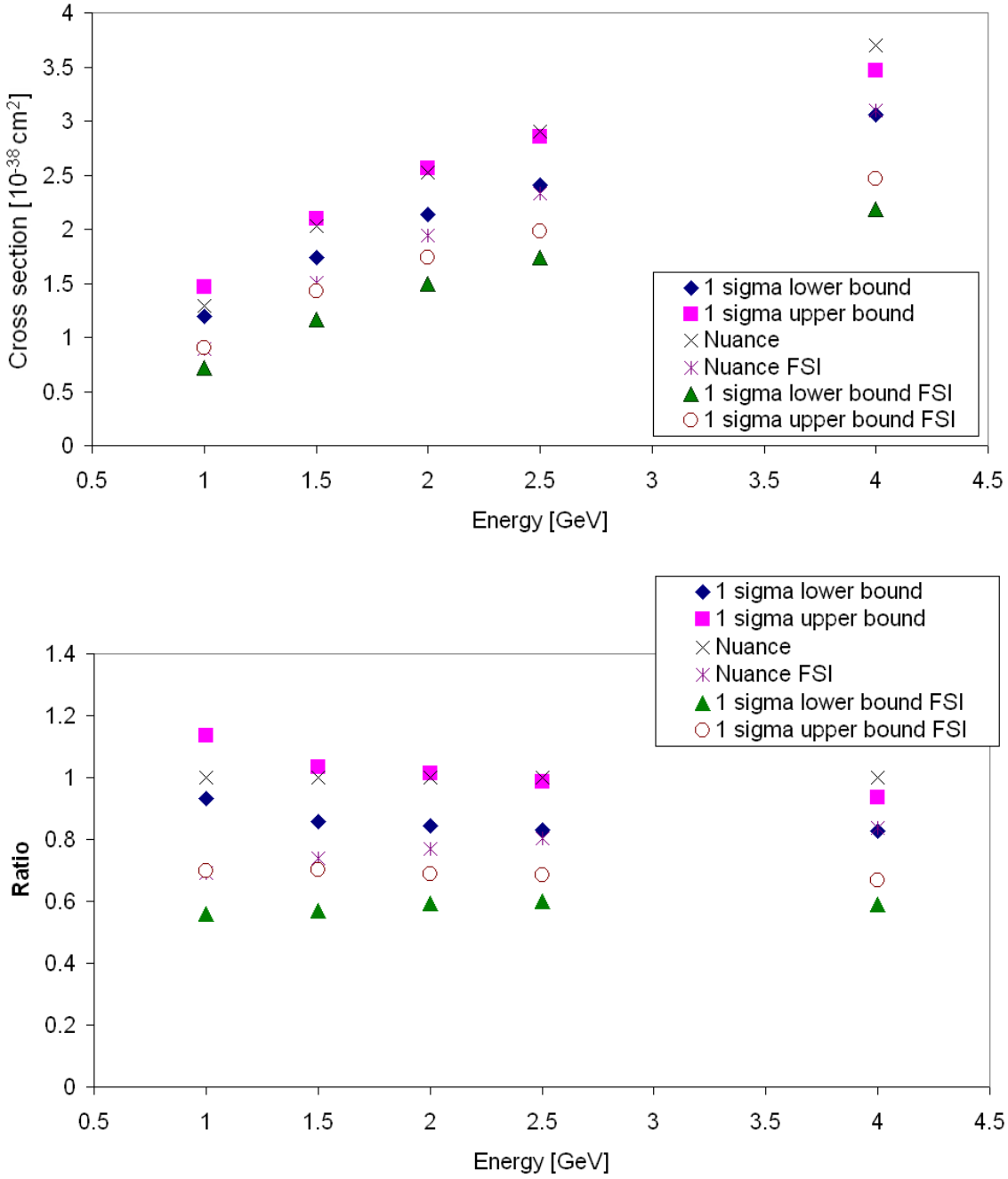

Fig. 48. Cross sections per nucleon of pion production on water - NC π^0 channel. Upper figure - NC π^0 production absolute cross-section, lower figure - NC π^0 production cross-section normalized to Nuance results without FSI. NuWro points show 1σ error ranges, Nuance points are shown here for reference.

We decided to examine the fit that used dipole parameterization of axial form factors in which two parameters: M_A and $C_5^A(0)$ were fitted. The error ellipse, presented in Fig. 46 is calculated for CC π^+ production. However, we can scan this ellipse, calculating NC neutral pion production cross-section for each point on it, and find minimum and maximum value (which correspond to 1σ range). By doing this for a broad range of incident neutrino energy we can obtain M_A and $C_5^A(0)$ parameters corresponding to lower and upper 1σ bound at each energy and then use them in NuWro simulations, which will allow us to calculate cross-sections for the channels of interest. NuWro simulation package was using exactly the same form factors as the ones that were used in the fit.

The idea of this comparison is to see how uncertainty of pion production depends on energy of incoming neutrino. For this purpose, a sample consisting of 500,000 events was generated for neutrino energies 0.5, 1, 1.5, 2, 2.5 and 4 GeV for each of the parameterizations chosen. Resonant and deep inelastic channels were taken into account. Using cross section per nucleon value calculated by NuWro and number of events in the channels of interest one was able to obtain the result, presented in Figs. 47, 48. All simulations were conducted using water as target. Only muon neutrino interactions were taken into account as they dominate in the beam.

Figs. 47, 48 show how cross section uncertainty depends on energy of incoming neutrino. Two sets of points illustrate 1σ bounds on cross-sections (cf. Fig. 46) obtained using NuWro, others are Nuance results. In order to show how inclusion of FSI modify the cross sections we present separately results with nuclear effects turned off. All comparisons were done in the two pion production channels described earlier. Lower plots in Figs. 47, 48 show all cross-sections divided by Nuance results without FSI. It is seen that uncertainties due to form factor determination inaccuracies decrease with energy and are most notable in low energy region. Application of FSI makes the cross-sections and uncertainties smaller. In particular at 1 GeV the uncertainty for NC π^0 production is about $\pm 10\%$.

There is a notable difference between NuWro and Nuance in the high energy region. This is probably due to different models being used in the two generators: Nuance uses Rein-Sehgal model, while NuWro single delta resonance approximation, which is good only for lower energies. We consider the Nuance result in the high energy region more trustworthy.

We also notice that Nuance predicts higher (with respect to NuWro) single pion production cross-sections on nuclear targets. This is caused by different assumptions for pion absorption cross section at higher values of kinetic energy. This is a region where the experimental data

for pion nucleus absorption are missing and Monte Carlo predictions have to rely on some theoretical assumptions.

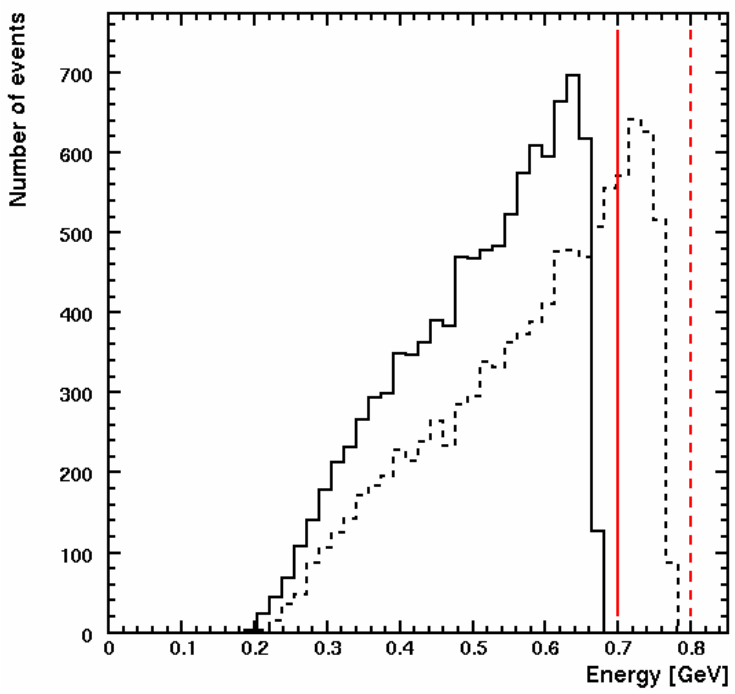

Fig. 49. Electron energy distributions for mono-energetic electron neutrino beams. Red lines denote neutrino energies for which the electron energy distributions (black) were made. Solid line – 700 MeV neutrino energy, dotted line – 800 MeV. 10,000 events were generated for each energy using Nuance with water set as target. Only CCQE interactions were taken into account as these are used for electron neutrino appearance measurements.

In order to evaluate what neutrino energies are relevant for T2K ν_e appearance search, one has to look at the typical energies of pions that constitute background. The oscillation signal from $\nu_\mu \rightarrow \nu_e$ is located in the range 500 – 900 MeV with a peak at around 700 MeV of neutrino energy (see Chapter 2). If we try to translate it into electron energies (using Fig. 49), we will see that majority of electrons produced in CCQE interactions of neutrinos in this energy range have energies close to energy of incident neutrino. The energy of π^0s that we can consider the most dangerous is therefore approximately in the 300 - 900 MeV bracket. On the other hand, using Ref. [N04] we can state that for neutral pions of energies above 600 MeV the detection efficiency for NC π^0 events drops way below 50% in comparison to the efficiency for pions at rest (for which the two Cherenkov rings are easiest to distinguish; see Fig. 3b in Ref. [N04]), and in further considerations we will assume that "dangerous" neutral

pions are of energies above 600MeV. Following these two hints, we can look at pion energies in the range between 600 and 900 MeV. Neutrino energies for those pions coming from NC π^0 interactions are shown in Fig. 50 (in three pion energy bins). We can then conclude that neutrino of 1 – 4 GeV are the most important in the context of ν_e appearance searches in T2K experiment. Therefore the expected uncertainty varies between 6% and 10% (see Fig. 48). However, it is important to note that the errors discussed here come only from uncertainties in form factors and do not take into account other model approximations, e.g. non-resonant background in pion production or an influence of matter on the width of Δ resonance.

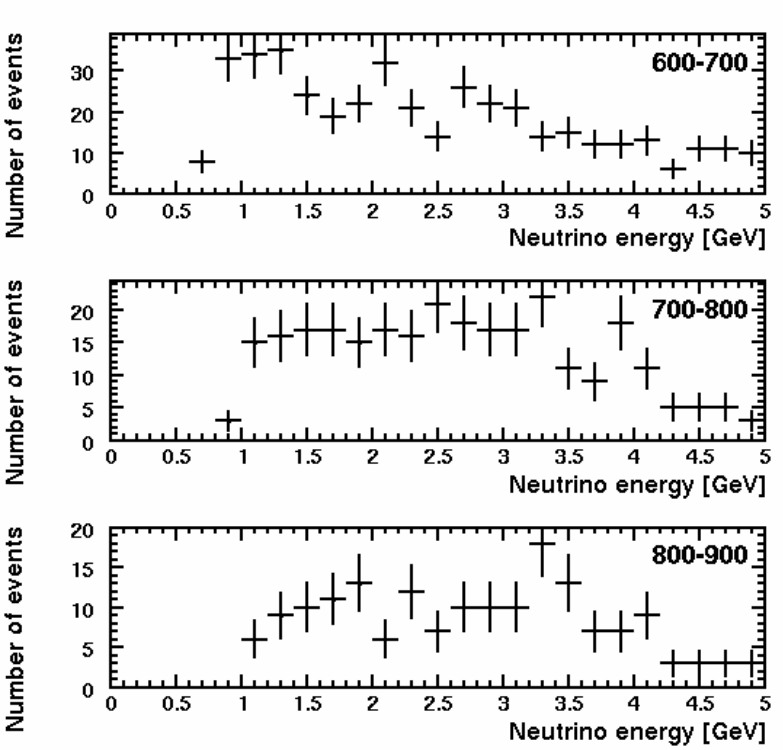

Fig. 50. Energy of incoming neutrino in three π^0 energy bins - from top to bottom: 600-700 MeV, 700-800 MeV, 800-900 MeV. Nuance simulation sample was used with T2K neutrino beam energy spectrum as an input. It is visible that neutrino energy area between 1 and 4GeV is the most populated.

6.4 Multi-pion background

In this section, we will look at events that may seem to be a single pion production in Super-Kamiokande, but are in fact a multi pion production with some charged pions invisible because they carry too little energy (neutral pions are almost always visible in Cherenkov detector). These can contribute to single pion background (this contribution is therefore

important for systematic error calculations) and haven't been carefully studied before in context of T2K experiment.

Let's start with a short summary. The process in question:

$$\nu_e + N \rightarrow e^- + N'$$

is a signature of electron neutrino appearance. It can however be faked by a single π^0 production:

$$\nu_\mu + N \rightarrow \nu_\mu + N + \pi^0$$

since some neutral pions can mistakenly be taken for electrons.

In this section our aim is to look at events of the following type (from now on we will call these events *multi-pion*):

$$\nu_\mu + N \rightarrow \nu_\mu + N + \pi^0 + n \times \pi^\pm$$

and evaluate their contribution to the total number of muon neutrino induced NC neutral pion production events. In the analysis we have used Nuance muon neutrino samples for T2K beam described in Chapter 5. Options with and without FSI has been taken into account.

First, we've looked at the statistics in the simulation file. The results are presented in Table 8. The numbers in the table correspond to raw events i.e. no visibility cuts were applied (all particles were considered visible). We can see that potentially more than 20% of single π^0 events can in fact be multi-pion events.

To verify this in real detector environment, we employed visibility analysis, to find out how many charged pions are detectable in Super-Kamiokande. As have already been said in Chapter 4, only charged particles with velocity exceeding velocity of light in the detector medium can be seen in Cherenkov detector. Technically, this corresponds to a condition on particle's energy (called here a *basic cut*):

$$E > 1.5 \times m$$

where m is a rest mass of the particle. This does not affect neutral pions (as they are not visible directly but through their decay products) – they are visible regardless of their energy.

The condition above is a threshold one – if the energy is over the threshold, the light is emitted. It may be however difficult to reconstruct a particle with the energy near the threshold due to small number of photons emitted and weak rings they form. This is particularly valid if there are some other rings in the vicinity which distort the image. That is why the second, stronger condition is also taken into account (called hereafter a *+50 MeV cut*):

$$E > 1.5 \times m + 50MeV$$

50MeV over the threshold can be considered safe regarding detector reconstruction capabilities.

	Without FSI	**With FSI**
Single π^0 events whole sample	**33632**	**26377**
Single π^0 events with no charged pions	28378±168 (84%)	20841±144 (79%)
Single π^0 events with 1 charged pion	3100±56 (9%)	3218±57 (12%)
Single π^0 events with 2 charged pions	1652±41 (5%)	1723±42 (7%)

Table 8. Number of events of specified types in both (with and without FSI) muon neutrino samples generated with T2K beam. No visibility cuts were applied. Single π^0 refers to events that have one neutral pion and possibly other charged pions as well.

One can now look once again at the multi-pion events and verify how many of them appear as single π^0 after the above cuts have been applied. Table 9 presents the results obtained with the visibility cuts taken into account.

	All events visible as single π^0	**Events that fake single π^0 (being in fact multi-pion)**
without FSI, basic cut	28536±169	158±13 (0.5%)
without FSI, +50MeV cut	28797±170	419±20 (1.5%)
with FSI, basic cut	21232±146	391±20 (1.8%)
with FSI, +50MeV cut	**21649±147**	**808±28 (3.7%)**

Table 9. Number of events of specified types in both samples. Visibility cuts described in the text are included. The more stringent the visibility cut, the fewer particles are visible, and the more events can be mistakenly counted as single π^0.

The most important result is contained in the lowest row of the table – for FSI sample, with the most stringent (and realistic) visibility cut used. The contribution of multi-pion events in the single neutral pion sample can be estimated as reaching 4%. Fig. 51 shows π^0 momentum distribution for all apparent single π^0 events (solid line) and the multi-pion contribution to it (dashed line).

To summarize, a contribution at the level of 4% is not large enough to be bothered with in the first stage of T2K experiment starting in 2009, especially knowing that neutral pion cross-section uncertainty is of the order of 10% or even higher. It is possible, however, that in the second stage, when more precise measurements are planned, the 4% of multi pion events can

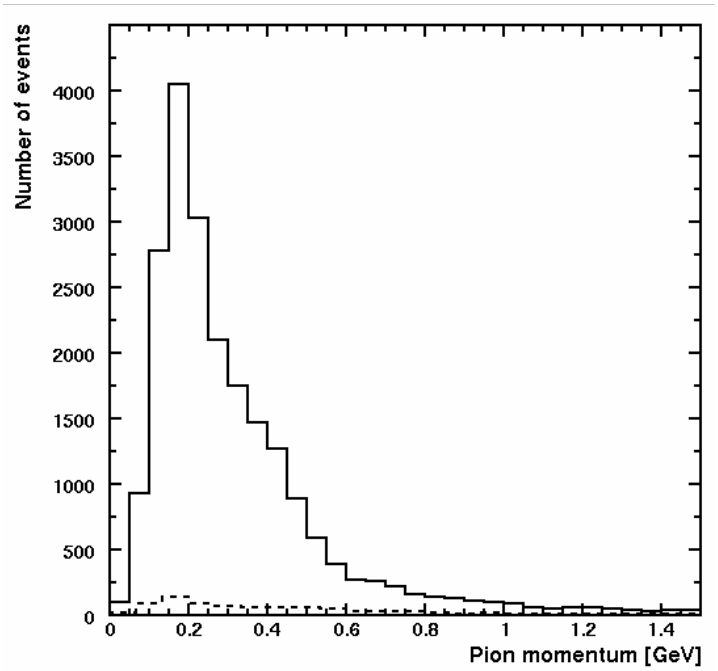

Fig. 51. Momentum distribution of neutral pions for single pion events (solid line) and multi-pion events that look like single pi when *+50MeV* cut is applied (dashed line).

be significant and become a subject of further studies. One idea would be to utilize for that purpose a planned LAr TPC detector in 2 km station of T2K experiment, which is expected to be built during experiment's operation in the first stage. LAr TPCs are known to have excellent particle reconstruction capabilities (see also the analysis presented in Chapter 7). The other option (if 2 km station cannot be used) would be to carry out the multi-pion analysis on measurements from ND280 off axis detector.

Chapter 7
Prospects for a precise estimation of π⁰ background using liquid argon detector of 2 km station

In order to determine beam contamination coming from electron neutrino component in the T2K beam, necessary measurements will be carried out in ND280 off-axis detector. However, due to differences in neutrino spectrum discussed in Chapter 4, building a second detector farther from the beam source may become a necessity. Its liquid argon high resolution time projection chamber (LAr TPC, see Chapter 4) would be ideal for such studies - it is an imaging detector, with excellent particle type recognition capability and good calorimetric features. It allows for precise reconstruction of events and can lead to good estimation of ν_e component. It can also supplement measurements carried out using other detectors in the 2km station: water Cherenkov detector and muon ranger.

In this chapter we will focus on neutral pion identification methods for LAr TPC, keeping in mind that it is essential for efficient background rejection when determining ν_e component of the beam. The analysis presented here was performed at the time when it was not clear what some of the key design features of the detector will be (and at the time of writing of this thesis, it is still unclear whether the 2 km station will be built). Therefore it should be treated as a crude one, testing the capabilities of a new and promising detection technique.

7.1 Neutral pion signature in liquid argon

The LAr TPC is an imaging detector and, as opposed to Cherenkov detector, one can see in it the whole electromagnetic cascade (shower) with all electron tracks (see Fig. 52, 53). Such a cascade is produced by an electron emerging from ν_e CCQE interaction. However, cascades are also present in ν_μ NC interactions with single π^0 production, where they are initiated by two gamma quanta from neutral pion decay. If one shower is for some reason invisible, the NC muon neutrino event can easily be confused with one induced by an electron neutrino.

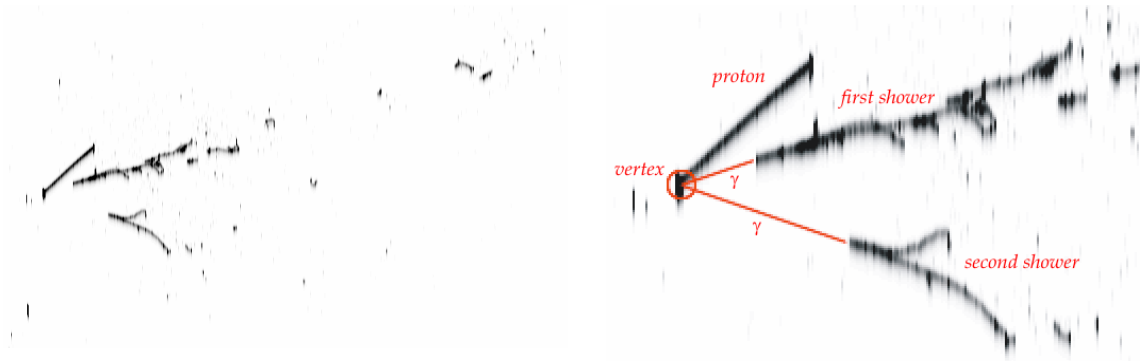

Fig. 52. A simulated neutral pion event, induced by a 3 GeV muon neutrino (collection view). Left: view of the whole event. Right: vertex region magnified, with all the elements labeled in red. Two electromagnetic showers (cascades) are visible, as well as a proton track.

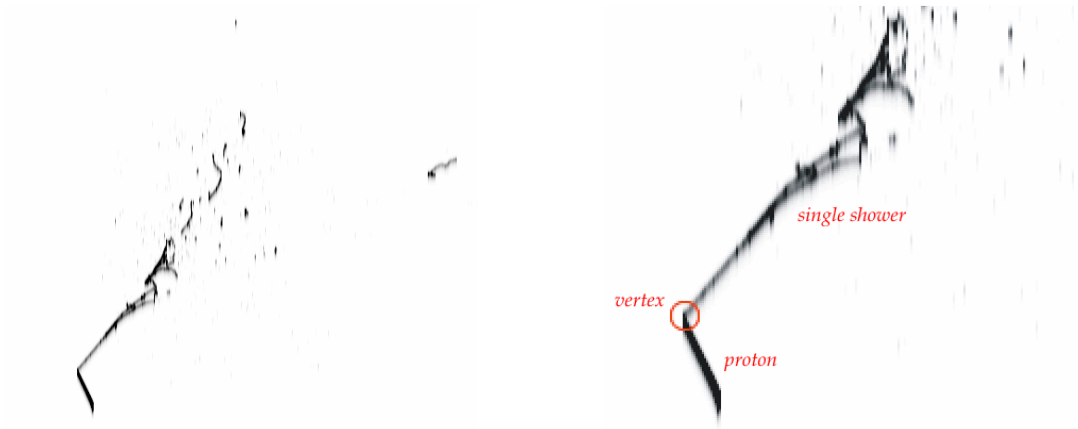

Fig. 53. A simulated electron event, induced by 0.7 GeV electron neutrino (induction view). Left: view of the whole event. Right: vertex region magnified, with all the elements labeled in red. An electromagnetic cascade and a proton track are visible.

The electron component constitutes about 1% of the beam neutrinos (which corresponds to around 2% of electron neutrino interactions in the total number of interactions; 30% of these interactions are CCQE events). The NC events with single neutral pion production constitute 4% of all muon neutrino and antineutrino interactions, which are the remaining 98% of all neutrino interactions seen in the detectors. This means that neutral pion background is almost 7 times more abundant than electron signal.

The typical event display for CCQE electron neutrino interaction (*electron event* in short) and NC muon neutrino interaction with neutral pion production (π^0 *event*) are shown in Fig. 52 and 53. Invisible tracks of two gammas emerging from neutral pion decay are marked in red. Besides the showers, one can see also proton tracks coming from the primary vertex and some

"garbage" – short proton tracks induced by neutrons produced in primary and secondary interactions (the neutrons are themselves invisible). It is worth to notice, that in case of a π^0 event, the two showers are spatially separated from the vertex (incident gammas travel a certain distance before converting into electron-positron pair and forming cascades) while in the electron case the electron shower comes directly from the vertex.

7.2 Neutral pion separation methods

Since our aim is to identify electron events in the detector, we have to develop some methods of distinguishing them from their main background, i.e. π^0 events. If such an event looks similarly to the one presented in Fig. 52, the task is easy. However, in many cases the situation is not that clear: one of the cascades might be not visible due to shower overlapping or gamma escaping from the detector (if interaction vertex is located too close to the walls). The interaction vertex can be hard to identify, if there is no visible proton. There is therefore a need to establish a procedure to separate π^0 events also in those more difficult cases.
Three methods can be used for the separation, in the order of simplicity:

- *Two shower method* – the easiest way to recognize π^0 events is to check whether one or two showers can be seen on the display. If we can see two showers, the event is a π^0 one. Unfortunately, some neutral pion events can have only one shower visible, and these cannot be identified using this method.
- *Gap method* – neutral pion events have showers originating from the different location than the primary vertex. Seeing the gap identifies the event as a π^0 one. However, if the gap is small, it is sometimes hard to notice. Also note that one has to know where the vertex is located, and this is only possible if other particles coming from the vertex are visible. If an interaction produces neutrons, they are invisible and the vertex cannot be identified.
- *Energy loss (dE/dx) method* – one can examine the ionization energy loss pattern of a visible shower. In a π^0 case the loss should be twice as large as in the electron case – the shower is formed by a electron-positron *pair*. However, sometimes a gamma induces a single-electron shower due to Compton scattering effect ($\gamma + e^- \rightarrow \gamma + e^-$), in which gamma scatters on a free electron and looses some energy in its favor. This process is dominant for photon energies of the order of MeV and smaller.

To achieve best results, these three methods should be combined. In this study two shower and gap methods were studied. The results were then combined with the results of previous energy loss analysis performed for ICARUS detector [I04], taken from Ref. [G03].

7.3 Two shower method

The simplest method of identifying π^0 events is looking for two showers on the display. If one can see two showers, it is for sure a π^0 event. One visible shower may indicate an electron event, but it is also possible that:

- the interaction vertex was close enough to the walls of the detector to let one gamma out of it. If the gamma converts outside the liquid argon volume, it is invisible in the detector,
- the π^0 showers are overlapping, and what we take for one shower is in fact a superposition of two.

In order to estimate how many gammas escape from the detector without leaving a trace, a dedicated study using full detector simulation was carried out. Nuance was used for neutrino interaction generation; then, the interaction products were propagated through the medium using dedicated LAr TPC detector simulation built on the basis of GEANT4 [K05]. As a result one obtains data files, that can be viewed and reconstructed by an application called Qscan, utilizing Fullreco library (developed initially for ICARUS experiment and tailored to the needs of T2K LAr). Two views are available for each event: induction and collection.

Neutral pion events were generated and the events were reconstructed with the number of hits produced by each gamma determined for both detector views. The study was performed for 5 choices of fiducial volume of the detector. In the experiment one has to neglect interactions happening close to the walls, because their reconstruction is uncertain. If we choose large active volume (which gives larger statistics and larger systematic errors in the same time), we have to get close to the walls; the farther away from the walls, the smaller active volume. In Ref. [H03] the fiducial volume proposed is 50cm away from the walls of the detector – this choice is equivalent to 100ton of active LAr. In this study the distances from the walls taken into account were: 10cm, 20cm, 30cm, 40cm and 50cm.

Two conditions for a shower to be categorized as visible were taken into account:

- there is at least one hit reconstructed as belonging to the shower on both views,
- there are at least ten hits reconstructed as belonging to the shower on both views.

One hundred events were simulated for each wall distance. The results are shown below.

Fiducial cut	1 hit criterion	10 hit criterion
10 cm	10 ± 3	12 ± 3
20 cm	5 ± 2	11 ± 3
30 cm	6 ± 2	7 ± 3
40 cm	2 ± 1	3 ± 2
50 cm	3 ± 2	4 ± 2

Table 10. Number of neutral pion events with only one shower visible using 5 different fiducial cuts (per 100 events). Two criteria of shower visibility were used, as described in the text.

Misidentifiability increases for low distance values – for the vertex near the walls the probability that gamma converts outside the detector is much larger.
In order to evaluate how many neutral pion events can be confused with electron ones due to overlapping showers, an additional visual scanning was performed. It showed that 10%-20% of events can be misidentified due to absence of clear distinction between two showers.

7.4 Gap method

For π^0 events, we expect a gap between the vertex and the point at which the showers begin. We can use this feature to tell such events apart from electron events, with showers originating precisely at the vertex. However, to carry out such an analysis, we have to deal with two issues. First, the position of the vertex is not a priori known. We have to have at least one visible particle originating from the vertex and it is usually a proton or charged pion. This limits our capability to events that have at least one proton or charged pion with sufficiently high energy to be visible. Second, if a gap is small, one can easily make a mistake and decide that there is no gap at all. Therefore, we have to consider only events for which the gap is large enough. Fortunately, taking into account events with the gap larger than 1 cm excludes only 5.4% of all the events. This number is obtained by assuming exponential gamma attenuation probability [P00]:

$$I(x) = I_0 \exp\left(-\frac{x}{\lambda_0}\right),$$

where I is photon beam line intensity, I_0 is its initial intensity, x is the thickness of a medium in which pair production takes place and λ_0 is conversion length of photon in liquid argon (18 cm).

In the analysis presented here, we were looking at visible particles at the vertex, which is a necessary prerequisite to see the gap. We required the particle at the vertex to be visible (give a signal) on at least three consecutive wires of the detector. For such particles we are able to determine their direction. In the analysis, version 3.006 of Nuance was used with argon as a target and T2K beam profile. Around 25,000 NC ν_μ events were generated. A dedicated program was used instead of detector simulation. The program calculated number of wires on which the ionizing signal from each particle produced can be observed. As at the time of conducting this study it was not yet clear what the wire pitch for T2K LAr will be, we assumed an ICARUS wire pitch of 3 mm. The program utilized the following algorithm:

- it took into account every charged particle (protons, charged pions, muons, electrons, charged kaons), and calculated length of its track using energy-range dependence for each type of particle,
- it made two consecutive projections: first onto the wire plane, and then second onto 2 directions perpendicular to the wires' directions. This way two quantities were obtained, corresponding to the length of track in two directions perpendicular to the wires,
- and if greater of these quantities exceeded 9 mm (3 wires multiplied by the wire pitch) it concluded that the track was visible.

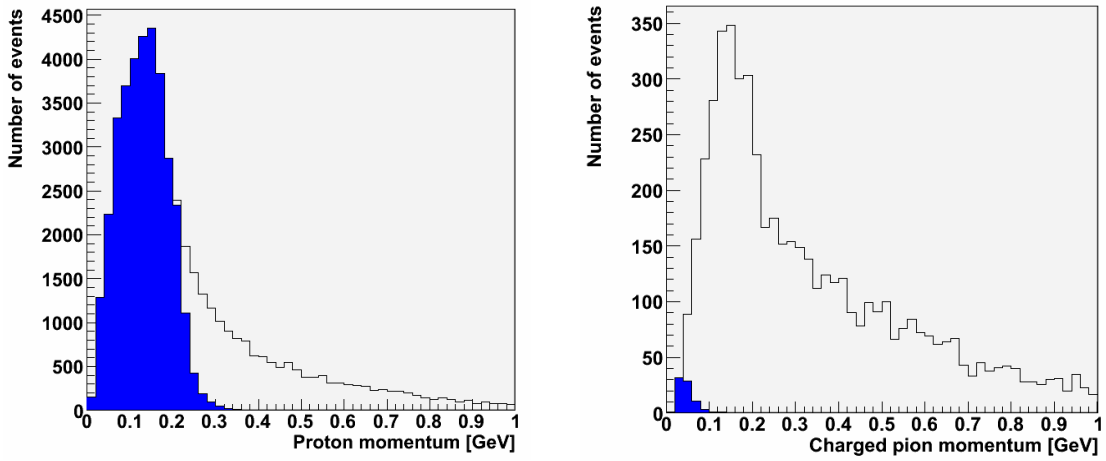

Fig. 54. Momentum of pions and protons using three wires visibility criterion. White histograms: momentum distribution of all particles; blue histogram: momentum distribution of invisible particles. Left: protons, right: charged pions.

The results are shown in Fig. 54 and Table 11.

Particle	Visibility	
	visible	invisible
Protons	0.67 tracks/event 33%	1.3 tracks/event 67%
Charged pions	0.24 tracks/event 99%	0.003 tracks/event 1%
Charged kaons	0.004 tracks 97%	0.0001 tracks/event 3%

Table 11. Number of tracks of different particle types per event in the sample (~25,000 NC ν_μ events) taking into account the 3 wire visibility criterion described in the text.

One can see that there is a multitude of protons generated by Nuance in the low energy range, but most of them are in fact invisible. Other particles are almost always visible (but they are rare and do not significantly contribute to the visibility analysis).

To conclude this part of the study, one has to check how many neutral pion events have at least one visible particle in the vertex. The results are presented in the table below. We see that 64% of all π^0 events have the primary vertex visible, which enables us to use the gap method. Remaining 36% cannot be identified using this method.

Description	Number of events
All NC events in the sample	**25636**
Events with 1 or more π^0	**4301±66** (**17%**)
π^0 events with 1 or more visible track	**2762±53** (**11%** of all, **64%** of all π^0 events)
π^0 events with no visible tracks	**1539±39** (**36%** of all π^0 events)

Table 12. Results of vertex visibility analysis using 3 wire criterion described in the text.

7.5 Energy loss analysis

In this section we describe for completeness the analysis conducted in Ref. [G03]. The analysis was carried out for ICARUS experiment. ICARUS (Imaging Cosmic and Rare Underground Signals) is an experiment aimed at proton decay search and studying interactions of atmospheric, solar and beam neutrinos. It consists of two T600 (600 ton) time projection chamber modules filled with liquid argon placed in underground laboratory in Gran Sasso, Italy. Its construction is similar to the 2 km liquid argon detector for T2K (the T2K detector design is actually based on ICARUS design and experiences). A half-module (T300) of the detector is an aluminum box (3.6 m wide, 3.9 m high, 19.9 m long) - a cryostat - filled with 300 tons of liquid argon. A cathode is placed in the middle to sustain an electric field inside. Three anode wire planes are installed along the sidewalls of the detector - they serve as a readout equipment. A wire plane is a plane of multiple parallel wires, with a distance between consecutive wires of 3 mm. Wires on each plane are oriented in different directions (i.e. -60, 0, 60 degrees with respect to the bottom of the detector). Several photomultipliers are also mounted on the walls for scintillation light triggering. The detailed description of ICARUS modules is given in Ref. [I04]. The detector is capable of recording tracks of charged particles traversing the active liquid argon volume.

In the analysis single electron and gamma showers were studied. If one sees a single shower from neutral pion decay, the only chance of distinguishing it from an electron shower is to analyze the energy loss pattern (also called ‘dE/dx pattern’) at the beginning of a cascade (before it starts to shower). Gamma converts into collimated electron – positron pair and gives an ionizing signal which is two times stronger than a single electron signal in electron case. However, one has to remember that a different process from pair production can also occur – Compton scattering, in which the photon scatters on a free electron, and this electron induces a shower, this time with an electron energy loss signature.

In the study electrons and gammas of several energies (250 MeV, 500 MeV, 1 GeV and 2 GeV) were generated using dedicated Fluka detector simulation for ICARUS T600 geometry. The energy loss on several first wires of cascades (before showering starts) was examined. For each cascade, the average energy loss on these wires was calculated and this value was used as a discriminator. The results as a function of particle energy for 90% electron efficiency are presented in Fig. 55. For 0.5 and 1 GeV, energies typical for gammas from neutral pion decay in T2K, the separation inefficiency of 5.5% and 3.7% respectively is

reported (i.e. these fractions of gamma showers were mistakenly identified as electron ones assuming that 90% of electrons are identified properly).

The separation of events of the two types gets better with the energy of incoming particles. This is due to decrease of Compton scattering effect with energy. It is worth to note, that this is just the opposite to Cherenkov water detectors, for which the higher the energy, the worse the separation (high energy gammas tend to travel in the same direction, leaving overlapping rings). In this regard the measurements of T2K LAr can be considered complementary to water Cherenkov detector's measurements.

7.6 Summary

To get the final answer one has to combine the results of the three different studies discussed above. The identification efficiencies were as follows:

- Two shower method: 10% of misidentified neutral pions because of escaping gammas, 10%-20% because of overlapping showers. In effect 20-30% of neutral pion events should be analyzed using the other two methods.
- Gap method: 36% of events that could not be identified with two shower method,

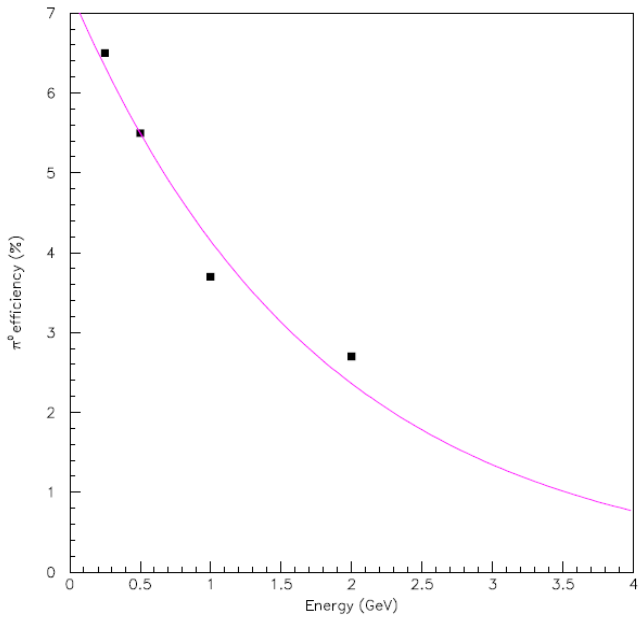

Fig. 55. Energy loss pattern analysis: neutral pion separation inefficiency as a function of particle (electron, gamma) energy. Electron identification efficiency of 90% is assumed. An exponential fit is superimposed (taken from [G03]).

cannot be also tagged by observing a gap, as there are no visible particles emerging at the vertex.. One should note that we took into account only events in which gamma converted farther than 1 cm from the vertex and this excluded 5.4% of events. Finally the inefficiency of this single method is 40% (36%+(100%-36%)*5.4%), and combining it with the first one gives 8-12% of inefficiency.

- Energy loss pattern method, used as a last resort when two above methods fail: in Ref. [G03] it is reported that 3.7-5.5% gammas of relevant energies is being confused with electrons (for 90% electron efficiency). In the most pessimistic scenario the three methods combined give 0.6% of neutral pion identification inefficiency.

Summarizing, we can say that the technique is promising, as the separating capability is very high – combining the three types of analyses described above give the misidentification fraction value well below 1%. In future more precise studies should be carried out taking into account final design of the detector and experimental setup of the T2K experiment.

Chapter 8
Discussion and summary

The thesis presents several analyses important for T2K experiment.

The primary aim of the thesis was to study background to electron neutrino appearance in T2K experiment. The main contribution to this background is NC neutral pion production. The pion production uncertainty analysis, presented in Chapter 6, is a central study for this thesis. Historical bubble chamber data have been reanalyzed, for the first time properly taking into account flux normalization errors. Resulting fit was used as a starting point for a simulation study that yielded 6-10% uncertainty for resonant NC neutral pion production channel in the neutrino energy range that is interesting in context of T2K experiment.

The analysis described above is accompanied by a study of neutral pion identification capabilities of liquid argon time projection chamber detector. Liquid argon imaging technique has an excellent reconstruction capabilities. The study took into account a detector in the planned 2 km station of T2K. Two methods of neutral pion identification have been verified: two shower method and gap method. Combination of those two and a third, energy loss pattern method (results for this method were taken from literature) gave a result of less than 1% of neutral pion misidentification. Such high identification level is very promising and situates the liquid argon technique above the water Cherenkov detectors in terms of π^0 identification.

Two separate analyses of neutrino energy and four-momentum transfer squared reconstruction have also been conducted. Methods of neutrino energy reconstruction were presented, along with listing of conditions in which they give inaccurate results. Problems associated with Q^2 reconstruction were also shown. The detector study indicated that in CC charged pion production most of low Q^2 events cannot be reconstructed and tagged properly.

Finally, the SMRD detector optimization, presented in Chapter 4, was the most practical and immediately useful part of the work. The experimental requirements included provision of reconstruction capability for muon tracks coming from neutrino interactions that cannot be handled by tracker detectors and enabling the detector to serve as cosmic muon trigger. Basing on simulation of detector responses, we were able to meet the requirements and design the layout of scintillator modules in the ND280oa magnet. Using that design ND280oa detector will be able to reconstruct 99% of muons coming from all interactions and 99.3% of muons from CCQE interactions. The SMRD detector was assembled using the suggestions formulated in this analysis and is now ready for operation. At the time of writing of this Chapter (February 2010) first neutrino events have been successfully recorded.

Appendix
Fitting of form factor parameters to the data

We are to fit the calculated differential cross-sections for ANL $\sigma_{th}^{ANL}\left(Q_i^2\right)$ to the data $\sigma_{\text{ex}}^{ANL}\left(Q_i^2\right)$, and each i-th bin of data has a known error $\Delta\sigma_i$ (see Chapter 6). The data are binned in Q^2 and averaged over neutrino energies. The same applies to the fit for BNL. In general, $\sigma_{th}\left(Q_i^2\right)$ are functions of *j* parameters (like M_A and $C_5^A(0)$), which we would like to determine.

In the simplest case, where $\sigma_{\text{ex}}\left(Q_i^2\right)$ are uncorrelated, the χ^2 function to minimize can be constructed as follows:

$$\chi_1^2 = \sum_{i=1}^{k_{ANL}} \left(\frac{\sigma_{th}^{ANL}\left(Q_i^2\right) - \sigma_{\text{ex}}^{ANL}\left(Q_i^2\right)}{\Delta\sigma_i} \right)^2 + \sum_{i=1}^{k_{BNL}} \left(\frac{\sigma_{th}^{BNL}\left(Q_i^2\right) - \sigma_{\text{ex}}^{BNL}\left(Q_i^2\right)}{\Delta\sigma_i} \right)^2$$

for which the number of degrees of freedom is $dof = k_{ANL} + k_{BNL} - j$.

However, the values of $\sigma_{\text{ex}}\left(Q_i^2\right)$ are strongly correlated, as there is a common systematic error that applies to all $\sigma_{\text{ex}}\left(Q_i^2\right)$. Let's try to separate this factor from the bin-to-bin variation and write:

$$\sigma_{\text{ex}}\left(Q_i^2\right) = f \cdot N_i$$

where N_i is a number of events in a given Q_i^2 bin (so that total number of events $N = \sum_{i=1}^{k} N_i = \frac{\sigma_{tot-ex}}{f}$) and f is a factor containing neutrino flux, number of targets (related to mass of the detector), live time of the experiment, etc. This factor is approximately the same for all the bins.

We can now calculate the total error as:

$$\left(\frac{\Delta\sigma_i}{\sigma_i} \right)^2 = \left(\frac{\Delta f}{f} \right)^2 + \left(\frac{\Delta N_i}{N_i} \right)^2 = f_{rel}^2 + \frac{1}{N_i}$$

assuming poissonian errors for N_i, $\Delta N_i = \sqrt{N_i}$. Relative error $f_{rel} = (10-20)\%$ comes mainly from flux uncertainty, as other quantities are known with a much better precision.

In experiments like ANL and BNL one measures *k* values of N_i, which can be treated as random variables. For cross-section determination one also has to know the neutrino flux $\phi \pm \Delta\phi$ (which is

another independent random variable) and that gives us $f \pm \Delta f$, since flux errors dominate f_{rel} ($\frac{\Delta\phi}{\phi} = \frac{\Delta f}{f}$).

We have therefore a vector of $k+1$ random variables $x^{ex} = \left(N_1^{ex}, N_2^{ex}, \ldots, N_k^{ex}, f\right)$. In order to construct a χ^2 function:

$$\chi^2 = \sum_{i=1}^{k} \left(\frac{x_i^{ex} - x_i^{th}}{\Delta x_i^{ex}} \right)^2$$

we need a corresponding vector of theoretical values $x^{th} = \left(N_1^{th}, N_2^{th}, \ldots, N_k^{th}, f_{th}\right)$. They can be any functions of parameters that will be fitted (like M_A and $C_5^A(0)$ in the fit described in Chapter 6). One of those parameters is f_{th} and the last function in the vector is equal to this parameter.

Now a χ^2 function can be written the following way:

$$\chi^2 = \sum_{i=1}^{k} \left(\frac{\frac{1}{f_{th}} \sigma_i^{th} - N_i^{ex}}{\Delta N_i^{ex}} \right)^2 + \left(\frac{f_{th} - f}{\Delta f} \right)^2$$

where, again, $\left(N_1^{ex}, N_2^{ex} \ldots\ldots N_k^{ex}, f\right)$ are experimental values and $\left(N_1^{th}, N_2^{th} \ldots\ldots N_k^{th}, f_{th}\right)$ are theoretically calculated expectations, $N_i^{th} = \frac{\sigma_i^{th}}{f_{th}}$.

Usually, a total cross-section value is given as an experimental result instead of value of f:

$$\sigma_{tot}^{ex} = f \cdot N^{ex}, \quad N^{ex} = \sum_{i=1}^{k} N_i^{ex}$$

It is also convenient to define a normalization parameter, which will be fitted instead of f_{th}:

$$p \equiv \frac{f_{th}}{f} = \frac{\sigma_{tot}^{th} N^{ex}}{\sigma_{tot}^{ex} N^{th}}$$

and experimental normalization error (which is derived from data):

$$r \equiv \frac{\Delta f}{f}$$

The final formula is then as follows:

$$\chi^2 = \sum_{i=1}^{k} \left(\frac{\sigma_i^{th} - p\sigma_i^{ex}}{p\Delta\sigma_i^{ex}} \right)^2 + \left(\frac{p-1}{r} \right)^2$$

and this formula was used in the fitting procedure.

References

[A86] L. A. Ahrens et al., *Determination of the neutrino fluxes in the Brookhaven wide band beams*, Phys. Rev. D 34, 75, 1986.

[A98] J. N. Abdurashitov et al., Phys. Rev., C59, 2246–2263, 1999, [hep-ph/9803418].

[A01] S. H. Ahn et al., Phys. Lett., B511, 178–184, 2001, [hep-ex/0103001].

[AG01] A. Aguilar et al., Phys. Rev., D64, 112007, 2001, [hep-ex/0104049].

[A03] S. Agostinelli et al. [GEANT4 Collaboration], *GEANT4: A simulation toolkit*, Nucl. Instrum. Meth. A506, 250–303, 2003.

[AH03] S. Ahmed et al., Phys. Rev. Lett., 92, 181301, 2004, [nucl-ex/0309004].

[AP03] M. Apollonio et al., Eur. Phys. J., C27, 331, 2003, [hep-ex/0301017].

[A04] Y. Ashie et al. [Super-Kamiokande Collaboration], Phys.Rev.Lett.93:101801,2004 [hep-ex/0404034].

[AR04] F. Ardellier et al., 2004, [hep-ex/0405032].

[A05] Y. Ashie et al. (Super-Kamiokande Collaboration), *A Measurement of Atmospheric Neutrino Oscillation Parameters by Super-Kamiokande I*, Phys. Rev. D 71, 112005, 2005 [arXiv:hep-ex/0501064].

[AH05] B. Aharmim et al., Phys. Rev., C72, 055502, 2005, [nucl-ex/0502021].

[A06] C. Andreopoulos, *The GENIE universal, object-oriented neutrino generator,* Nucl. Phys. Proc. Suppl. 159, 217–222, 2006.

[A08] C. Amsler et al. [Particle Data Group], *Review of Particle Physics*, Physics Letters B667, 1, 2008 and 2009 partial update for the 2010 edition.

[A09] C. Andreopoulos [for the GENIE Collab.] *The GENIE neutrino Monte Carlo generator,* Acta Phys. Pol. B 40, 2461, 2009

[B76] S. M. Bilenky and B. Pontecorvo, Sov. J. Nucl. Phys., 24, 316–319, 1976; S. M. Bilenky and B. Pontecorvo, Nuovo Cim. Lett., 17, 569, 1976.

[B77] Barish et al. *Study of neutrino interactions in hydrogen and deuterium: Description of the experiment and study of the reaction* $\nu+d\rightarrow\mu^-+p+p_s$ Phys. Rev. D 16, 3103, 1977

[B81] Baker et al. *Quasielastic neutrino scattering: A measurement of the weak nucleon axial-vector form factor* Phys. Rev. D 23, 2499 – 2505, 1981

[B97] R. Brun and F. Rademakers, *ROOT: An object oriented data analysis framework,* Nucl. Instrum. Meth. A389, 81–86, 1997.

[B01] J. N. Bahcall, M. H. Pinsonneault, and S. Basu, Astrophys. J., 555, 990–1012, 2001, [astro-ph/0010346].

[BO01] F. Boehm et al., Phys. Rev., D64, 112001, 2001, [hep-ex/0107009].

[B02] G. Battistoni, A. Ferrari, A. Rubbia, P.R. Sala, *The FLUKA nuclear cascade model applied to neutrino interactions,* Proceedings of the "Second International Workshop on Neutrino-Nucleus Interactions in the few-GeV Region", NUINT02, December 2002, University of California, Irvine, USA.

[B04] S. M. Bilenky, *A lecture on neutrinos*, 2004 [arXiv:hep-ph/0402153v1].

[C71] Y. Cho et al. PRD 4, 1967, 1971.

[C98] B. T. Cleveland et al., Astrophys. J., 496, 505–526, 1998.

[C02] D. Casper *The nuance neutrino physics simulation, and the future,* Nucl. Phys. Proc. Suppl. 112, 161, 2002.

[C04] A. Cervera-Villanueva, J.J. Gómez-Cadenas and J.A. Hernando, *"RecPack" a reconstruction toolkit*, Nucl.Instrum.Meth.A534:180-183, 2004.

[D04] S. Desai *High energy neutrinos astrophysics with Super-Kamiokande,* Ph. D. thesis, 2004.

[D06] [The T2K Collaboration], *Document for ND280 review*, 2006 [internal T2K document].

[E02] K. Eguchi et al., Phys. Rev. Lett., 90, 021802, 2003, [hep-ex/0212021].

[F96] Y. Fukuda et al. [Kamiokande Collaboration], Phys. Rev. Lett., 77, 1683–1686, 1996; Y. Fukuda et al. [Super-Kamiokande Collaboration], Phys.Rev.Lett. 81, 1158-1162, 1998; Erratum-ibid. 81, 4279, 1998

[F98] Y. Fukuda et al. (Super-Kamiokande Collab.), *Evidence for oscillation of atmospheric neutrinos,* Phys.Rev.Lett.81:1562-1567,1998

[F05] A. Ferrari, P.R. Sala, A. Fassò, J. Ranft, CERN-2005-010, INFN/TC_05/11 (2005); G. Battistoni, S. Muraro, P.R. Sala, F. Cerutti, A. Ferrari, S. Roesler, A. Fassò, J. Ranft, Proc. of the Hadronic Shower Simulation Workshop 2006, Fermilab 6–8 September 2006, M. Albrow, R. Raja eds., AIP Conf. Proc. 896, 31, 2007.

[G03] Y. Ge, P. Sala, A. Rubbia, *e/π^0 Separation in ICARUS Liquid Argon Time Projection Chamber,* Icarus internal note ICARUS-TM-03-05, 2003.

[G07] C. Giunti, C. W. Kim, *Fundamentals of Neutrino Physics and Astrophysics*, Oxford University Press, 2007.

[G09] K. M. Graczyk, D. Kielczewska, P. Przewlocki, and J. T. Sobczyk, *C5A axial form factor from bubble chamber experiments,* Phys. Rev. D 80, 093001, 2009.

[H99] W. Hampel et al., Phys. Lett., B447, 127–133, 1999.

[H03] Y. Hayato et al. *Letter of Intent, Neutrino Oscillation Experiment at JHF*, 2003 http://neutrino.kek.jp/jhfnu/loi/loi.v2.030528.pdf

[H09] Y. Hayato *A neutrino interaction simulation program library NEUT*, Acta Phys. Pol. B 40, 2477, 2009.

[I04] ICARUS Coll., *Design, construction and tests of the ICARUS T600 detector,* Nucl. Inst. Meth., A527, 329-410, 2004.

[J05] C. Juszczak, J. A. Nowak and J. T. Sobczyk, *Simulations from a new neutrino event generator*, Nucl. Phys. Proc. Suppl. 159, 211, 2006.

[K86] T. Kitagaki et al., *Charged current exclusive pion production in neutrino deuterium interactions*, Phys. Rev. D 34, 2554, 1986.

[K90] T. Kitagaki et al., *Study Of Neutrino D → Mu- P P(S) And Neutrino D → Mu- Delta++ (1232) N(S) Using The Bnl 7-Foot Deuterium Filled Bubble Chamber*, Phys. Rev. D 42, 1331, 1990.

[K05] E. Kearns et al. *A Proposal for a Detector 2 km Away From the T2K Neutrino Source,* 2005, http://hal.in2p3.fr/docs/00/40/91/76/PDF/2km-proposal-05-05-30.pdf

[K09] G. Karagiorgi for the MiniBoone Collaboration, *New Results from MiniBooNE: A Search for Electron Antineutrino Appearance at ~1 eV^2,* to appear in the proceedings for Les Rencontres de Physique de la Vallee d'Aoste, LaThuile, Italy, March 1-7, 2009, [hep-ex/0910.0263]

[KA09] H. Kakuno, *Status of the T2K experiment*, presented at 22nd International Workshop on Weak Interactions and Neutrinos, Perugia, Italy, September 16, 2009, http://www.t2k.org/docs/talk/012

[LS72] C.H. Llewellyn-Smith, Phys. Rep. C3, 261, 1972.

[L09] M. Lindner, *Status of the T2K 280m Near Detector,* proceedings of ICHEP08, 2009, http://www.t2k.org/docs/proc/001/

[LA09] Private communication with J. Łagoda from T2K SMRD group (Warsaw Neutrino Group, Warsaw University), 2009.

[M62] Z. Maki, M. Nakagawa, and S. Sakata, Prog. Theor. Phys., 28, 870, 1962.

[M01] K. McDonald, *An Off-Axis Neutrino Beam,* 2001 [arXiv:hep-ex/0111033v1].

[M06] D. G. Michael et al. [MINOS Collaboration], Phys.Rev.Lett.97:191801,2006 [hep-ex/0607088].

[M08] S. Mine et al. (K2K Collaboration), *Experimental study of the atmospheric neutrino backgrounds for proton decay to positron and neutral pion searches in water Cherenkov detectors,* Phys. Rev. D 77, 032003, 2008 [arXiv: hep-ex/0801.0182].

[M09] K. Matsuoka *Development and production of the ionization chamber for the T2K muon monitor*, presented at TIPP09 conference, 2009,
http://www-he.scphys.kyoto-u.ac.jp/member/matsuoka/talk/TIPP09.pdf

[N05] S. Nakayama et al. (K2K Collaboration), *Measurement of single pi0 production in neutral current neutrino interactions with water by a 1.3-GeV wide band muon neutrino beam,* Phys. Lett. B 619, 255, 2005 [arXiv:hep-ex/0408134].

[P57] B. Pontecorvo, Sov. Phys. JETP, 6, 429, 1957; B. Pontecorvo, Sov. Phys. JETP, 7, 172–173, 1958.

[P00] D. H. Perkins, *High Energy Physics,* Cambridge University Press, 2000.

[P10] Private communication with M. Posiadała from T2K and NA61 experiments (Warsaw Neutrino Group, Warsaw University), 2010.

[R81] D. Rein, L.M. Sehgal, *Neutrino Excitation Of Baryon Resonances And Single Pion Production* Ann. Phys. 133, 79, 1981.

[R82] G. M. Radecky et al., *Study Of Single Pion Production By Weak Charged Currents In Low-Energy Neutrino D Interactions*, Phys. Rev. D 25, 1161, 1982.

[R83] D. Rein, L.M. Sehgal, Nucl. Phys. B223, 29, 1983.

[R01] A. Rubbia, *NUX – neutrino generator,* presented at 1st Workshop on Neutrino–Nucleus Interactions in the Few GeV Region (NuInt01), Tsukuba, Japan, 13–16 December 2001

[R07] D. Rein, L.M. Sehgal, Phys. Lett. B657, 2007.

[S72] R.A. Smith, E.J. Moniz, Nucl. Phys. B43, 605 (1972); Erratum: B101, 547, 1975.

[S04] J. T. Sobczyk, J. A. Nowak and K. M. Graczyk, WroNG: *Wroclaw neutrino generator of events for single pion production,* Nucl. Phys. Proc. Suppl. 139, 266, 2005 [arXiv:hep-ph/0407277].

[S08] T. Schwetz, M. Tortola, J. Valle, *Three-flavor neutrino oscillation update*, 2008, updated 2010 [arXiv:hep-ph/0808.2016v3].

[S10] Private communication with Robert Sulej, member of T2K SMRD group (A. Soltan Institute for Nuclear Studies, Warsaw Neutrino Group), 2010.

[T08] J. A. Thomas, P. L. Vahle (editors), *Neutrino Oscillations: Present Status and Future Plans*, World Scientific, 2008.

[V07] A. Vacheret for the T2K Collab., *The T2K beam line and near detectors,* in proceedings of NuInt 07 conference, 2007,

http://www.imperial.ac.uk/research/hep/preprints/07-22.pdf.

[W09] M. O. Wascko *Experimental measurements of neutrino cross-sections near 1 GeV,* Acta Phys. Pol. B 40, 2421, 2009

[Z07] J. Zalipska, *Search for transformation of muon neutrinos into electron neutrinos in K2K experiment,* Ph.D. thesis, 2007.

[Z08] G. 'S.' Zeller, Low Energy Neutrino Cross Sections, presented at Neutrino '08 Conference, Christchurch, New Zealand, 2008,

http://www2.phys.canterbury.ac.nz/~jaa53/presentations/Zeller.pdf